AD-A065 914 DEFENCE RESEARCH ESTABLISHMENT SUFFIELD RALSTON (ALBERTA) F/G 18/3
FREE-FLIGHT MEASUREMENT OF THE DRAG FORCES ON CYLINDERS IN EVEN--ETC(U)
FEB 79 A W GIBB, D A HILL

UNCLASSIFIED DRES-TP-453 NL

1 OF 2

AD A065914

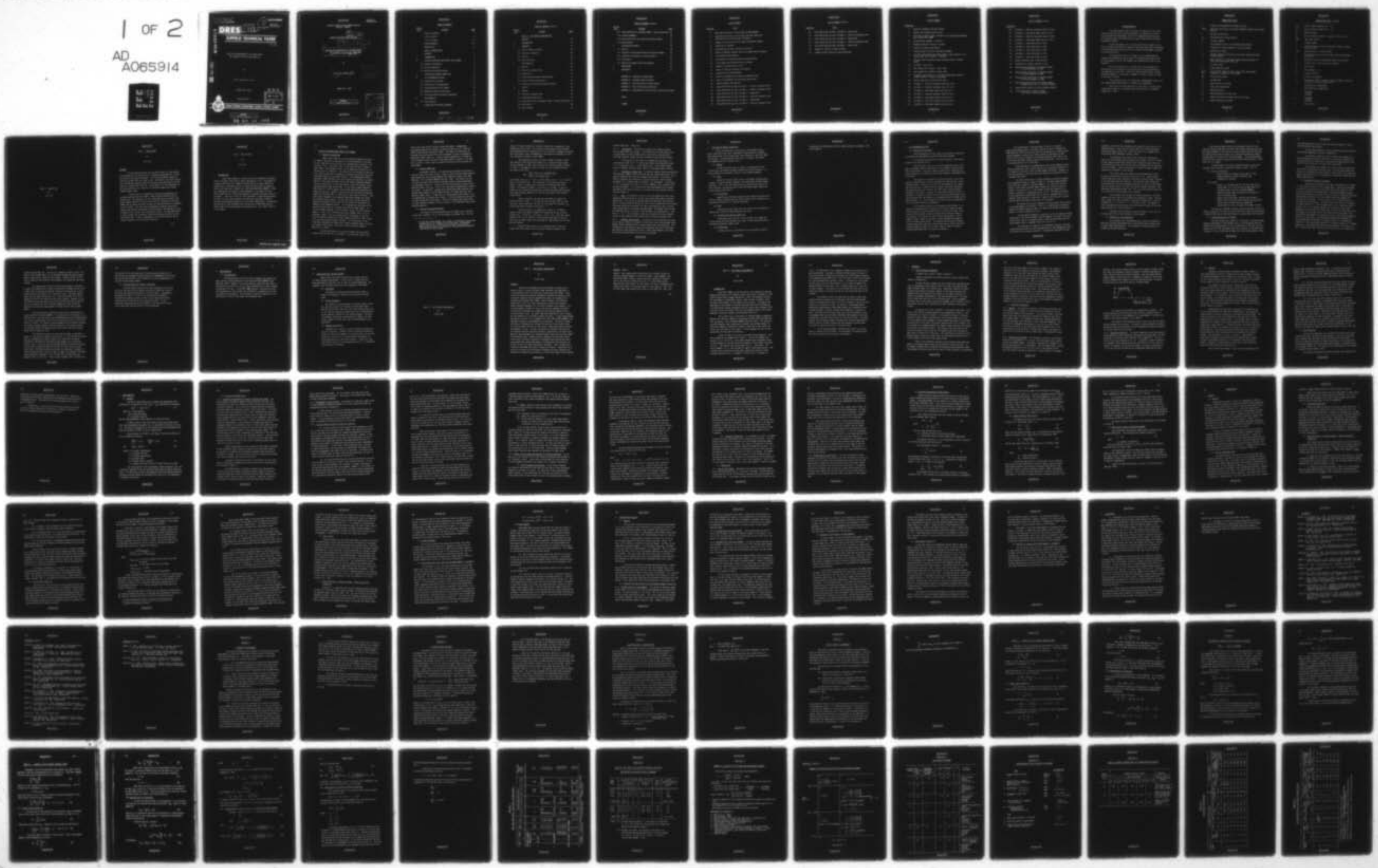

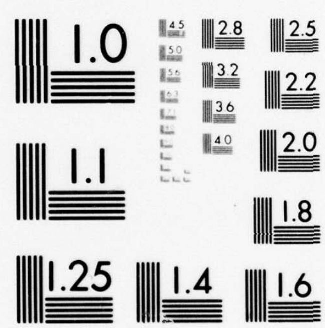

MICROCOPY RESOLUTION TEST CHART
NATIONAL BUREAU OF STANDARDS-1963-A

UNCLASSIFIED

UNLIMITED
DISTRIBUTION

DRES

SUFFIELD TECHNICAL PAPER

NO. 453

FREE-FLIGHT MEASUREMENT OF THE DRAG FORCES ON CYLINDERS IN EVENT DICE THROW (U)

by

A.W.M. Gibb and D.A. Hill

PROJECT NO. 21K52

February 1979

CANADA DEFENCE RESEARCH

DEFENCE RESEARCH ESTABLISHMENT SUFFIELD : RALSTON : ALBERTA

WARNING
The use of this information is permitted subject to recognition of proprietary and patent rights.

UNCLASSIFIED

UNLIMITED
DISTRIBUTION

DEFENCE RESEARCH ESTABLISHMENT SUFFIELD
RALSTON ALBERTA

(14) DRES-TP-

SUFFIELD TECHNICAL PAPER NO. 453

(9) Technical paper,

(6)

FREE-FLIGHT MEASUREMENT OF THE DRAG FORCES ON CYLINDERS IN EVENT DICE THROW ~~(U)~~

by

(11) Feb 79

(10) A.W.M. Gibb ~~and~~ D.A. Hill

(12) 15p.

PROJECT NO. 21K52

ACCESSION for
NTIS White Section ☒
DDC Buff Section ☐
UNANNOUNCED ☐
JUSTIFICATION
BY
DISTRIBUTION/AVAILABILITY CODES
Dist. AVAIL. and/or SPECIAL
A

UNCLASSIFIED

403104

TABLE OF CONTENTS

Section No.	SECTION	Page
	Table of Contents	i
	List of Tables	iv
	List of Figures	vi
	Acknowledgements	viii
	Nomenclature	ix
	Part I - PLAN OF TEST	
	ABSTRACT	1
1.	INTRODUCTION	3
2.	REVIEW OF UNSTEADY DRAG FORCES ON CYLINDERS	4
2.1	General Introduction	4
2.2	Previous DRES Work	5
2.3	Review of Unsolved Problems	5
3.	SELECTION OF PROJECT OBJECTIVES	8
4.	THE EXPERIMENTAL DESIGN	10
4.1	Selection of Cylinders	10
4.2	Selection of Instrumentation	13
4.3	Predicted Motion of Cylinders	14
4.4	Mechanical Design of Cylinders	14
4.5	The Associated Dust Density Experiment	16
5.	DATA ANALYSIS	17
5.1	Error Analysis	17
6.	SUGGESTIONS FOR FURTHER RESEARCH	18

TABLE OF CONTENTS (Cont'd)

Section No.	SECTION	Page
	Part II - TEST RESULTS AND ANALYSIS	
	ABSTRACT	19
1.	INTRODUCTION	21
2.	APPARATUS	23
2.1	Test Cylinders and Mounts	23
2.2	Velocity Transducers	24
2.3	Cameras	26
2.4	Dust Collectors	27
3.	DATA ANALYSIS	29
3.1	General	29
3.2	Velocity Transducer Data	30
3.3	Camera Data	35
3.4	Free-Field Overpressure Measurements	37
3.5	Impact Pressure Calculations	38
3.6	Calculation of Mach and Reynolds Numbers	39
4.	RESULTS	40
4.1	General	40
4.2	Velocity Transducer Data	40
4.3	High-Speed Camera Data	41
4.4	Drag Coefficient vs Reynolds Number - Before Corrections	41
4.5	End Effects	42
4.6	Dust Loading	45

TABLE OF CONTENTS (Cont'd)

Section No.	SECTION	Page
4.7	Drag Coefficient vs Reynolds Number - After Corrections	45
4.8	Surface Roughness	46
4.9	Drag Coefficients for Supercritical Mach Numbers	46
4.10	Blast Anomaly	47
5.	DISCUSSION OF RESULTS	48
5.1	General	48
5.2	Variation of Drag Coefficient with Reynolds Number	48
5.3	Comparison with Results of Other Workers	50
5.4	End Effects	51
5.5	Results for Supercritical Mach Numbers	52
6.	CONCLUSIONS	53
7.	REFERENCES	55
	APPENDIX A: Statement of Requirement	
	APPENDIX B: Cylinder Motion Estimates	
	APPENDIX C: Blast-Resistant Cylinder Design	
	APPENDIX D: Test of Velocity Calibration	
	APPENDIX E: Philosophy of Curve-Fitting to Velocity-Time Data	
	TABLES	
	FIGURES	

LIST OF TABLES

Table No.	TITLE
1.	DRES drag force data - free-flight cylinder method
2.	$C_D(M,L/D)$ for finite L/D calculated from DIAL PACK data and infinite L/D from the open literature
3.	Summary of L/D ratio effect *vs* Mach and Reynolds numbers
4.	Selection of cylinders
5.	Contributions of each cylinder to the goals
6.	Values of dynamic pressure used in cylinder motion estimates
7.	Calculated cylinder motion
8.	Calculations for blast-resistant cylinder design
9.	Size, weight and location of test cylinders
10.	Summary of cameras used in trial
11.	Check of velocity transducer calibration
12.	Comparison of fitting methods
13.	Best-fit polynomials for velocity transducer data
14.	Best-fit polynomials for high speed camera data
15.	Impact pressure calculations
16.	Drag coefficient *vs* time, cylinder 2 - velocity transducer data
17.	Drag coefficient *vs* time, cylinder 3 - velocity transducer data
18.	Drag coefficient *vs* time, cylinder 3 - camera data
19.	Drag coefficient *vs* time, cylinder 4 - velocity transducer data
20.	Drag coefficient *vs* time, cylinder 4 - camera data
21.	Drag coefficient *vs* time, cylinder 5 - velocity transducer data

LIST OF TABLES (Cont'd)

Table No.	TITLE
22.	Drag coefficient vs time, cylinder 5 - camera data
23.	Drag coefficient vs time, cylinder 6 - velocity transducer data
24.	Drag coefficient vs time, cylinder 6 - camera data
25.	Drag coefficient vs time, cylinder 7 - velocity transducer data
26.	Drag coefficient vs time, cylinder 7 - camera data
27.	Summary of results for each cylinder
28.	Summary of best values for drag coefficient

LIST OF FIGURES

Figure No.

1. $C_D(M)$ for different L/D and R values
2. $C_D(D/L)$ for different (M,R) values
3. The range of (M,R) values included in all previous measurements and in Event DICE THROW
4. Cylinder drag assembly - location 1
5. Mechanical design of typical cylinder
6. Layout of cylinder drag project
7. Close-up view of velocity transducer assembly
8. Pre-shot view showing high speed camera, light reflector, and greasy stake dust collector - location 1
9. Pre-shot view of Canadian sector showing extent of treated ground
10. Cylinder 1 (post shot)
11. West support for cylinder 1 (post shot)
12. East support for cylinder 1 (post shot)
13. Cylinder 5 (post shot) at 7 psi peak overpressure location showing extent of lateral displacement
14. Greasy stake dust collector (post shot)
15. Cylinder 2 - velocity transducer data (20.1 psi)
16. Cylinder 3 - velocity transducer data (9.7 psi)
17. Cylinder 3 - high speed camera data (9.7 psi)
18. Cylinder 4 - velocity transducer data (6.7 psi)
19. Cylinder 4 - high speed camera data (6.7 psi)
20. Cylinder 5 - velocity transducer data (6.7 psi)
21. Cylinder 5 - high speed camera data (6.7 psi)

LIST OF FIGURES (Cont'd)

Figure No.

22. Cylinder 6 - velocity transducer data (9.7 psi)
23. Cylinder 6 - high speed camera data (9.7 psi)
24. Cylinder 7 - velocity transducer data (9.7 psi)
25. Cylinder 7 - high speed camera data (9.7 psi)
26. Cylinder 3 - drag coefficient vs time
27. Cylinder 4 - drag coefficient vs time
28. Cylinder 5 - drag coefficient vs time
29. Cylinder 6 - drag coefficient vs time
30. Cylinder 7 - drag coefficient vs time
31. Impact pressures used in data analysis
32. Uncertainty in impact pressure vs time
33. Measured drag coefficient vs Reynolds number - 3.5 inch diameter cylinder
34. Measured drag coefficient vs Reynolds number - 9.5 inch diameter cylinder
35. Measured drag coefficient vs Reynolds number - 18.0 inch diameter cylinder
36. Measured drag coefficient vs Reynolds number - composite plot for all cylinder diameters
37. Measured end effects for finite-length cylinders
38. Drag coefficient vs Reynolds number - best values (after corrections)

ACKNOWLEDGEMENTS

The authors would like to thank Mr. R. Naylor for many stimulating discussions about the drag experiment, for agreeing to conduct the associated dust experiment, and for his suggestion on better ways of calculating the fluid flow behind the shock front than by using the Friedlander formula.

One of the authors (Dr. A. Gibb) would like to thank Dr. G.V. Price for making available his computer codes which were used to determine the Friedlander decay constant and to calculate flow parameters required in the data analysis.

The assistance of Mr. S.A. Cyganik is also appreciated for discussions of mechanical design ideas, for expediting the fabrication of the equipment, and for the assembly and preparation of parts of the apparatus.

One of the authors (Dr. A. Gibb) would like to express his appreciation to all those who assisted with the setup and execution of the experiment in the field. Particular thanks are due to Mr. Cyganik, and also to Messrs. F. Winfield, R. Campbell, W. Ngo, J. Vesso, R. Moss, M. Fach and C. McIvor.

The assistance of Mr. N.A. Bannister, Head/Computer Group, with the computer-based data analysis is gratefully acknowledged.

Much of the previous DRES data in this report, including data reanalysed in Table 2, is extracted from reports by Mr. S.B. Mellsen (1969a, 1971, 1974).

NOMENCLATURE TABLE

A	Frontal area presented by cylinder to fluid
AN/FO	Explosive consisting of 94 percent ammonium nitrate and 6 percent fuel oil
a	Cylinder acceleration
C_D	Drag coefficient (dimensionless)
D	Cylinder diameter
F	Time-dependent factor in Friedlander decay formula
f	Frequency of vortex shedding at rear of cylinder
I	Overpressure impulse
I_o	Impulse received by cylinder during shock diffraction phase of drag loading
k	Decay constant in Friedlander formula describing decay of blast wave overpressure with time
L	Cylinder length
M	Free-stream Mach number
M_c or M_{c1}	Critical Mach number at which local fluid speed becomes supersonic at some point on cylinder
M_{c2}	Critical Mach number
m	Cylinder mass
P_D	Drag pressure on cylinder
p	Blast wave overpressure
p_a	Ambient pressure
p_o	Peak overpressure in blast wave
q	Dynamic pressure on cylinder due to fluid flow
q_I	Impact pressure on cylinder

NOMENCLATURE TABLE (Cont'd)

q_{Io}	Initial impact pressure (at t = o)
q_o	Initial dynamic pressure (at t = o)
R	Reynolds number
R_c	Critical Reynolds number, in range 3×10^5 to 5×10^5
RMS	"Root mean square"
S	Strouhal number
T	Time from start of velocity transducer signal to signal crossover point
TNT	High explosive, tri-nitro-toluene
t	Elapsed time after arrival of shock front at front edge of cylinder
t_+	Duration of positive overpressure phase of blast wave
t_T	Transit time of shock front over cylinder
u	Fluid speed
u_o	Fluid speed at t = o
v	Cylinder velocity
x	Cylinder displacement
x_o	Distance of travel of velocity tranducer magnet from start of signal to signal crossover point
η	$\dfrac{C_D(\text{finite L/D, steady flow})}{C_D(\text{infinite L/D, steady flow})}$
η'	$\dfrac{\text{"unsteady"}}{\text{"steady"}}$
η''	$\dfrac{\text{"unsteady"}}{\text{"unsteady"}}$
ρ	Fluid density

PART I: PLAN OF TEST

by

D.A. Hill

PART I: PLAN OF TEST

by

D.A. Hill

ABSTRACT

Previous determinations of drag coefficients for both steady and unsteady flow are reviewed for all reported experiments at critical and supercritical Reynolds numbers. The unsolved problems remaining from earlier DRES work were found to be: end effects, dust drag loading, the discrepancies between steady and unsteady flow drag forces, and the need for a further data analysis. A new analysis is also presented for the drag coefficient as a function of flow Mach number and cylinder length-diameter ratio.

A plan of test is presented for drag force measurements on cylinders during Event DICE THROW, a 628-ton AN/FO explosion held in October 1976. The objectives of this experiment were to provide drag force support data for the lattice mast and all antennas in Event DICE THROW, and to extend the table of data for drag coefficients to diameters up to 18 inches. The free-flight measurement technique, using both cameras and velocity transducers for data sources, was employed on seven cylinders at 20, 10 and 7 psi overpressure levels. The expected motion of each cylinder was calculated, based on the predicted value for the drag coefficient. Finally, suggestions for the data analysis and for further research in this area are discussed.

(U)

Part I: Plan of Test

by

D.A. Hill

1. INTRODUCTION

Event DICE THROW was a large blast trial conducted on October 6, 1976 at the White Sands Missile Range, New Mexico, U.S.A. The explosive charge was 628 tons of an ammonium nitrate-fuel oil mixture (AN/FO) at ground level, considered similar in explosive energy yield to previous 500-ton TNT explosions (PRAIRIE FLAT, DIAL PACK and MIXED COMPANY). DRES was requested by the Canadian Forces (Appendix A) to design and carry out an experiment on further measurements of unsteady-flow drag forces on cylinders. The plan of test for this experiment is described separately as Part I of this report because the author was relocated at Defence Research Establishment Ottawa prior to the DICE THROW event. The execution and analysis of the experiment were carried out by other DRES workers. These aspects of the experiment are described by Dr. A.W. Gibb in Part II of the report.

2. REVIEW OF UNSTEADY DRAG FORCES ON CYLINDERS

2.1 General Introduction

When a fluid flows in a given direction towards and around an object, the force on the object in the flow direction is defined as the "drag force" and any force in a perpendicular direction is defined as "lift". The classic text in the area of drag is Hoerner's book (1958), "Fluid-Dynamic Drag", which summarizes virtually all of the work prior to that date. The drag forces are further divided into skin friction drag, due to tangential stresses in the fluid, and form or pressure drag, due to normal stresses. From dimensional analysis (Owczarek, 1968) the drag force can be shown to be given by $C_D\ (\frac{1}{2}\rho U^2)A$ where A is the cross-sectional area of the object presented perpendicularly to the flow, U is the fluid speed, ρ the fluid density and C_D the dimensionless drag coefficient. It can also be shown (Owczarek, 1968) that for a set of objects of the same shape and orientation but arbitrary size, $C_D = C_D(M,R,\gamma)$ where M and R are the Mach and Reynolds numbers for the flow and γ is the specific heat ratio of the gas. Note that surface roughness on the object effectively changes the "shape" and therefore the C_D value. The form drag force can be computed by knowing the pressure on each point on the surface of the object and summing up the component forces. This technique has been used to calculate the drag force on a cylinder by Bishop and Rowe (1967). As the flow speed increases so that R becomes $>R_c$ (R_c, critical Reynolds number, = (3-5) x 10^5) the drag coefficient changes from 1.2 to 0.3 (Owczarek, 1968). This can be explained by the change in the pressure distribution around the cylinder (Gowen and Perkins, 1953, figure 5) as the flow pattern becomes turbulent. For discussions of the relationship between the laminar and turbulent boundary layers and the von Karman vortex street, see Hoerner (1958), Owczarek (1968) or Martin et al. (1965).

The main difference in drag force between the flow behind a shock front and that in a wind tunnel is in the early stage of the

flow as the shock front diffracts around the object. Shadowgraphs and drawings showing this process are given by Martin et al. (1965 and 1967) and by Mellsen and Naylor (1969). The effect of diffraction on the drag force during the first few milliseconds of flow is sketched by Wolkovitch (1968, figure 4). The net impulse imparted to a cylinder by this diffraction phase has been fitted empirically in figure 3.1 of Long et al. (1975), a result used to estimate the motion of the cylinders for DICE THROW.

2.2 Previous DRES Work

Experiments similar to the present one have been carried out in previous large scale blast trials. Those in which the free-flight measurement method[1] was used include PRAIRIE FLAT (Mellsen, 1969a), DIAL PACK (Mellsen, 1971) and MIXED COMPANY (Mellsen, 1974). The results for the circular and square cross-section cylinders tested in those experiments are presented in Table 1. In each case the flow started at supercritical Reynolds number, $R>R_c$ ($R_c = (3\text{-}5) \times 10^5$) and usually progressed to subcritical values. In each case average drag coefficients were reported, even though large changes in C_D are known to occur in steady flow over this Reynolds number range. In addition, for overpressure levels above 12 psi the compressibility effects due to $M>M_{c1} = 0.48$ are obscured by the use of a single average drag coefficient. The use of average drag coefficients to cover important changes in M and R values is less desirable than a more detailed analysis.

2.3 Review of Unsolved Problems

The values of the drag coefficient are known to be a function of the four variables: M, R, L/D and steady vs unsteady flow. For the

---

1 In the free-flight method, the cylinder is permitted to accelerate through the air in response to the blast wave. Acceleration (hence drag force) is derived as the slope of the measured velocity-time history and curvature of the measured displacement-time history of the cylinder.

regions of those variables of interest there exist no complete or comprehensive sets of data. The available limited data will be analysed and presented below to indicate some of the scientific problems associated with the present state of knowledge of drag forces on cylinders for the flow conditions relevant to DICE THROW.

The measured C_D values from finite length cylinders in DIAL PACK (Mellsen, 1971) have been examined as a function of Mach number (M) and compared to other values reported for infinite length cylinders in Table 2. Although the data are rough, one can estimate the average value of the ratio

$$\eta(M) = \frac{C_D(M, \text{ finite } L/D, \text{ unsteady flow})}{C_D(M, \infty\ L/D, \text{ steady flow})}$$

The average values of $\eta' = 0.65 \pm 0.18$ for $M>M_{c1}$ and $\eta' = 1.9 \pm 0.35$ for $M<M_{c1}$ will be used later. The importance of M_{c1} to the C_D value is shown in Figure 1, where $C_D(M)$ is plotted for different D/L and R values. The dramatic change in the value of C_D at $M \approx M_{c1}$ is due to a change in the flow pattern around the cylinder resulting from the local flow speed becoming supersonic at the top and bottom of the cylinder cross-section.

Figure 2 presents the same data replotted as $C_D(D/L)$ for different (M, R) values. It can be seen that for $M<M_{c1}$ and $R<R_c$ the classical results show that L/D ratio in the range of 5-20 gives a C_D figure appreciably different from $C_D(L/D = \infty)$.

The above results are summarized in Table 3. Different regions of Mach and Reynolds numbers are marked off by the critical values of $M_{c1} = 0.48$, $M_{c2} \approx 0.9$ and $R_c = (3\text{-}5) \times 10^5$. Only the regions labelled I-III are of interest to the present experiment but the results for the other regions are presented for completeness and for comparison purposes.

Using the above analysis as a reference point it was concluded that there remain several important unsolved problems from

previous DRES work. These are:

2.3.1 End effects. The effect of using finite length cylinders has not been taken into account. The previous use of side plates near to and parallel to the cylinder end is of no help as the end plate must make complete contact with the cylinder to avoid the end effects.

The severity of the effect is estimated by the values of η'' calculated in Table 3 ($\eta'' = 1$ implies end effects are negligible) where $\eta'' \doteq 1.5$ (Region I) and $\eta'' \doteq 0.65$ (Region III). These rough figures serve to indicate that end effects must be investigated more carefully.

2.3.2 Unsteady vs steady flow. In previous reports (Naylor and Mellsen, 1973; Mellsen, 1969b) it was concluded that the steady-flow values for C_D agreed reasonably well with the unsteady-flow results. The ratio ϕ of Table 3 indicates the difference in the two values for finite length cylinders ($\phi = 1$ implies that C_D (steady) = C_D (unsteady)). The values $\phi = 1.2 \pm 0.3$ (Region III) and $\phi = 1.9 \pm 0.5$ (Region I) are estimated from the data available. It is evident that more measurements with reduced end effects and further analysis are required for this problem, particularly for Region I.

2.3.3 Dust. The presence of dust in the flow behind the blast wave, especially after about 50 ms of flow, has usually been noted on previous camera data. This causes an unknown amount of additional drag loading, due to a larger effective density for the "fluid" flowing past the cylinder. Since dust would not be present for masts and antennas at sea, the dust drag loading should be measured and subtracted. An attempt would be made to condition the soil in front of the cylinders for reducing dust. Note that $\eta' = 1.9 \pm 0.4$ for Region I could be an indication of dust loading as well as the problem of end effects and of steady vs unsteady flow.

2.3.4 Complete data analysis. No realistic error estimates have been put on the C_D values at each point in the flow, nor on the averaged values. Without these, subsequent blast loading predictions lose precision. The differences in the measured camera and transducer data (up to 30% either way) have not been explained, nor has it been shown whether or not they are within the measurement error for each technique.

3. SELECTION OF PROJECT OBJECTIVES

After consideration of the needs of the Canadian Forces, and of the state of our basic knowledge of drag forces on cylinders from blast waves, the following goals were selected for the DICE THROW drag project. The abbreviated titles such as "support" and "table" are intended for use in Tables 4 and 5.

(i) Support

Provide drag force data in support of experiments on the lattice mast, the VHF/UHF Polemast antenna and the whip antenna, i.e., test cylinders with diameters similar to the antenna diameters.

(ii) Table

Extend the current table of data of unsteady flow drag coefficients to larger cylinder diameters, for effectively infinite length cylinders. This is for both future potential applications and scientific interest, and applies both to the diffraction phase loading and to the pressure drag forces.

(iii) End Effects

Measure the differences between finite length and effectively infinite length cylinders both for this project and for correlation to, and possible correction of, previous DRES work.

(iv) Dust

Estimate the extra drag force due to dust for the purpose of subtracting it from the total measured drag force.

(v) Unsteady Flow versus Steady Flow

Obtain more data from all of the cylinders for comparison of the steady flow and unsteady flow values of the drag coefficient at the Mach and Reynolds numbers used.

(vi) Diffraction

Collect data for a contribution to the scientific study of

diffraction for effectively infinite length cylinders in Regions I and III of Table 3.

4. THE EXPERIMENTAL DESIGN

4.1 Selection of Cylinders

From considerations of both goals and practical limitations, the methods and measurements described below were selected.

The free-flight method was used again because it had proven successful on previous trials.

Since the blast trial is a one-shot experiment with a minimum of equipment proofing beforehand, as few changes as possible were made to the method. Only those changes necessary for correcting previous problems or for meeting a new cylinder diameter requirement were carried out.

The problem of end effects has been discussed. One of the solutions considered was to add a hemisphere to each end of a finite length cylinder. Since the C_D value for a hemisphere is well known, the idea would be to subtract off the "known" end effect and deduce the drag force per unit length on the effectively infinite length cylinder in the middle. However, the drag coefficient of the sum of the parts is unlikely to equal the sum of the drag coefficients of the parts, because the flow patterns of a hemisphere and a cylinder do not join smoothly, i.e., the cylinder-flow vortices have no counterpart in the flow pattern around the hemisphere.

An alternate solution to the problem of end effects is to attach thin perpendicular end plates to the finite length cylinder. The truncated flow patterns here would be closer to the ideal effectively-infinite length, especially during the diffraction phase of the loading. This design also more closely approximates a finite-length cylinder joined at each end to other perpendicular members, with or without gusset plates. By changing the end plate thickness (causing negligible additional drag forces) one can adjust the total cylinder weight and hence the cylinder range of motion to permit optimum measurement with the velocity transducers.

One disadvantage of the end plates is that in a sidewise blast-force anomaly such as occurred at the 25 psi level in MIXED COMPANY (Mellsen, 1974) the force strikes the end plates at a glancing angle causing diagonal, possibly oscillatory, motion of the whole cylinder. There could also be a problem if a turbulent boundary layer flow is set up over the end plate, causing excessive end plate drag. The worst case is estimated below to be a 10% effect.

From examination of shadowgraphs of the vortex shedding process, (Naylor and Mellsen, 1973, figures 10B and C) an end plate extension of 1.5 diameters at the end of the cylinder appears desirable. However, to limit the problems of end plate drag and vibration an extension of only 1 diameter was chosen.

The final selection of cylinder diameters, end plate diameters and overpressure levels is shown in Table 4. The same length-diameter ratio (L/D) was chosen for cylinder numbers 1, 3, 4 and 5 so that the effects of end plates and Mach number regions for fixed L/D could be studied. The value of L/D = 5 was chosen to keep the length of the largest cylinders at a reasonable value, 7.5 ft. The known end effects are not appreciably changed when the L/D ratio is changed from 5 to 10 (Hoerner, 1958, Section 3, figure 28). Table 5 lists the ways in which each cylinder contributed to the goals of the project.

By restricting cylinder diameters to three values, more overlap in the measurements was possible. The 9.5 in. diameter was included to support the VHF/UHF antenna project, as there were no DRES drag measurements of a similar diameter at 10 psi.

For the smaller diameter, a value of 3.5 in. was chosen as being equivalent to the larger diameter vertical members to be used in the test lattice mast, and as a reasonable value to use for correlation with the whip antenna, which is tapered from 2.5 in. to 5.5 in.

For drag data in support of the structures projects, the drag information must cover the first quarter period of the fundamental mode of oscillation of the related structure. From previous DRES work and new

estimates, this period was estimated to be about 70 ms or less for the VHF/UHF antenna, < 50 ms for the lattice mast (25 - 30 ms previously (Long and Laidlaw, 1973)) and < 100 ms for the 18 in. cylinder (86 ms for the DIAL PACK TACAN mast (Coffey, 1971)).

For completing the table of data, the basic scaling parameters for fluid dynamic drag are known to be M and R. But for a series of near-identical equivalent charge-weight explosions such as we have in the 500-ton series, then the psi level and diameter are an equivalent pair of variables. These relationships are shown in Figure 3 where our selection of cylinders is also marked.

This figure shows the regions below and above the critical M value of 0.48 and the critical R value of 5×10^5. Each straight line through the origin represents the range of M and R values traversed by one cylinder after the explosion. The straight lines through the origin make the simplifying assumption that $M \propto R$, that is, they assume that the speed of sound, viscosity and density changes involved in the shock wave approximately cancel out. This is an over-simplification but is sufficient for the purposes of this drawing.

Each straight line through the origin represents a different diameter and the latter are recorded on the drawing in inches. All the other ranges of M and R covered in literature available to us are also recorded for $R > 5 \times 10^5$ or $R > 1 \times 10^5$ and $M > 0.48$. The legend explains the meaning of the curves, and the reference letters A-J are the same references as listed in Table 3.

The paths to be taken by our seven cylinders, as well as the starting position for each cylinder, are also marked.

4.2 Selection of Instrumentation

All cylinders were instrumented with a velocity transducer at each end, and were photographed with a high-speed camera (framing rate of order 1000 frames/second). The transducers on each end were calibrated and recorded separately.

The overlap between cameras and transducers was felt to be necessary because experience has shown that either recording device may fail when subjected to the violent air blast loading from the explosion. The position where each cylinder first strikes the ground was marked and measured as a further fail-safe measurement. This one measurement gives the total impulse received by the cylinder from the blast if negligible lift is assumed.

A second reason for the dual recording system is that each technique gives secondary information unique to itself. That is:

(i) velocity transducers
- record from each cylinder end for angle of yaw,
- measure degree of cylinder vibration, and frequency of vibration.

(ii) cameras
- record if a cylinder end falls off the mount due to ground shock, as it did for one cylinder about 100 ms before time of arrival for MIXED COMPANY,
- indicate through image obscuration the presence of dust in the blast wave,
- observe any flying debris hitting the cylinders,
- permit vertical and horizontal motions and rotational motion about cylinder axes to be measured,
- record time of arrival of shock (red ribbon flutter).

The vertical component of motion could be measured in order to check for possible lift due to non-horizontal blast flow direction and/or a choking effect due to the flow between a large cylinder and the ground.

4.3 Predicted Motion of Cylinders

As each cylinder was a model for a particular structural member (whether represented in DICE THROW or not), it was necessary that the duration of recorded motion for each cylinder be not less than the first quarter period of the fundamental mode of oscillation of the particular structure. Each cylinder was designed with a mass large enough to cause

the predicted motion to fall within the desired distance of travel over the desired time interval.

The C_D values chosen for these calculations and the detailed calculations themselves are given in Appendix B.

The internal structure of each cylinder was designed to be more rigid against transverse vibrations than previous designs, and to have sufficiently strong walls to withstand collapse when hit with the full initial force of the shock front (see below).

The estimates are conservative by 20% in the C_D values used and by 20% in the desired recording time. This 40% safety factor was felt to be sufficient to protect against likely errors in C_D values and against the possibility of an unexpectedly strong shock front from the 628-ton AN/FO charge.

4.4 Mechanical Design of Cylinders

The overall arrangement of cylinders and supporting equipment is illustrated in Figure 4, the assembly photo. Most of the equipment is similar to that described in the DIAL PACK report (Mellsen, 1971) with a few changes as described below. The outside diagonal support plates were designed to minimize the possibility of side-plate vibrations and yet keep cross bars out of the centre flow region between the cylinder and the ground. In fact, there will be a certain amount of flow choking in that region. The worst case is for the 18 in. diameter cylinders centred 6 ft. off the ground which leave a separation gap of only 63 ins. or 3.5 diameters between the cylinder and the ground. Assuming a flat solid ground surface and a vertical original shock front, the method of flow images can be used along with previous DRES "solidity-effect" measurements to estimate the size of the ground interference effect on the C_D value. The flow pattern between the idealized flat solid ground and the cylinder 3.5 diameters above it is regarded as identical to the flow pattern between two isolated cylinders of 7 diameter separation. Approximate DRES data (Long and Laidlaw, 1973, Table 2.1) for a related experiment indicate that the effect for this separation is

likely not more than 10%. The flow will, however, produce a small lift force on the cylinder which will be detected through the camera measurements of the vertical motion of the cylinder. Another reason for the 5-6 ft. height of the cylinders above ground is to reduce the dust drag loading.

The camera marker plate served the dual purpose of providing an upper scale marked off in inches to record the cylinder position, and a lower scale to provide black/white contrast for possible use in estimating relative dust density as a function of time. The camera marker plate and the support plates were 9 in. from the cylinder so as not to impede the flow of air around the end of the cylinder. Because of this, the camera lens was adjusted to have both the scale and the cylinder in focus at the same time, and a constant geometrical scale factor was applied to the position measurements to relate them to true cylinder motion.

The cylinders were connected to the velocity transducers by a system modified from MIXED COMPANY. The connecting rod was longer to reduce the error in the horizontal speed measurement due to the approximately 2 in. drop in height under the force of gravity which occurs in the first 100 ms of flight. The flexible aluminum segment of the connector reduced the chance of broken magnets resulting from yaw in the cylinder motion. For the same reason, the gimbal mounts were farther from their support plates than in previous trials.

The internal structure of one of the cylinders is depicted in Figure 5. The internal support discs and the 1 in. rod through the centre were to strengthen the structure against the transverse vibrations observed to interfere with the velocity measurements on all previous similar trials. They also provide strength against the possible collapse of the front cylinder wall when hit by the full force of the initial shock front. Pertinent design calculations are contained in Appendix C. As some transverse oscillation of these cylinders was expected, the fundamental vibration frequency of each cylinder with its end plates was measured prior to the trial. There is some evidence that in certain pre-

vious blast trials the observed oscillations grow and diminish in a way that may be analogous to beats between the fundamental oscillations and the forcing function of the frequency of vortex shedding which is related to the Strouhal number.

4.5 The Associated Dust Density Experiment

The drag loading from dust has been estimated to be as high as 20% of the total force by Naylor and Mellsen (1973) but, since it has never been measured accurately, it may be larger. Consequently, the ground for 100 ft in front of the cylinders was treated to minimize the presence of dust, and one or two simple passive dust collectors were installed at each overpressure level. It was hoped that they would provide an estimate of the total mass of dust in the shock wave and the particle size distribution.

5. DATA ANALYSIS

5.1 Error Analysis

The data analyses of both velocity transducer and camera data were similar to those employed for data from the MIXED COMPANY Event (Mellsen, 1974). However, in previous analyses, there has never been a discussion of the errors in the C_D values calculated for a given cylinder at each point in time. In the DICE THROW analysis, the effect of noise and fluctuations in the raw data was reflected in a quoted error in the C_D values for each method. This permitted a realistic appraisal of the consistency of results from camera and transducer data.

6. SUGGESTIONS FOR FURTHER RESEARCH

Many factors are known to affect the C_D values, but not all have yet been investigated. In most cases, it would take too many experiments to map out a set of data of limited importance. Consequently, the following effects were not examined in DICE THROW:

(a) Turbulence

The degree of turbulence behind the shock front is known to be important, especially for multiply-reflected waves.

(b) Surface Roughness

The effect of varying degrees of cylinder surface roughness has been shown to be important in wind tunnel work. Despite the fact that real masts will have rough surfaces due to ice covering and general weathering, this is considered to be too complex a problem for the current program. The masts and antennas tested were aerodynamically "smooth"; for that reason, smooth cylinders were used in the aerodynamic drag experiment.

(c) Shading and Solidity

"Shading" and "solidity" are two interference effects on the mast structure. "Shading" refers to mutual interference effects of two or more members in a plane parallel to the flow direction; "solidity" is a similar effect for members in a plane perpendicular to the flow direction. There exist some simple DRES results of limited generality but it is recognized that more data are needed.

PART II: TEST RESULTS AND ANALYSIS

by

A.W.M. Gibb

PART II: TEST RESULTS AND ANALYSIS

by

A.W.M. Gibb

ABSTRACT

Results are presented from an experiment to measure aerodynamic drag on circular cylinders under unsteady flow conditions in a long duration free-field blast wave during Event DICE THROW. These results provided drag loading information required for analysis of the structural response tests on Canadian Navy masts and antennae also conducted during Event DICE THROW. Seven cylinders, distributed at nominal 20, 10 and 7 psi peak overpressure locations and spanning three different diameters (3.5, 9.5 and 18 inches), were studied. The 18-inch diameter cylinder at 20 psi with 48-inch diameter end plates was partially destroyed by a sidewise blast pressure anomaly travelling from east to west. No useful data were obtained for this cylinder, but the remaining six cylinders yielded valid data. A free-flight method, developed in earlier trials (PRAIRIE FLAT, DIAL PACK, MIXED COMPANY), was employed to measure time-dependent drag pressures. For every cylinder, one velocity transducer was attached to each end of the central shaft to record cylinder velocity vs time, while a high-speed camera recorded displacement vs time. Cylinder acceleration, and hence drag pressure, was obtained from the slope and curvature, respectively, of these curves. Generally good agreement was obtained between results derived from camera and transducer data. Dynamic pressure (needed to extract drag coefficients) was calculated, assuming a Friedlander-type overpressure decay, from ground-level gauge measurements of overpressure-time histories at the 20, 10 and 7 psi peak overpressure locations. Some cylinders were fitted with extended end plates to reduce end effects. Comparison of results for cylinders with and without extended end plates indicated the presence of substantial end effects at critical and supercritical Reynolds

ABSTRACT (Con't)

numbers. Dust samples were collected at each cylinder location on vertical aluminum channels filled with grease. These samples, combined with camera records, suggest that dust loading was insignificant at the initial cylinder positions 5 or 6 feet above ground. Measured drag coefficients for Mach number <0.4 were in agreement with steady-state values for Reynolds numbers in the range (4 - 30) x 10^5, but were lower than steady-state values in the range (30 - 40) x 10^5.

(U)

PART II: TEST RESULTS AND ANALYSIS

by

A.W.M. Gibb

1. INTRODUCTION

Event DICE THROW, a free-field blast trial employing a 628-ton Ammonium Nitrate/Fuel Oil explosive charge, took place on October 6, 1976 at White Sands Missile Range, New Mexico. One of the Canadian projects, the measurement of aerodynamic drag on right circular cylinders, using the free-flight method, is the subject of this report. The project was undertaken at the request of Director Maritime Facilities and Resources to provide blast-loading information for the lattice mast (Laidlaw, 1977), pole mast (Price and Coffey, 1977) and whip antennae (Price, 1977) which underwent structural response testing during this trial.

This project was a continuation of research begun in Operation PRAIRIE FLAT (Mellsen, 1969a) and continued in Events DIAL PACK (Mellsen, 1971 and Naylor, 1973) and MIXED COMPANY (Mellsen, 1974). The choice of cylinder diameter, peak overpressure location, and cylinder design for Event DICE THROW are discussed in detail in the Plan of Test which comprises the first part of this report. A brief summary only will be presented here for the sake of continuity.

Seven cylinders of circular cross-section were employed. Their basic properties are summarized in Table 7. Two of the diameters employed, 3.5 in. and 9.5 in., were chosen because they correspond closely to the diameters of the main structural members of the related structures (3.5 in. - whip antenna and lattice mast; 9.5 in. - pole mast). The third diameter, 18 in., was included to support future mast designs. The cylinders were located at the same peak overpressure levels as their related structures (3.5 in. diameter at 10 psi, 9.5 in. diameter at

7 psi). An additional 3.5 in. diameter cylinder was located at 20 psi peak overpressure. The major unresolved problem chosen for study in this test was the influence of end effects for finite-length cylinders on the measured drag coefficient. With this goal in mind, the cylinders of a given diameter were grouped in pairs. In each pair, one cylinder had end plates with the same diameter as the cylinder diameter; the second cylinder had end plates with a diameter which was 3 times the cylinder diameter. The purpose of the extended end plates was to eliminate end effects by cutting off the air flow around the ends of the cylinder.

The methods of data recording were the same as those developed and used in previous trials employing the free-flight method. Velocity transducers were used on all test cylinders to record cylinder velocity as a function of time. In addition, a high-speed camera, operating at approximately 1000 frames/second, was stationed at each cylinder location to record cylinder displacement as a function of time. The slope of the velocity-time curve and the curvature of the displacement-time curve provided independent measurements of cylinder acceleration, and hence drag force, as a function of time. The camera records also provided secondary information on possible complicating factors such as cylinder rotation and the presence of solids (both fine dust or massive particles) in the blast wave.

All of the measurements reported herein refer to the drag phase of loading on the cylinder. No measurements of loading during the initial shock diffraction phase are reported.

2. APPARATUS

2.1 Test Cylinders and Mounts

A typical test set-up is shown in Figure 4.

Figure 6 indicates the relative position of each cylinder with respect to Ground Zero.

At each location, support for the cylinders was provided by two vertical rectangular plates made of 0.25 inch steel, with their bottom edges fastened firmly to a concrete base. Additional rigidity for these plates was provided by triangular support in the form of two one inch diameter steel bars welded to the outside of the support plates at an angle of 30 degrees approximately 5 feet above ground level. The lower ends of these bars were set into the concrete base. This arrangement provided a more rigid support than the arrangement used in previous trials (horizontal parallel bars connecting the inner surfaces of the support plates).

The design of the test cylinders is discussed extensively in the Plan of Test and the cylinder properties are summarized in Table 9. The construction of a typical cylinder is illustrated in Figure 5. Briefly, each was a right circular cylinder with a solid centre shaft of 0.75 or 1.0 inch diameter which extended 14 inches beyond each end of the cylinder. Flats were cut in the shaft nine inches from each end of the cylinder, and the cylinder was suspended between the support plates with the flats resting on the tops of the support plates. The purpose of the flats was to prevent the cylinders from rolling off the supports under the influence of small gusts of wind prior to the shot. The coefficient of sliding friction between support plate and cylinder shaft was minimized by application of silicone grease to the top of the support plate.

There is one additional feature of the cylinder design which was added at an advanced date and was not discussed in the Plan of Test. In an attempt to dampen shaft vibrations by providing better mechanical coupling between the central shaft and the shell of each cylinder, O-ring grooves

were cut in the outer edges of the interior support discs (Figure 5) and 3/16 or 1/4 inch diameter O-rings were inserted. This addition helped to fill in any small gaps between the inner surface of the cylindrical shell and the outer edges of the interior support discs. As well, an additional plywood support disc was placed 4 inches in from each end of the cylinder. Wood was used because of its low density; the intention was to provide extra support for the shaft close to the cylinder end without seriously affecting uniformity of mass distribution along the cylinder length. The additional support close to the cylinder end was provided in an attempt to increase the vibration frequency of the end of the cylinder shaft; this was felt to be necessary because calculations had shown that the fundamental vibration frequency of the solid centre shaft could be low enough to complicate analysis of the velocity transducer data.

2.2 Velocity Transducers

2.2.1 General. The velocity transducers for measuring cylinder velocity directly as a function of time consisted of seven pairs of Hewlett-Packard Sanborn 7LV9 transducers. On a given cylinder, two transducers were used, one coupled by a mechanical linkage to each end of the cylinder shaft. The transducer signals were recorded separately, on a tape recorder with nominal DC to 4KHz recording bandwidth. This provided two independent measurements of velocity for each cylinder. A close-up view prior to the shot showing the transducer coil in its gimbal mount, and the mechanical linkage which couples the magnet inside the coil to the end of the cylinder shaft, is presented in Figure 7.

2.2.2 Principle of operation. The transducers consist of two toroidal hollow-core wire-wound coils in series, along the common core of which travels a permanent magnet. The magnet is mechanically coupled to the object whose velocity is to be measured. When the object moves, pulling the magnet through the coils, the flux lines of the magnet cut the coils and induce a voltage in them which is proportional to the magnet

velocity. The two-coil design gives rise to two regions of equal length over which the transducer velocity response is uniform, separated by a short region of highly non-uniform response. Over the second working length, however, the sensitivity is reduced by a factor of two and the polarity reversed with respect to the first working length. A typical constant-velocity trace would have the following shape:

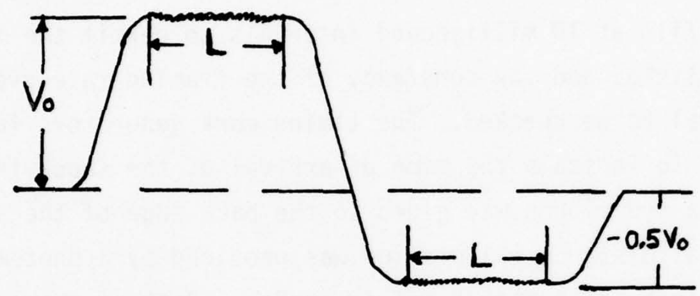

The useful working lengths are denoted by the symbol L. This diagram explains why the velocity traces from the cylinders shown in Figures 15 to 25 are in two segments with a gap between: only data collected in the working lengths, L, are usable.

The Sanborn 7LV9 transducers used in this trial had two nominal working lengths, each 9 inches. The overall recording length of approximately 20 inches was sufficient to permit between 80 and 200 milliseconds of cylinder motion to be recorded.

2.2.3. Velocity calibration. The electro-mechanical calibration method, which employed a Kistler standard accelerometer and shake table, has been described in a previous report (Mellsen, 1971, Appendix A). The calibration error was estimated to be ± 3%. In addition, careful inspection of transducer traces indicated possible variations of ± 2% in the uniformity of response over any working length. An overall uncertainty of ± 5% in the velocity calibration was assumed when analyzing the data.

2.3 Cameras

Photosonic framing cameras, operating at nominal speeds of 1000 frames/second, were set on camera posts at each cylinder location to record displacement of the cylinders as a function of time. A camera set on its mounting post can be seen in Figure 8. Relevant information on the cameras and their locations is given in Table 10.

The cameras provided internal timing marks which were projected onto the film at 10 millisecond intervals to permit the framing rate to be established and the constancy of the framing rate over the recording interval to be checked. The timing mark generators functioned on all cameras. To indicate the time of arrival of the shock front in the film frame, a red ribbon was glued to the back edge of the support plate. Horizontal distance calibration was provided by a photomarker plate with a 12-inch scale marked off in inches. Both of these aids can be seen clearly in Figure 7.

Approximately one week before shot day, Test Command moved the shot time forward from 1300 hours to 0800 hours. This change provided potentially serious problems for the camera recording system. The angle and position of the sun at 0800 hours were such that it shone almost directly into the camera lenses. The cylinder ends to be photographed were in shadow, and the high background light level caused extremely poor image contrast. To improve contrast, reflector panels were constructed of sheets of aluminum foil taped to a 4 ft x 4 ft sheet of plywood backing. One panel was bolted to each camera post, and each was oriented to reflect sunlight onto the cylinder end to be photographed. One such panel is visible in Figure 8. These hastily-constructed reflectors provided sufficient reflected light to permit pictures of acceptable contrast to be recorded at shot time by all cameras. However, a slightly denser cloud cover at shot time could have ruined the camera experiment entirely.

Such a significant change in shot time was unexpected on the

basis of DRES experience on previous trials. It should be recognized, however, that a decision to change the shot time is possible on any future trials. In view of the DICE THROW experience, the following suggestions are made to minimize the risk to the camera records in future trials:

(1) The most serious problem would arise near sunrise or sunset. Before choosing which end of the cylinder is to be photographed, information should be obtained on the predicted position of the sun at sunrise and sunset on shot day. All else being equal, the cylinder end to be photographed should be chosen according to the camera orientation which promises least interference from a rising or setting sun.

(2) In the case that back-lighting by the sun or low light intensity prove to be a problem, a contingency plan to provide sources of artificial light at each camera location should be seriously considered. Such a light source must be capable of providing light of sustained intensity for a period of approximately 200 milliseconds from the time of shock arrival at any location. Candidates for consideration would be (i) flares, (ii) flash lamps, or (iii) spotlights, possibly used in conjunction with parabolic or planar reflectors. Integrity of the light source under blast loading is an important factor to be considered. In view of the fact that the test area is cleared of personnel approximately two hours before shot time, another factor for consideration is the ability to activate the light source by remote control close to shot time.

2.4 Dust Collectors

Since it was known that dust entrained in the blast wave could significantly alter the measured drag pressure, it was felt to be important to obtain some indication of the contribution of dust loading. A series of simple passive dust collectors consisting of 7-foot high vertical aluminum channels filled with grease were located at strategic points on the layout (Figure 14). The results of this experiment are the subject of a separate report (Naylor, 1977).

The ground surrounding the Canadian projects was treated with a

sprayed-on oil-based coating approximately 1/8 inch thick. Camera records and dust collectors confirmed that the coating was highly effective in suppressing dust. The extent of the treated ground can be clearly seen in Figure 9.

Production of a relatively dust-free blast wave was desirable in order to relate experimental conditions as closely as possible to real-life conditions encountered by Navy materiel.

3. DATA ANALYSIS

3.1 General

The goal of the analysis was to obtain the aerodynamic drag coefficient as a function of time, $C_D(t)$. C_D is defined by the equation:

$$P_D(t) = C_D(t)\, q(t) \tag{1}$$

where P_D is drag pressure
C_D is drag coefficient
q is dynamic pressure

and the time-dependence of each quantity is noted explicitly.

A power series in time was fitted to the velocity-time data, v(t), and displacement-time data, x(t), as described in Sections 3.2 and 3.3. The best-fit polynomials to the velocity-time and displacement-time data are recorded in Tables 13 and 14 respectively.

Drag pressure is related to the slope of v(t) and curvature of x(t), through the relations:

$$\frac{dv(t)}{dt} = a(t), \qquad \frac{d^2x(t)}{dt^2} = a(t) \tag{2}$$

and $$P_D(t) = \frac{m}{A}\, a(t) \tag{3}$$

where x is cylinder displacement
v is cylinder velocity
a is cylinder acceleration
m is cylinder mass
A is frontal area of cylinder
t is elasped time after arrival of shock front at cylinder.

For the purposes of this experiment, dynamic pressure, q(t), was replaced in Equation (1) by the closely-related quantity impact pressure, $q_I(t)$. The derivation of $q_I(t)$ from measured free-field overpressure-time histories, and the reason for replacing q(t) with $q_I(t)$, are elaborated in Sections 3.4 and 3.5.

3.2 Velocity Transducer Data

3.2.1 Conversion from analog to digital velocity-time signal. The analog signals recorded on magnetic tape during the trial were digitized after the trial at a digitizing rate of 16 KHz using an analog-to-digital converter. Up to 100 msec of smooth baseline (unaffected by ground shock) was retained on either side of the signal. A straight line was fitted to the baseline data. After subtracting the baseline, and accurately determining the crossover point at which the transducer signal changed polarity, the second half of the transducer signal was multiplied by -2 (see Section 2.2.2). Using a digitized 1 volt reference signal of approximately 1 second duration recorded just before the transducer signal, the calibration values in ft/sec/volt (which had been measured in the laboratory at DRES prior to the trial) were applied to the digitized signal to produce a final velocity-time signal. The starting point of the signal, determined by inspection of the digitized data, was taken as zero time in the subsequent analysis. The uncertainty in this zero position is 0.25 msec. The first 3 msec of data were omitted to exclude from the fit the initial diffraction phase which can last for as long as 1.5 msec.

After establishing by visual inspection that digital smoothing of the transducer signals would not suppress any significant features in the data, a smoothing was performed by averaging each consecutive interval of 8 points. At the time that the curve fitting was performed, the interval between data points was 0.5 msec.

A method of checking the velocity calibration for each transducer is described in Appendix D and the results of this investigation are recorded in Table 11.

The characteristic transducer response time (approximately 2 msec) was not fast enough to follow the abrupt change in velocity occurring during the initial diffraction phase of shock loading on the cylinder, which lasts for about 1 millisecond. There was, therefore, little point to analyzing velocity-time data during the initial re-

covery time of the transducer. For this reason, only data from 3 msec onward were retained for analysis. No analysis of the diffraction phase of shock loading was attempted.

3.2.2 Philosophy of curve-fitting. The reasons for choosing a power series in time (polynomial regression method) to fit the velocity-time data are thoroughly discussed in Appendix E.

A least squares criterion was applied to determine the best fit to the velocity data. All data points were weighted equally. The data were fitted by a power series of increasing order up to N=6 (7 coefficients). It was necessary to have some criteria for determining which order of polynomial provided the best fit to the data.

3.2.3 Factors affecting choice of best-fit function.

(a) From the theory of least squares fitting (Appendix E, Part II), it was clear that the addition of a higher order term to the fitting function provided an extra degree of freedom and automatically ensured that a smaller root mean square deviation was obtained. However, if the improvement in the RMS deviation was small, the uncertainties in the fitting coefficients themselves actually increased because the effect of adding an extra degree of freedom more than offset the small improvement in the RMS deviation. In this case, since acceleration was a function of these coefficients, the uncertainty in acceleration (and hence drag pressure) increased as the order of the fit increased. To minimize this effect, the lowest order fit which satisfied the conditions set forth in items (b) and (c) below was chosen as the best fit.

(b) The drag pressure-time curve was derived directly from the first derivative of the curve fitted to the velocity-time data. As the order of the fitting polynomial was increased, in general the shape of the derived drag pressure-time curve changed. However, if the scatter in the velocity-time data was not too large, a point was quickly reached for which addition of the next higher order term in the fitting function did not significantly change the shape of the derived drag pressure-time

curve (i.e., fitting procedure had produced a stable first derivative). One could then claim with some confidence that adding the next higher order term produced no significant new information on the shape of the drag pressure-time curve. In other words, if a fit of order N and a fit of order N+1 produced essentially the same shape for $P_D(t)$, the fit of order N was chosen as the one which contained all of the available information on the shape of $P_D(t)$.

(c) While the overall shape of the drag pressure-time curve cannot be known with certainty, two characteristics of the curve are known, based on the shape of the dynamic pressure curve: (1) initially, the *slope is negative*; (2) *at large* times, when the dynamic pressure approaches zero asymptotically, the drag pressure approaches zero asymptotically.

When one performs a least squares fit to the velocity data with a power series, however, there are no special constraints to guarantee that the drag pressure derived from the best-fit polynomial will have these two characteristics. When the scatter in the velocity data is small, the data themselves provide sufficient constraint to ensure that the curve for drag pressure derived from the fit will have these characteristics. However, if the scatter in the velocity data is sufficiently large, the derived drag pressure may fail to exhibit either one or both of these characteristics. When this occurs, it is necessary to exercise judgment to rule out such a fit on the grounds that it is not physically reasonable. This is particularly true for cases in which the derived drag pressure drops to zero and becomes negative before the end of the fitting region is reached.

Since one is relying entirely upon the data themselves to constrain the fitting function to have the proper behaviour at late times, it would seem to be important for the transducer time record to extend up to the point where the slope of the velocity-time curve is approximately zero (i.e., where the dynamic pressure is negligible compared to its initial value). While this was the case for all of the

transducer data collected in Event DICE THROW (except for a couple of truncated signals caused by broken magnets, etc.), it was not always the case in previous trials, where transducers with shorter working lengths were used.

In summary, before a fitted function was accepted as an accurate description of the variation of drag pressure with time, three conditions had to be satisfied:

(1) reasonable limits on uncertainty (low order of polynomial),
(2) stable first derivative, and
(3) correct physical behaviour at early times (when dynamic pressure is large) and at later times (when drag pressure is decreasing to zero asymptotically).

If the fitting function failed to meet these criteria for a particular data set, then all high order fits were rejected as unsuitable and a linear fit to drag pressure was chosen as the best-fit function. Since the dynamic pressure curve is non-linear, it is clear (Equation 1) that a linear fit cannot, in general, represent the detailed shape of $P_D(t)$. It is, however, useful in showing the trend of $P_D(t)$ and can be considered as a coarse averaging function. For data sets which fit $P_D(t)$ with a linear function, it should be noted that the detailed shape of the derived $C_D(t)$ curve is not significant. Only C_D values averaged over 25 msec intervals were accepted as meaningful in these cases.

3.2.4 Effect of non-random fluctuations in velocity-time data. As was the case in all previous trials, non-random fluctuations were evident in all transducer signals. These could be subdivided into two categories: (1) pure (damped) sinusoidal oscillations; (2) irregular fluctuations.

(1) Pure Sinusoidal Oscillations. Large single-frequency oscillations were observed in the velocity-time spectra from transducers attached to cylinders 3, 4 and 5. By inspection of the corresponding camera records, it was established that they were oscillations of the solid centre shaft of the cylinder to which the transducers were attached.

The fact that the amplitudes of oscillation were larger in general than those observed in velocity-time traces from previous trials may be attributed to two factors: (1) the centre rod in this trial was continuous and of order 5 to 8 feet in length (cf. the short - approximately 1 foot long - end rods of previous trials); (2) the absolute length of rod protruding beyond the cylinder end was 14 inches for DICE THROW, compared to only 6 inches for previous trials. Each of the above factors (1) and (2) would tend to favour a higher initial displacement for the end of the centre rod relative to the cylinder axis.

An attempt was made to remove the prominent single-frequency component by performing a Fourier transform of the velocity-time spectrum, subtracting the unwanted component, and reconstructing the filtered velocity-time function by performing an inverse Fourier transform. Due to the short length of the v(t) spectrum, the presence of gaps at the beginning and in the middle of the spectrum, and the fact that the oscillation was damped, it proved impossible to apply a sufficiently precise frequency filter which would remove the oscillatory component without simultaneously distorting the shape of the main velocity-time signal.

The next approach employed was an attempt to fit the velocity-time spectrum with a function of the form:

$$v(t) = v_1(t) + v_2(t) \qquad (4)$$

where

$$v_1(t) = a_1 + a_2t + a_3t^2; \quad v_2(t) = a_4e^{-a_5t}\sin(2\pi a_6t + a_7). \qquad (5)$$

This function, which includes an explicit sinusoidal term, contained seven fitting parameters (a_1- - - - a_7). A least squares best-fit criterion was adopted, and the best-fit function was found by a parameter search method. Because the computer time consumed increases rapidly with the number of parameters using this method, it proved necessary to limit the polynomial part of the fitting function to second order in order to keep the overall number of parameters manage-

able. While it was recognized that a second order polynomial was not of sufficiently high order to describe adequately the v(t) trace, the results of this fit were still of interest because the model function attempted to take into account the damped sinusoidal oscillation. It was useful to compare the best-fit coefficients a_1, a_2, a_3 obtained using this function with the best-fit coefficients obtained by linear least squares fitting procedure using a second order power series only (described in Appendix E). The results of the two procedures are summarized in Table 12. They indicate that, at least for a second order polynomial fit to velocity, the two methods give similar answers for the polynomial describing the velocity-time curve. In fitting the velocity-time records with a polynomial of order higher than 2, the implicit assumption is made that any oscillations about the mean velocity are sufficiently rapid that they do not seriously affect the choice of best-fit polynomial. The results in Table 12 lend some credence to this assumption.

(2) Irregular Fluctations. For cylinders 2, 6 and 7, irregular fluctuations were superimposed on the sinusoidal oscillations. The fluctuations were most likely caused by friction between the moving magnet and the surrounding coil housing. This type of fluctuation is the most problematic because it is neither completely random nor periodic. It is impossible to assess accurately the uncertainty in the fitted function attributable to the irregular nature of these fluctuations. No attempt was made to do so, and in the error analysis it was assumed that the fluctuations were random. Because the fluctuations are rapid compared to the slope of the v(t) curve, this is not a bad assumption. There is no *a priori* means of knowing if this is the case, however; it must be assumed.

3.3 Camera Data

3.3.1 Use of film reader. Developed films from the high-speed cameras were analyzed with the aid of a precision film reader. Timing marks projected onto the film at 10 millisecond intervals were used to establish the framing rate. A horizontal distance scale in each film frame was pro-

vided by a photomarker plate attached to the support plate nearest the camera and marked off over a 12 inch interval in alternate black-and-white 1-inch wide bands. The zero of coordinates was defined for each film frame to be the junction of the photomarker plate with the vertical back edge of the support plate.

For those cameras with 50 mm focal length lenses (Table 10), non-linearity across the field of view could be neglected. For those cameras with 13 mm lenses, a correction had to be applied. It would be an advantage in future trials to use cameras with focal lengths longer than 13 mm to minimize the importance of this correction.

The measuring position on the cylinder was defined by the junction of alternate black and white sectors painted onto the end plates. Because the end plate is 9 inches farther from the camera than the photomarker plate, a simple geometrical correction had to be applied to the measured position coordinates. It was also necessary to apply a correction to account for motion of the camera and mounting post under blast loading. This correction was necessitated by a shift in the optic axis of the camera with respect to the object being photographed. Since no cross-hairs were present on the camera lens to define the optic axis, a reference point on the edge of the film frame was used to keep track of the camera motion. The accuracy of position measurement was estimated to be ± 0.04 inches before any corrections were applied.

3.3.2 Philosophy of curve-fitting. The same considerations which governed the fitting of the velocity-time data discussed in Section 3.2 applied to the fitting of the displacement-time record from the high-speed cameras, except that one was interested in the second, rather than first, derivative, and the record was continuous. In addition, the ability to observe the cylinder end, rather than the end of the cylinder shaft, meant that the oscillations of the cylinder shaft, so prominent in the velocity transducer data, were absent in the camera data.

3.4 Free-Field Overpressure Measurements

Side-on pressure gauges mounted at ground level were used to record overpressure-time histories at strategic points on the Canadian layout. These measurements are the subject of a related Suffield Technical Paper (Winfield, 1977). Four side-on pressure gauges were located in the vicinity of the 20 psi overpressure position, six gauges in the vicinity of the 10 psi overpressure position, and four gauges in the vicinity of the 7 psi overpressure position.

Each overpressure-time curve was assumed to follow the empirical Friedlander decay formula:

$$p(t) = p_o F \qquad (6)$$

where

$$F = \left(1 - \frac{t}{t_+}\right) e^{-k\frac{t}{t_+}}$$

with p_o = peak overpressure (psi)

t_+ = duration of positive overpressure phase

k = Friedlander decay constant (empirically determined).

The positive duration, t_+, was determined by visual inspection of the digitized pressure-time records.

The overpressure impulse, I, defined by:

$$I = \int_0^{t_+} p(t)\, dt \qquad (7)$$

was obtained by numerical integration of the area under the measured pressure-time record from $t = o$ to $t = t_+$. Integration of Equation 6 from $t = o$ to $t = t_+$ leads to the equation:

$$\frac{I}{p_o t_+} = \left[\frac{1}{k} - \frac{(1 - e^{-k})}{k^2}\right] \qquad (8)$$

The function on the right is an unique function of the decay constant k only. This function was plotted and the value of k determined

graphically for each pressure gauge by calculating the ratio $\frac{I}{p_o t_+}$ using experimental values of I, p_o and t_+ determined directly from the measured pressure-time records. Once the parameters I, p_o, t_+ and k were determined for each gauge at a given nominal peak overpressure location, a best value was determined for each parameter by averaging the results from all the gauges at that peak overpressure location. The scatter in the values of the parameters about the mean value was used to provide an estimate of the uncertainty in each parameter. The results of this procedure are summarized in Table 15.

3.5 Impact Pressure Calculations

The dynamic pressure q and impact pressure q_I were assumed to decay as F^2 (Glasstone, 1957), i.e.,

$$q(t) = q_o F^2 \tag{9}$$

$$q_I(t) = q_{Io} F^2 \tag{10}$$

where the peak dynamic pressure, q_o, is determined from the Rankine-Hugoniot relations at the shock front to be (Glasstone, 1957):

$$q_o = \frac{5}{2} \frac{p_o^{\,2}}{(p_o + 7p_a)} \tag{11}$$

and the peak impact pressure is determined to be (Kinney, 1962):

$$q_{Io} = q_o + \frac{q_o^{\,2}}{2.8(p_o + p_a)} \tag{12}$$

where

p_o = peak overpressure

p_a = ambient pressure.

It has been the practice in recent years at our Establishment to define drag coefficient in terms of impact pressure, rather than dynamic pressure (see Equation 1), because drag force for compressible fluids is directly related to impact, rather than dynamic, pressure. This practice has been continued in this part of the present report. The ratios of impact pressure to dynamic pressure at the

20.1, 9.7 and 6.7 psi peak overpressure locations were 1.103, 1.039, 1.022, respectively, based on Equations 9, 10, 11 and 12.

In calculating impact pressure for a given peak overpressure location, the average values of the parameters from all of the pressure gauges at that overpressure location, as listed in Table 15, were used. To obtain an estimate of the uncertainty in impact pressure at that location, impact pressure-time curves were calculated using the values of p_o, t_+ and k determined for each gauge. At 10 msec intervals, the RMS deviation of these curves from the "average" curve was calculated. This RMS deviation, expressed as a percentage, is plotted as a function of time for each peak overpressure location in Figure 32.

The impact pressure curves used in the data analysis are plotted in Figure 31.

3.6 Calculation of Mach and Reynolds Numbers

Free stream Mach and Reynolds numbers were calculated using standard definitions. Fluid velocity was assumed to decay as:

$$u = u_o F \tag{13}$$

where

F is defined in Equation 6,

and u_o was derived in terms of p_o and p_a from the Rankine-Hugoniot relations across the shock front.

The temperature of the flow behind the shock front was approximated by the isentropic relation. The kinematic velocity was described by a power series in temperature, where the coefficients of the series were obtained by fitting a power series to values of kinematic viscosity for air at specific temperatures.

Details of these calculations are given in a previous report (Mellsen, 1974).

4. RESULTS

4.1 General

A qualitative summary of results is presented in Table 27. Cylinder 1 failed to undergo free flight and suffered severe damage due to a blast anomaly which moved up the east side of the Canadian sector. The anomaly is discussed in Section 4.10. Post-shot views of the cylinder and the east and west support plates are presented in Figures 10, 11 and 12 respectively. Figure 13 presents a post-shot view of cylinder 5, showing the lateral displacement caused by a lateral pressure component associated with the blast anomaly. Figure 14 is a post-shot view of one of the 7-foot high greasy stake dust collectors. The height of the dust cloud is indicated by the change in reflectivity of the greased surface at a height of 3 to 3.5 feet.

Figures 15 through 25 present results of fits to velocity transducer data and camera data for cylinders 2 through 7 (except for cylinder 2 where only transducer data are available). Figures 26 through 30 and Tables 16 through 26 present derived drag pressures and drag coefficients for cylinders 3 through 7 from both camera and transducer data. A qualitative summary of results for each cylinder, with qualifying remarks, is presented in Table 27. A summary of best values for the measured drag coefficients is presented in Table 28.

4.2 Velocity Transducer Data

The data from east and west ends on a given cylinder were analyzed separately. The best-fit curve is drawn through the velocity-time data as a solid line. The dotted lines in the figures represent ± one root mean square (RMS) deviation in the scatter of data about the best-fit curve. It was assumed for purposes of error analysis, and in the absence of better information, that the RMS deviation had a constant value at all points on the curve. The acceleration curve is the first derivative of the best-fit velocity function. The dotted lines on the acceleration-, drag pressure-, and drag coefficient-time curves, however,

represent ± three standard deviations (99% confidence interval).

Power series with terms up to the fourth power in time (5 parameters) were fitted to the velocity data for cylinders 3, 4, 6 and 7. Velocity data for cylinders 2 and 5 were fitted by power series with terms up to the second power in time (3 parameters).

4.3 High-Speed Camera Data

Cameras recorded the motion of the west cylinder ends only. In the figures, the best-fit power series curve is drawn as a solid line through the displacement-time data. Dotted lines representing ± one RMS deviation are also drawn, but are not evident on most drawings because the deviation is so small. On the velocity-, acceleration-, drag pressure-, and drag coefficient-time curves, however, the dotted lines represent ± three RMS deviations about the best-fit curve (99% confidence interval). Displacement data for cylinders 3, 4, 5 and 6 were fit by a power series with terms up to the fifth power in time (6 parameters). Displacement data for cylinder 7 were fit by a power series with terms up to the third power in time (4 parameters).

4.4 Drag Coefficient vs Reynolds Number - Before Corrections (Figure 36)

For a given record, the drag pressure-time curve was divided by the appropriate impact pressure-time curve (Figure 31) to obtain drag coefficient as a function of time, $C_D(t)$. The $C_D(t)$ curves are plotted in Figures 26 through 30 for each cylinder. Dotted lines represent ± three standard deviations of uncertainty.

In Figure 36, the resultant $C_D(t)$ curves are plotted as a function of Reynolds number for all cylinders for which the free stream Mach number is less than the critical value $M_c = 0.48$. For this Mach number range, the dependence of C_D upon Mach number is slight.

In Figure 36, data which required a linear fit to drag pressure have not been included because a linear fit was felt to provide no detailed information on the shape of the drag pressure-time curve (see Sec-

tion 3.2). The $C_D(t)$ values are presented as bands of uncertainty for three reasons:

(1) To permit a visual comparison of the relative accuracies of the velocity transducer and high-speed camera techniques.

(2) To emphasize that, for a given data record, the uncertainty in the derived drag coefficients is not constant across the record. The uncertainty is least near the middle of each record.

(3) To show the measure of agreement between drag coefficients obtained using the velocity transducer and those obtained using the high-speed camera technique.

In this figure, and in the plots of $C_D(t)$ in Figure 26 through 30, no uncertainty in the calculated impact pressure has been included. This has been done so that the ratio of drag coefficients with and without extended end plates could be formed directly to assess the importance of end effects. In such a ratio impact pressure cancels out, so the uncertainties in Figures 26 through 30 and Figure 36 are the appropriate ones to use for assessing end effects.

Included for completeness in Figure 36 is a solid curve representing drag coefficients measured in a wind tunnel under steady-state flow conditions (Delaney and Sorensen, 1953; Gowen and Perkins, 1953). The extension of the steady-state results to higher Reynolds numbers (Roshko, 1961) is represented by the dotted portion of the curve.

4.5 End Effects (Figure 37)

The flow of air over the ends of finite-length cylinders can produce a measured drag coefficient which is different from the value that would be measured for an infinitely-long cylinder. Since the main structural members of the Canadian Navy masts and antennae tested in DICE THROW either had relatively large length/diameter (L/D) ratios or were attached at either end to other members, drag coefficients for infinite-length cylinders were the appropriate input to structural response calculations for these structures.

In the present experiment, thin extended end plates were attached to the ends of some cylinders (Figures 4 and 5) to prevent air flow around the ends of the cylinders, thereby eliminating end effects.

There was, of course, a contribution to the overall drag on the cylinder due to drag on the end plates themselves. However, because the end plates had bevelled knife edges, and the air flow was expected to be nearly parallel to the faces of the end plates, the main contribution to end plate drag was skin friction drag, for which the maximum drag coefficient, according to Hoerner (1958), is 0.008. Using this value for C_D, the fractional contribution by the end plates to the overall measured cylinder drag pressure was assumed to be given by:

$$\frac{(C_D A)_{\text{end plate}}}{(C_D A)_{\text{end plate}} + (C_D A)_{\text{cylinder}}}$$

where

$A_{\text{end plate}}$ is the total exposed surface area of the two end plates

A_{cylinder} is the frontal area of the cylinder

$(C_D)_{\text{end plate}} = 0.008$

$(C_D)_{\text{cylinder}}$ = measured value from experiment.

These calculated contributions from the end plates to the measured drag coefficient (approximately 10% for cylinder 7, 7% for cylinder 5, and less than 1% for cylinder 2) were then subtracted from the measured coefficients to produce a set of corrected coefficients appropriate to infinite-length cylinders. It is these corrected coefficients which are plotted in Figure 38.

Since the experiment included pairs of identical cylinders with and without extended end plates, at the same peak overpressure locations, it was possible to measure end effects directly by forming the ratio

$$\frac{C_D \text{ (with extended end plates, corrected for end plate drag)}}{C_D \text{ (without extended end plates)}} .$$

These ratios were formed, using drag coefficients averaged over 25 msec intervals, for cylinders 6 and 7 (velocity transducer data) and cylinders 4 and 5 (camera data). The results are plotted in Figure 34 as a function of elapsed time after shock arrival.

For cylinders 6 and 7, with an L/D ratio of 17, the first two points in Figure 37 covering 50 msec of motion correspond to Reynolds numbers (9-5) x 10^5, i.e., just above the critical Reynolds number range (5-3) x 10^5. For these points, the C_D ratio lies below 1. A slight tendency for the ratio to decrease with time after shock arrival is noted. All points are consistent with the weighted average value of 0.78.

For cylinders 4 and 5, which have an L/D ratio of 5, all of the data points correspond to Reynolds numbers in the supercritical range (16-9) x 10^5. Initial values of the C_D ratio are substantially greater than 1 and are not consistent with unity within error. Moreover, the ratio increases markedly for later times. The average value for the first 50 msec of motion is 1.43 while for the second 50 msec of motion it is 1.95. The average value for the first 100 msec of motion is 1.58, but not all of the data points agree with this value within error.

Due to the failure of cylinder 1, the 18-inch diameter cylinder with extended end plates, it was not possible to measure end effects directly using cylinders 1 and 3. In view of the large end effects observed for cylinders 4 and 5 in the supercritical Reynolds number range with an L/D ratio of 5, it was felt that substantial end effects could also be expected for the 18-inch diameter cylinder 3, whose motion spanned a somewhat higher Reynolds number range and which also had an L/D ratio of 5. Since no direct information was available for cylinder 3, the average end effect factor of 1.58 measured for cylinders 4 and 5 was applied to the camera data for cylinder 3. These corrected data are plotted in Figure 38. It is notable in this Figure that, even after substantial end effect corrections, the two data points at highest Reynolds number (first 50 msec

of motion) for the 18-inch diameter cylinder lie well below steady-state values. To obtain agreement with the steady-state values, the measured drag coefficients (before end effect corrections) would have to be multiplied by an approximate factor of 2. If, instead of an average end effect factor, one employed the measured values for each 25 msec interval recorded in Figure 37, the two points at highest Reynolds numbers in Figure 38 would be depressed a further 10%, while the third point would be elevated a further 20% to lie above the steady-state value.

4.6 Dust Loading

Both the greasy dust collectors described in Section 2.4 and the high-speed camera records provided qualitative information on the amount of dust entrained in the blast wave during the cylinder motion. Both dust collectors (see 7-foot tall dust collector in Figure 14) and camera records confirmed that a significant dust cloud existed only to a height of about three feet above ground, and that relatively little dust existed at the initial cylinder height 5 to 6 feet above ground. One would expect any dust loading to increase the effective drag force on the cylinder, thereby increasing the measured drag coefficient. The insignificance of dust loading is supported by the fact that the measured drag coefficients in Figure 38 were consistent with steady-state values over most of the range of measurement. The oil-based coating sprayed onto the ground in the Canadian sector proved highly effective in suppressing dust, as evidenced by the relatively low dust levels in this trial compared to previous trials in which dust clouds were observed to rise to a height of 7 to 8 feet (Leech et al., 1973).

4.7 Drag Coefficient vs Reynolds Number - After Corrections (Figure 38)

Figure 38 is a composite semi-log plot showing measured drag coefficients for "infinitely long" smooth cylinders in unsteady flow conditions for Reynolds numbers from (3 to 40) x 10^5. For the 3.5-inch and 9.5-inch diameter cylinders, data from cylinders with extended end plates were used, after subtracting a correction for end plate drag. For the 18-inch diameter cylinder without extended end plates, the average end effect factor

of 1.58 measured for the 9.5-inch diameter cylinder was applied to the results to convert them to values appropriate to a cylinder of infinite length. The error bars on the data points in this Figure include the uncertainties in impact pressure plotted in Figure 31. As in Figure 36, the solid line represents results from wind-tunnel experiments in steady-state flow conditions (see Section 4.4). The extension by other workers of these results to higher Reynolds numbers is represented by the dashed portion of the curve.

4.8 Surface Roughness

All of the cylinders were sanded and polished, after deep scratches were filled with body-filler compound, to ensure that all surface imperfections were less than 1/1000 of the cylinder diameter and that all scratches present were in the direction of air flow over the cylinder. Under these conditions, according to Hoerner, the cylinder could be considered aerodynamically smooth and the effect of surface imperfections on the air flow would be negligible.

4.9 Drag Coefficients for Supercritical Mach Numbers - Cylinder 2

For cylinder 2 at 20.1 psi peak overpressure, the flow Mach number fell from 0.63 to 0.50 during the first 20 msec of motion, and 0.50 to 0.38 during the next 20 msec of motion. During these intervals, the Mach number was above $M_{critical} = 0.48$, so a large drag coefficient was expected. For cylinder 2, only one transducer record provided useful data and these data contained large irregular fluctuations on the main signal. It was necessary to accept a linear fit to drag pressure to obtain reasonable uncertainty limits; only average drag coefficients over 20 msec intervals were accepted as meaningful (see Section 3.2.2). The large scatter in results from pressure gauges adjacent to the cylinders at the 20 psi peak overpressure location caused a correspondingly large uncertainty in impact pressure, an uncertainty which reached 100% after only 60 msec of cylinder motion (Figure 32). The net result was that only average drag coefficients for 0-40 msec were obtained, and these had large uncertainties associated with them. The results were:

For 0-20 msec $C_D^{avge} = 0.76 \pm 0.20.$

For 20-40 msec $C_D^{avge} = 0.98 \pm 0.21.$

4.10 Blast Anomaly

High-speed camera records showed that the large end plates on cylinder 1 distorted and separated from the main body of the cylinder shortly after the cylinder left the support stand. Available evidence suggests that a blast anomaly, in the form of a surface precursor jet moving up the east side of the Canadian sector, was responsible for the failure of cylinder 1. This anomaly produced a secondary pressure wave which moved diagonally from east to west across the layout behind the main shock front. The dust-raising precursor jet could be clearly seen on overhead photographs of the charge just after detonation. The evidence for the laterally-moving pressure wave follows:

(1) Small secondary pressure peaks were observed on pressure records at the 20 and 10 psi peak overpressure locations. Correlation of the time of arrival of these secondary pulses with the gauge positions indicated that the pressure wave responsible was moving diagonally from east to west.

(2) All cylinders which translated laterally did so from east to west (Figure 13).

(3) The west support stand for cylinder 1 had been twisted toward Ground Zero and the stand had been collapsed (Figure 11). The east support stand was somewhat distorted but still upright (Figure 12). The only explanation consistent with these and other minor pieces of evidence is that the cylinder or cylinder end plates delivered a series of rapid blows to each support plate. The fact that the west support plate collapsed first suggested that it had received the first major blow from the cylinder. This conclusion in turn implied that the cylinder initially had to translate laterally from east to west. An east-west force would have been required to produce this motion.

5. DISCUSSION OF RESULTS

5.1 General

The principal information gained from the present experiment is (1) the variation of drag coefficient in the range of critical and supercritical Reynolds numbers under unsteady flow conditions of a free-field blast wave, and (2) a measurement of end effects under these same conditions for cylinders with length/diameter ratios of 5 and 17.

All of the measurements recorded in Figures 36, 37 and 38 are for Mach number less than the critical value ($M_c = 0.48$). For $M<M_c$, C_D is primarily a function of Reynolds number. For $M>M_c$, C_D depends mainly upon Mach number. As M increases through M_c, an abrupt rise in C_D from 0.3 to approximately 1.2 is observed. This is a result of the fact that, for $M = M_c$, flow becomes supersonic at some point on the cylinder. The local shock wave which forms causes a buildup in thickness of the boundary layer and a rapid movement of the separation point forward on the cylinder with an attendant rapid rise in drag coefficient.

The principal difference between measurements made in steady and unsteady flow arises from the fact that the unsteady flow is preceded by a shock front which diffracts over the cylinder, sending reflections back and forth several times across the cylinder. It is possible that passage of the shock front may "condition" the following air blast flow to produce drag coefficients which are different from those one would measure in the steady-flow conditions encountered in wind tunnel tests.

5.2 Variation of Drag Coefficient with Reynolds Number (Figure 38)

5.2.1 Cylinder with 3.5-inch diameter. The points for Reynolds number in the range 5×10^5 to 8×10^5 are in good agreement with steady-state values. The points between 3×10^5 and 5×10^5, in the critical range, fall well below steady-state values. This result might be attributable to surface roughness, which tends to move the critical Reynolds region toward lower Reynolds numbers (Hoerner, 1958). However, as discussed

in Section 4.8, precautions were taken to ensure that the cylinder surface was aerodynamically smooth, so this explanation is an unlikely one. It is more probable that the lack of agreement is caused by the simple fact that the low order power series used to fit the data is not capable of responding to the rapid change in C_D which occurs in this range of Reynolds number.

5.2.2 Cylinder with 9.5-inch diameter. Drag coefficients derived for the 9.5-inch diameter cylinder for Reynolds numbers in the range 9×10^5 to 17×10^5 are consistent with the steady-state values within error, but tend to lie somewhat higher on average.

5.2.3 Cylinder with 18.0-inch diameter. The two C_D values spanning the first 50 msec of motion ($R = 43 \times 10^5$ to 29×10^5) lie well below steady-state values. The C_D value for the 50-75 msec interval ($R = 29 \times 10^5$ to 24×10^5) is slightly larger than the steady-state value, but consistent with it within error.

It is possible that the discrepancy between steady and unsteady C_D values observed at highest Reynolds numbers is due to an inadequate end effect correction over this range of Reynolds number. However, to obtain agreement with steady-state values for all three points, it would be necessary to apply an end effect correction which decreased with time after shock arrival. This is contrary to the observed end effect variation for the 9.5-inch diameter cylinder.

If one accepts the data as presented in Figure 38, they suggest that, in the early stage of unsteady flow for Reynolds numbers of order 40×10^5, C_D is lower than the steady-state value. As time progresses, the drag coefficient increases to a value somewhat higher than, but consistent with, the steady-state value. The mechanism responsible for the increase in drag coefficient for $R > 10^6$ is not completely understood, but Roshko (1961) has pointed out the strong similarity in shape of the C_D vs R and 1/S vs R curves, where S is Strouhal number ($S = (fd)/u$ where d is cylinder diameter, u is free-stream velocity, and f is the frequency of vortex shedding at the rear of the cylinder). This similarity suggests

that drag coefficient is related to the frequency of vortex shedding. If the initial shock front conditioned the following flow pattern in such a way as to increase artificially the frequency of vortex shedding, it is likely that a decreased drag coefficient would result. One might then expect drag coefficient to increase as quasi-steady flow developed, in agreement with observations.

5.3 Comparison with Results of Other Workers

A limited number of drag coefficient measurements in unsteady flow are available. These have been carried out primarily at AWRE (U.K.) in shock tubes and by DRES in previous free-field blast trials. In several instances, drag coefficients well in excess of steady-state values were observed. In the case of past DRES results, some of this difference may be attributable to dust entrained in the free-field blast wave. Dust loading seems to have been a more serious problem in previous trials than in DICE THROW (see Section 4.6). Some work is underway at DRES to examine the problem of dust loading on circular cylinders using a mathematical model in order to provide some theoretical limits on the potential seriousness of the problem for some representative field conditions.

In the case of at least one set of results from AWRE (Bishop and Rowe, 1967), the high measured drag coefficient of 0.67 for $M<M_c$ may be attributable to the fact that, early in the flow history, the flow Mach number M was $>M_c$. The authors suggest that the drag coefficient measured for $M<M_c$ may depend upon "conditioning" of the flow while $M>M_c$. This contention that, in unsteady flow conditions, the measured drag coefficient may depend upon the history of the flow is carried forward in other work at AWRE by Martin, Mead and Uppard (1967). In this work the authors show, from shadowgraph records during the shock diffraction phase, that the boundary layer separation point has been moved well forward on the cylinder, and they argue that, because it is unlikely to re-attach downstream during the subsequent flow, an abnormally high drag coefficient is expected (in agreement with observations).

The present data are notable because they are consistent with steady-state values over a wide range of Reynolds number. The data for the 18-inch diameter cylinder are new. Until now, no known unsteady flow measurements existed at such high Reynolds number and low Mach number ($M<M_c$ at all times). Dryden and Hill (1930) measured C_D for a 12-foot diameter, 120 foot long smoke stack (L/D = 10) in a natural wind of about 25-40 mph, which corresponds to Reynolds numbers of 30×10^5 to 50×10^5. These measurements were, however, for extremely low Mach numbers, and were not made in a decaying blast wave which was preceded by a shock front.

5.4 End Effects (Figure 37)

It has been shown from shadowgraph records (Martin, Mead and Uppard, 1967) that it can take as long as 10 msec for quasi-steady flow to develop over the cylinders after passage of the shock wave. It is somewhat surprising, however, to find that the ratio of C_D's for infinite/finite length cylinders is strongly varying as late as 75 msec into the motion (Figure 37). Before any conclusions can be drawn, it will be necessary to re-analyze the data to ensure that the observed strong variation in C_D ratio for the 9.5-inch diameter cylinders is not simply an artifact of the data analysis. The average value of the ratio over 100 msec of motion, 1.58, is quite close to the value of 1.67 measured by Dryden and Hill (see Section 5.3) for very low Mach numbers and R in the range 30×10^5 to 50×10^5. The Reynolds number range covered in Dryden and Hill's experiment brackets the range covered by our 18-inch diameter cylinder ($R = 24 \times 10^5$ to 43×10^5). Their measured end effect was 1.67. The fact that this value is close to our average end effect factor of 1.58 (measured on the 9.5-inch diameter cylinder) lends support to the decision to apply the factor of 1.58 to the results for the 18-inch diameter cylinder.

The results for the 3.5-inch diameter cylinder are consistent with a C_D ratio of unity for Reynolds numbers just above the critical region. This ratio appears to drop below unity by as much as 25% as the

critical Reynolds region is entered. The indicated decrease in C_D ratio may not be significant, however, because it is likely that the low-order power series fit to the data is inadequate for modelling the rapid change in C_D which probably occurs in this region.

The number of end effect measurements in unsteady flow conditions is limited. A comparison with present results is made difficult, if not impossible, by the fact that some of the previous results are contradictory, and in most cases no estimates of the uncertainties in the quoted values have been reported. For these reasons, no detailed comparison of end effect results has been attempted.

5.5 Results for Supercritical Mach Numbers - Cylinder 2

The initial C_D value of 0.76 ± 0.20 measured for cylinder 2 is more consistent with the steady-state results for a finite-length cylinder, with L/D ratio of 17 (C_D = 0.9), than for an infinite-length cylinder (C_D = 1.3, Gowen and Perkins, 1953). Examination of the velocity-time curve in Figure 15 indicates that the initial acceleration values obtained from the fitted curve may well be too low. A more reliable determination of acceleration is not possible, however, given the large fluctuations which are present in the velocity-time data.

6. CONCLUSIONS

1. Aerodynamic drag coefficients measured for "infinite-length" aerodynamically smooth cylinders under unsteady flow conditions in a long-duration (160-300 msec) free-field blast wave were in generally good agreement with steady-state values for Reynolds numbers in the range 5×10^5 to 16×10^5 and Mach numbers <0.48. In the critical Reynolds number range 3×10^5 to 5×10^5, the measured drag coefficients lay well below the steady-state values, but this was felt to be due to the inability of the power series fitting function to respond to the very rapid changes in drag coefficient expected in this region. In the Reynolds number range 30×10^5 to 40×10^5, measured unsteady flow drag coefficients were approximately 30% lower than steady-state values. Further experiments would be necessary to establish whether this difference is due to an inadequate correction for end effects or to a real physical effect associated with the diffraction of the shock front across the cylinder.

2. Measurement of drag coefficients for identical cylinders with and without extended end plates permitted the direct measurement of end effects for finite-length cylinders by forming the ratio C_D(infinite)/ C_D(finite). For the cylinders with a length/diameter (L/D) ratio of 5, an average C_D ratio of 1.6 was observed over a Reynolds number range of 9×10^5 to 16×10^5 (M<0.48). For the cylinder with L/D of 17, an average C_D ratio of 0.8 was observed for Reynolds numbers in the range of 3×10^5 to 8×10^5. The ratio was observed to decrease as Reynolds number dropped from the supercritical to critical range. Further data analysis and experimentation are required to confirm the strong increase in end effect ratio with time after shock arrival which was observed for the cylinder with an L/D ratio of 5.

3. Greasy stake dust collectors and high-speed camera records confirmed that the oil-based coating sprayed onto the ground in the Canadian sector proved highly effective in suppressing dust. It is probable that the dust loading on the cylinders was negligible during the first

100-150 msec of motion over which measurements were taken.

4. Cylinder 1 at the 20.1 psi peak overpressure location failed due to the influence of a ground precursor type of blast anomaly which moved up the east side of the Canadian sector and produced a secondary pressure wave travelling diagonally from east to west across the Canadian layout.

7. REFERENCES

Bishop, V.J. and Rowe, R.D. 1967. The interaction of a long duration Friedlander shaped blast wave with an infinitely long right circular cylinder. AWRE Report No. 0-38/67. UNCLASSIFIED.

Coffey, C.G. 1971. Blast response of TACAN mast - Event DIAL PACK (U). Suffield Memorandum No. 13/71. UNCLASSIFIED.

Coffey, C.G. and Price, G.V. 1977. Blast response of UHF polemast antenna - Event DICE THROW (U). Suffield Technical Paper No. 449. UNCLASSIFIED.

Delany, N.K. and Sorensen, N.E. 1953. Low-speed drag of cylinders of various shapes. NACA Tech. Note No. 3038.

Dewey, J.M. 1964. The air velocity in blast waves from TNT explosions. Proc. Roy. Soc. A279, 366-385.

Dryden, H.L. and Hill, G.C. 1930. Wind pressure on circular cylinders and chimneys. Bureau of Standards Journal of Research, Washington 5, 653.

Glasstone, S. (Editor). 1957. The effects of nuclear weapons. Handbook prepared by U.S. Department of Defence, published by U.S. Atomic Energy Commission.

Gowen, F.E. and Perkins, E.W. 1953. Drag of circular cylinders for a wide range of Reynolds numbers and Mach numbers. NACA Tech. Note 2960.

Hoerner, S.F. 1958. Fluid-dynamic drag. Published by the author.

Kinney, G.F. 1962. Explosive shocks in air. Published by McMillan Company (New York).

Laidlaw, B.G. 1978. Blast response of lattice mast - Event DICE THROW (U). Suffield Technical Paper No. 452. UNCLASSIFIED.

Leech, J. (Maj, USAF), Lieberman, P., O'Neill, J.P., Gibbs, A.H., Pollack, S.A. 1973. Dynamic dust measurements - MIDDLE NORTH Series, MIXED COMPANY Event. TRW Systems Group.

Long, B.R. and Laidlaw, B.G. 1973. Shipboard lattice antenna masts under blast loading. Part II. Comparisons of experimental results with theoretical predictions by computer programs (U). Suffield Technical Paper No. 418. UNCLASSIFIED.

Long, B.R., Laidlaw, B.G. and Smith, R.J. 1975. The analysis of shipboard lattice antenna masts under air blast and underwater shock loading. Part III. Final report (U). Suffield Technical Paper No. 431. UNCLASSIFIED.

REFERENCES (Cont'd)

Martin, V.C., Mead, K.F. and Uppard, J.E. 1965. Blast loading on a right circular cylinder. AWRE Report No. 0-93/65. UNCLASSIFIED.

Martin, V.C., Mead, K.F. and Uppard, J.E. 1967. The drag on a circular cylinder in a shock wave. AWRE Report No. 0-34/67. UNCLASSIFIED.

Mathews, J. and Walker, R.L. 1965. Mathematical methods of physics. Published by W.A. Benjamin, Inc. (New York).

Mellsen, S.B. 1969a. Drag measurement on cylinders by the free-flight method - Operation PRAIRIE FLAT (U). Suffield Technical Note No. 249. UNCLASSIFIED.

Mellsen, S.B. 1969b. Correlation of drag measurements in Operation PRAIRIE FLAT with known steady flow values (U). Suffield Memorandum No. 12/69. UNCLASSIFIED.

Mellsen, S.B. 1971. Measurement of drag on cylinders by the free-flight method - Event DIAL PACK (U). Suffield Technical Paper No. 382. UNCLASSIFIED.

Mellsen, S.B. 1974. Measurement of drag on cylinders by the free-flight method - Event MIXED COMPANY (U). Suffield Technical Paper No. 419. UNCLASSIFIED.

Mellsen, S.B. and Naylor, R. 1969. Aerodynamic drag measurements and flow studies on a circular cylinder in a shock tube (U). Suffield Memorandum No. 7/69. UNCLASSIFIED.

Naylor, R. (In draft) Dust measurements in Event DICE THROW (U). Suffield Technical Note No. 398. UNCLASSIFIED.

Naylor, R. and Mellsen, S.B. 1973. Unsteady drag from free-field blast waves (U). Suffield Memorandum No. 42/71. UNCLASSIFIED.

Owczarek, J.A. 1968. Introduction to Fluid Mechanics. International Textbook Company.

Price, G.V. 1976. Private communication.

Price, G.V. and Coffey, C.G. 1977. Blast response of 35 ft. fibreglass whip antenna - Event DICE THROW (U). Suffield Technical Paper No. 448. UNCLASSIFIED.

Roark, R.J. 1954. Formulas for Stress and Strain. Third Edition. McGraw-Hill.

REFERENCES (Cont'd)

Roshko, A. 1961. Experiments on the flow past a circular cylinder at very high Reynolds number. J. Fl. Mech. 10, 345-356.

Welsh, C.J. 1953. The drag of finite-length cylinders determined from flight tests at high Reynolds numbers for a Mach number range from 0.5 to 1.3. NACA Tech. Note No. 2941.

Winfield, F.H. 1977. Event DICE THROW - Canadian air blast measurements (U). Suffield Technical Paper No. 451. UNCLASSIFIED.

Wolkovitch, J. 1968. Literature survey - Blast loads on cylinders and flat plate antenna components. Mechanics Research Incorporated MRI-C0255-TR1. UNCLASSIFIED.

APPENDIX A

STATEMENT OF REQUIREMENT

The original Canadian Forces request for further drag cylinder measurements in Event DICE THROW came from the Director of Maritime Facilities and Resources. The essence of the request is reproduced below (points 3 and 4 of the above reference):

> 3. "It is recommended that drag cylinders with approximately 3 inch, 18 inch and 24 inch diameters be tested each at two blast overpressures. The blast overpressures will be in the order of 10 psi but will become finalized through model mast considerations."
>
> 4. "The 18 inch and 24 inch diameter circular cylinders will provide an almost complete spectrum of drag loadings on cylinders. In addition, these cylinders should provide some guidelines for future designs of large pole-type masts. The 3 inch diameter cylinders will provide experimental results for useful correlation to actual members of the model masts."

After reviewing the current state of our knowledge of drag forces on cylinders and the limitations of the free-flight cylinder method we concluded that the original request for both 18 inch and 24 inch diameter cylinders is impractical at the higher diameter and is considered not desirable in light of the following arguments:

(i) The 18 inch cylinder stretches the technical limitations of our method, and the 24 inch cylinder even more so. Our 18 inch cylinders are 7.5 feet long, weigh 200 pounds and need to be centred 6 feet off the ground to avoid flow restrictions between the ground and the cylinder. The 24 inch cylinders would have to be 10 foot long, 350 pound objects centred 8 feet off the ground. There are problems fabricating a cylinder of that size to be both strong and yet as light in weight as 350 pounds. The expected motion of both these cylinders is beyond the recording limits of our velocity transducers, and is getting beyond the reasonable camera range when dust interference with the photography is taken into account.

(ii) In present thinking, there are no actual mast structures built or currently under consideration which go beyond 20 inch diameter. The largest diameter target in the past has been the TACAN mast, which had an O.D. of 20 inches in DIAL PACK and 17 inches in MIXED COMPANY. For the latter test, the measured strains were low, so that larger diameter designs in the future are not likely.

(iii) The 24 inch diameter is only 33% larger than the 18 inch diameter, and for the region of flow Mach numbers and Reynolds numbers that apply to both of them, we have a high degree of confidence in extrapolating the drag coefficient values. In fact, the one wind tunnel result published in this area shows very little change in the C_D value for the flow region of interest.

(iv) From the review of previous DRES work, we feel that the problem of end effects, and possible corrections to all previous DRES drag coefficients of about 30%, are more important to study this time than the 24 inch diameter cylinder.

The experiment chosen instead is described in the body of the text.

APPENDIX B

CYLINDER MOTION ESTIMATES

The motion of each cylinder has been estimated in the manner described below. From the review of Section 2, values of C_D were estimated as follows: for cylinders #5 and #7, with end plates, at 10 psi the value of $C_D = 0.5$ was assumed; for cylinders #3, #4 and #6, at 10 psi with no end plates, the constant value of $C_D = 0.6$ was chosen; for cylinders #1 and #2 with end plates at 20 psi the value of C_D was chosen to be 1.3 for the first 20 ms ($M>M_{c1}$), 0.7 for the next 20 ms ($M \approx M_{c1}$) and 0.5 thereafter ($M<M_{c1}$). These values are all about 20% larger than actually expected, giving a conservative estimate for the motion. The diffraction phase of the motion is then estimated using the results of Long et al. (1975) for the impulse, I_o, received during diffraction. Their result is re-expressed as:

$$I_o(\text{psi-ms}) = 3.3(p_o t_T(\text{psi-ms}))^{1.13} \qquad \begin{cases} p_o = \text{peak overpressure (psi)} \\ t_T = \text{transit time (ms)} \end{cases}$$

This was used as given for the 3.5 in. diameter cylinders but the estimate was halved for the 9.5 in. and 18 in. diameters, as it is known that the two points which lie appreciably below the I_o curve of Long et al. (1975) are from larger (12 in. diameter) cylinders. The motion following the diffraction phase was calculated using the equation:

$$F = ma = C_D\, A(144)q$$

where F is the drag force in lb_F, m is the cylinder mass in slugs, a the acceleration in ft/s^2, C_D the dimensionless drag coefficient, A the projected cylinder area (length x diameter) in ft^2, and q the dynamic pressure in psi. The constant 144 converts the dynamic pressure to lb_F/ft^2. The motion was calculated using a four-step integration process over steps covering 20 ms time intervals using the q values presented in Table 6, taken from published DRES reports. The simple four-step integration is able to predict the actual motion of cylinders previously tested to within about 20%. The calculated cylinder motions are given in Table 7.

Also presented there is the estimate of end plate drag for each cylinder. The end plate drag is calculated for both the inner and the outer surfaces of each end plate. As the air flow is essentially tangential to the end plate surface the drag force is frictional in nature and not "form" drag as for the cylinder.

Since the air density and particle speed vary in the same fashion for both the cylinder and the plate, the ratio of end plate drag to cylinder drag must be equal to $[C_D(\text{plate})A(\text{plate})]/[C_D(\text{cyl.})A(\text{cyl.})]$. For the frictional plate drag, assuming the worst case of turbulent flow, the C_D values from Hoerner (1958, Ch. 2, Fig. 5) are ≤ 0.008. Taking flow compressibility into account yields about the same value of C_D (Hoerner, 1958, Ch. 15, Fig. 13). The laminar flow C_D values are appreciably lower. The resulting estimates for end plate drag, presented in Table 7, show that in the worst case the additional drag force is only 8.9% of the cylinder drag force. In view of the need for end plates, this is a reasonable compromise, and the additional force can be estimated and subtracted.

APPENDIX C

BLAST-RESISTANT CYLINDER DESIGN

Most of the cylinders consist of hollow tubing with reinforcing discs and a welded centre rod. This design is a compromise between the light weight required for the desired flight path and the necessary strength to resist collapse during the diffraction phase loading. The maximum loading pressure on the one side of the cylinder is estimated in Table 8 as the diffraction phase impulse divided by two transit times. The maximum acceleration and pressure during the pressure drag phase is also tabulated for comparison; it is the average value estimated over the first 20 ms of the motion.

As it is difficult to estimate the one-sided pressure for collapse of a cylinder, the design estimates were made in another way. First, the uniform external pressure required for elastic buckling of the cylinder was calculated (see below), assuming a cylinder held circular in cross-section at equally spaced intervals of length ℓ. Then the design safety factor was calculated as the ratio (uniform pressure for elastic buckling)/(maximum diffraction pressure). The safety factor should be considered in light of the following points: (i) it does not take into account the extra rigidity introduced by the welded centre rod; (ii) it does not take into account the extra tendency to buckle due to the one-sided loading and to the effects of dynamic loading.

The formula for the pressure for external collapse is taken from Roark (1954, Table XVI, Formula Q, p. 318) as:

$$p' = 0.81 \frac{Et^2}{\ell r} \sqrt[4]{\left(\frac{1}{1-\nu^2}\right)^3 \frac{t^2}{r^2}}$$

where p' = uniform external pressure for elastic collapse (psi),

E = modulus of elasticity = 10^7 psi, - Values quoted for Al taken from Roark, 1954

ν = Poisson's ratio = 0.36 for aluminum,

ℓ = support disc spacing (in.)

t = wall thickness (in.)

and r = cylinder body radius (in.).

Note that $p' \propto \frac{t^2}{\ell r} \sqrt{\frac{t}{r}}$ so that wall thickness is the main variable useful for altering strength once the cylinder radius is chosen. In fact, the values of t used in the design, and presented in Table 8, were derived from this calculation.

APPENDIX D

TEST OF VELOCITY CALIBRATION

The velocity transducers were calibrated in the laboratory prior to the field trial using an electro-mechanical method. Since the circuit parameters varied slightly in the field from those used in the laboratory, the actual velocity calibration may have been in error by more than the 5% uncertainty allowed in the data analysis. A check on the accuracy of the calibration is provided by the following arguments.

Two positions of the magnet within the transducer coil are well-defined:

(a) the starting position, measured at setup time in the field to an accuracy of ± 1/16 inch;

(b) the position at which the transducer signal changes polarity (crossover point) determined to an accuracy of ± 1/16 inch in the laboratory.

Let the travel distance (b) - (a) be denoted by X_o. If the time from the start of the transducer signal to the crossover point is denoted by T, then:

$$\int_0^T v(t)dt = X_o \tag{1}$$

The quantity on the left can be determined entirely from the velocity-time transducer signal. T is determined directly to an accuracy of ± 0.25 msec by inspection of the digitized signal. The function v(t) is the best-fit polynomial curve fitted to the calibrated transducer signal, using the calibration value determined in the laboratory. If the calibration value is correct, the integral on the left-hand side should equal the independently-determined X_o on the right-hand side within the error of measurement. In Table 11, the values of:

$\int_0^T v(t)dt$, and X_o for each transducer are listed, as well as the percent difference expressed as a fraction of X_o.

PART II - THEORY OF LEAST SQUARES (Mathews 1965)

Consider a set of N experimental data points $\{y_i\}$ and a fitting function f with the corresponding set of N values $\{f_i\}$. The least squares fit criterion requires minimization of the function:

$$\sum_{i=1}^{N} \frac{(y_i - f_i)^2}{2\sigma_i^2} \tag{1}$$

where σ_i is the standard uncertainty in the i'th data point y_i. If f is a function of n parameters, a_1---a_n,

$$f = f(a_1 \text{---} a_n),$$

then the minimum in (1) is found by taking the partial derivative of (1) with respect to each of the n parameters.

$$\sum_{i=1}^{N} \frac{(y_i - f_i)}{\sigma_i^2} \frac{\partial f_i}{\partial a_m} = 0. \quad m = 1, 2, \text{---} n . \tag{2}$$

(i) Linear Least Squares Fit

The solution of the equations (2) can be cast into a convenient form if the f_i are linear functions of the parameters a_j; that is, if:

$$f_i = \sum_{m=1}^{n} C_{im} a_m \tag{3}$$

with known coefficients C_{im}. Conditions (2) can then be rewritten as:

$$\sum_i \frac{C_{im}}{\sigma_i^2} y_i = \sum_i \sum_\ell \frac{C_{im} C_{i\ell}}{\sigma_i^2} a_\ell \quad . \quad m=1, 2, \text{---} n \tag{4}$$

It is now useful to define a "data vector" Y and a "measurement matrix" M with components as follows:

$$Y_m = \sum_{i=1}^{N} \frac{C_{im}}{\sigma_i^2} Y_i \tag{5}$$

$$M_{m\ell} = \sum_{i=1}^{N} \frac{C_{im}\, C_{i\ell}}{\sigma_i^{\,2}} = M_{\ell m} \quad . \tag{6}$$

Note that Y depends upon the experimental results y_i and the errors σ_i whereas M depends only upon the errors σ_i. M is symmetric. (4) can then be rewritten as the matrix equation:

$$Y = Ma \tag{7}$$

with the solution:

$$a = M^{-1}\, Y \quad . \tag{8}$$

Note that the vector a is a unique solution for a given set of data $\{y_i\}$, errors $\{\sigma_i\}$, and given functional form (as determined by the coefficients $\{C_{i\ell}\}$). The only stipulation was that the fitting function should be linear in the coefficients a_ℓ.

(ii) Uncertainties in Parameters

To find the uncertainties in the parameters, it is necessary to calculate the expected mean-square deviations $<(a_m - \bar{a}_m)^2>$ or, more generally,

$$<(a_m - \bar{a}_m)(a_\ell - \bar{a}_\ell)> \tag{9}$$

where $\bar{a}_m$ is a theoretical quantity corresponding to a grand average value of a_m over a very large number of (theoretically-performed) identical experiments.

From (8) and (5), we have:

$$(a_m - \bar{a}_m) = \sum_k (M^{-1})_{mk}\, (Y_k - \bar{Y}_k)$$

$$= \sum_{kj} (M^{-1})_{mk} \frac{C_{jk}}{\sigma_j^{\,2}} (y_j - \bar{y}_j) \quad . \tag{10}$$

Furthermore,

$$<(y_j - \bar{y}_j)(y_i - \bar{y}_i)> = \sigma_i^{\,2}\, \delta_{ij} \tag{11}$$

APPENDIX E

PHILOSOPHY OF CURVE-FITTING TO VELOCITY-TIME DATA

PART I - CHOICE OF METHOD

The ultimate goal of the velocity-time measurement is to obtain the aerodynamic drag coefficient as a function of time, $C_D(t)$. *A priori*, one cannot claim a knowledge of the detailed shape of $C_D(t)$. Drag pressure is defined as the product of drag coefficient C_D and dynamic pressure q. The dynamic pressure q(t) has a shape that is well-defined: it is a monotonically decreasing function of time whose slope is always negative but decreases effectively to zero for large times.

Drag pressure is related to the slope of the velocity-time curve through the relations:

$$\frac{d_v}{d_t} = q \quad \text{and} \quad P_D = \frac{m}{A} a$$

where v is cylinder velocity

a is cylinder acceleration

m is cylinder mass

A is cylinder frontal area.

Since drag pressure, P_D, is defined to be the product of C_D and q:

$$P_D(t) = C_D(t)\ q(t).$$

$P_D(t)$ can assume a variety of shapes depending upon the shape of $C_D(t)$. The objective of fitting a curve to the velocity-time data is to derive the main features of the drag pressure-time curve, $P_D(t)$, without a detailed fore-knowledge of the true shape of this function.

To fit the velocity-time data, a polynomial function consisting of a power series in time was chosen primarily for three reasons:

(1) If $v(t) = \sum_{n=0}^{N} a_n t^n$, then the acceleration is very simply given by:

$$a(t) = \sum_{n=1}^{N} n\, a_n\, t^{n-1} \quad .$$

(2) Because the power series is linear in the coefficients (a_o, ---, a_N), a linear least squares criterion can be used to determine the best-fit function. This theory has the advantage that it provides a unique answer for the best-fit function for a given order of polynomial. A further advantage lies in the fact that the theory provides a straightforward prescription for the statistical uncertainties in the coefficients (a_o,---, a_n). This in turn permits a simple expression for the uncertainty in acceleration to be derived in terms of the uncertainties in these coefficients. The uncertainty in a(t) for any time t is an important quantity because it translates directly into an uncertainty in $C_D(t)$. The uncertainty in $C_D(t)$ is a measure of the confidence which one can place in the measured drag coefficient and is important for that reason.

(3) Available evidence on the expected shape of $C_D(t)$, and on the known shape of q(t), dynamic pressure, suggests that, for the Mach and Reynolds number ranges studied in this experiment, the variation of $P_D(t)$ is sufficiently smooth to be well-described by a low order power series in time.

A least squares criterion was applied to determine the best fit to the velocity data. All data points were weighted equally.

PART II - THEORY OF LEAST SQUARES (Mathews 1965)

Consider a set of N experimental data points $\{y_i\}$ and a fitting function f with the corresponding set of N values $\{f_i\}$. The least squares fit criterion requires minimization of the function:

$$\sum_{i=1}^{N} \frac{(y_i - f_i)^2}{2\sigma_i^2} \qquad (1)$$

where σ_i is the standard uncertainty in the i'th data point y_i. If f is a function of n parameters, a_1---a_n,

$$f = f(a_1\text{---}a_n),$$

then the minimum in (1) is found by taking the partial derivative of (1) with respect to each of the n parameters.

$$\sum_{i=1}^{N} \frac{(y_i - f_i)}{\sigma_i^2} \frac{\partial f_i}{\partial a_m} = 0. \quad m = 1, 2, \text{---} n . \qquad (2)$$

(i) Linear Least Squares Fit

The solution of the equations (2) can be cast into a convenient form if the f_i are linear functions of the parameters a_j; that is, if:

$$f_i = \sum_{m=1}^{n} C_{im}\, a_m \qquad (3)$$

with known coefficients C_{im}. Conditions (2) can then be rewritten as:

$$\sum_i \frac{C_{im}}{\sigma_i^2} y_i = \sum_i \sum_\ell \frac{C_{im} C_{i\ell}}{\sigma_i^2} a_\ell \quad . \quad m=1, 2, \text{---} n \qquad (4)$$

It is now useful to define a "data vector" Y and a "measurement matrix" M with components as follows:

$$Y_m = \sum_{i=1}^{N} \frac{C_{im}}{\sigma_i^2} Y_i \qquad (5)$$

$$M_{m\ell} = \sum_{i=1}^{N} \frac{C_{im}\, C_{i\ell}}{\sigma_i^2} = M_{\ell m} \quad . \tag{6}$$

Note that Y depends upon the experimental results y_i and the errors σ_i whereas M depends only upon the errors σ_i. M is symmetric. (4) can then be rewritten as the matrix equation:

$$Y = Ma \tag{7}$$

with the solution:

$$a = M^{-1}\, Y \quad . \tag{8}$$

Note that the vector a is a unique solution for a given set of data $\{y_i\}$, errors $\{\sigma_i\}$, and given functional form (as determined by the coefficients $\{C_{i\ell}\}$). The only stipulation was that the fitting function should be linear in the coefficients a_ℓ.

(ii) Uncertainties in Parameters

To find the uncertainties in the parameters, it is necessary to calculate the expected mean-square deviations $\langle(a_m - \bar{a}_m)^2\rangle$ or, more generally,

$$\langle(a_m - \bar{a}_m)(a_\ell - \bar{a}_\ell)\rangle \tag{9}$$

where $\bar{a}_m$ is a theoretical quantity corresponding to a grand average value of a_m over a very large number of (theoretically-performed) identical experiments.

From (8) and (5), we have:

$$(a_m - \bar{a}_m) = \sum_k (M^{-1})_{mk}\, (Y_k - \bar{Y}_k)$$

$$= \sum_{kj} (M^{-1})_{mk}\, \frac{C_{jk}}{\sigma_j^2}\, (y_j - \bar{y}_j) \quad . \tag{10}$$

Furthermore,

$$\langle(y_j - \bar{y}_j)(y_i - \bar{y}_i)\rangle = \sigma_i^2\, \delta_{ij} \tag{11}$$

where $\delta_{ij} = 1 \qquad i = j$

$= 0 \qquad i \neq j$

if the individual measurements y_i are assumed to be statistically independent. Then:

$$<(a_m - \bar{a}_m)(a_\ell - \bar{a}_\ell)> = \sum_{kj,p,i} (M^{-1})_{mk} \frac{C_{jk}}{\sigma_j^2} (M^{-1})_{\ell p} \frac{C_{ip}}{\sigma_i^2} \sigma_i \delta_{ij}$$

$$= \sum_{kp} (M^{-1})_{mk} (M^{-1})_{\ell p} \; M_{pk}$$

$$= (M^{-1})_{m\ell} . \qquad (12)$$

The standard error in a_m is given by:

$$\Delta a_m = <(a_m - \bar{a}_m)^2> = \sqrt{(M^{-1})_{mm}} . \qquad (13)$$

In general, the cross terms $<(a_m - \bar{a}_m)(a_\ell - \bar{a}_\ell)>$ with $\ell \neq m$ are not zero. This means that parameters a_m are not statistically independent and their errors are correlated.

(iii) Uncertainty in Quantity Which is a Function of the Parameters

Consider a quantity f which is a function of the vector $\underline{a}$

$$f = f(\underline{a}) \qquad (14)$$

$$\delta f(\underline{a}) = \sum_{k=1}^{N} \left(\frac{\partial f}{\partial a_k}\right) \delta a_k$$

and

$$(\delta f)^2 = \sum_{k=1}^{N} \left(\frac{\partial f}{\partial a_k}\right)^2 \delta^2 a_k + \sum_{i=1}^{N} \sum_{j=1}^{N} \left(\frac{\partial f}{\partial a_i}\right)\left(\frac{\partial f}{\partial a_j}\right) \delta a_i \; \delta a_j . \qquad (15)$$

Then $$(\sigma f)^2 = \sum_{k=1}^{N} \left(\frac{\partial f}{\partial a_k}\right)^2 <\delta^2 a_k> + \sum_{i=1}^{N} \sum_{j=1}^{N} \left(\frac{\partial f}{\partial a_i}\right)\left(\frac{\partial f}{\partial a_j}\right) <\delta a_i \delta a_j> . \qquad (16)$$

From (12), we know that:

$$\langle \delta^2 a_k \rangle = (M^{-1})_{kk} \qquad (17)$$

and $\langle \delta a_i a_j \rangle = (M^{-1})_{ij}$.

$$\text{Thus } (\sigma f)^2 = \sum_{k=1}^{N} \left(\frac{\partial f}{\partial a_k}\right) (M^{-1})_{kk} + \sum_{i=1}^{N} \sum_{j=1}^{N} \left(\frac{\partial f}{\partial a_i}\right)\left(\frac{\partial f}{\partial a_j}\right) (M^{-1})_{ij}. \qquad (18)$$

In general, the parameters a_m are not statistically independent, and the cross-correlation terms $(M^{-1})_{ij}$ are not zero.

(iv) Application to Fitting of Velocity-Time Data

The functional form of the velocity-time trace was chosen to be a power series in time:

$$v(t) = a_1 + a_2 t + a_3 t^2 + --- + a_n t^{n-1} .$$

This function is linear in the parameters (a_1---a_n) and can be re-written in the form (3), for a particular time, t_i:

$$v(t_i) = \sum_{m=1}^{n} C_{im} a_m$$

where

$$\begin{aligned} C_{i1} &= 1 \\ C_{i2} &= t_i \\ C_{i3} &= t_i^{\,2} \\ &\vdots \\ C_{in} &= t_i^{n-1} . \end{aligned}$$

The theory developed in (i), (ii) and (iii) above can then be applied. The experimental data points v_i consist of a set of velocities $\{v_i\}$ measured at particular times $\{t_i\}$. Because the uncertainties σ_i in these data points are not known *a priori*, it was felt that the fairest way to treat the data was to assume that the uncertainty was the same for all data points. It can then be shown that the best-fit parameters are independent of the particular value of σ. Once the best-fit curve was determined, the root-mean square deviation of the

data points about the best-fit curve was taken as the best estimate of σ.

From the fit to the velocity-time curve, one is interested in the first derivative, given by:

$$v' = a_2 + 2a_3t + 3a_4t^2 + \cdots + (n-1)a_nt^{n-2} .$$

The partial derivatives required in section (iii) to estimate the uncertainty in v' for various times t are given by:

$$\frac{\partial v'}{\partial a_2} = 1$$

$$\frac{\partial v'}{\partial a_3} = 2t$$

$$\vdots$$

$$\frac{\partial v'}{\partial a_n} = (n-1)t^{n-2} .$$

TABLE NO. 1

DRES DRAG FORCE DATA - FREE-FLIGHT CYLINDER METHOD

Cylinder No.	Diameter (in.)	L/D Ratio	P_o (psi)	Average Drag Coefficient 1st 24 ms	1st 40 ms	Over x ms	x = (ms)	Friedlander Decay Constant k
CIRCULAR CYLINDERS:								
A. PRAIRIE FLAT								
1	3.5	10.3	12.0	---	---	(.67)	50	1**
2	3.5	10.3	8.5	---	---	(.48)	50	1**
B. DIAL PACK								
1	12.0	10.0	5.9	.84(.94)	.79(.81)	.76(.72)	46(140)	1.0
2	3.5	17.1	11.0	.60(.71)	.61(.63)	.60(.75)	54(70)	1.0
3	3.5	17.1	14.3	.66	.61	.59	42	1.5*
4	3.5	17.1	17.0	.66	.53	.80	68	2.0
5	4.88	12.3	17.0	.68	.58	.62	50	2.0
6	3.5	17.1	20.5	.93	---	.92	26	2.0
7	5.73	10.5	20.5	1.07	---	1.07	24	2.0
C. MIXED COMPANY				1st 24 ms	1st 38 ms			
1	5.73#	10.5	23.1	---	---	---	---	2.22
2	3.50#	17.1	23.1	---	---	---	---	2.22
3	6.68†	12.6	9.1	.56(.67)	.59(.58)	.62(.62)	58(78)	1.63
4	6.68	12.6	9.1	.64	.70	.72	90	1.63
7	6.68†	12.6	7.0	.43	.50	.51	40	1.19
8	6.68	12.6	7.0	.47	.54	.52	86	1.19
SQUARE CYLINDERS - MIXED COMPANY								
5	6.0	14	9.1	2.02(1.77)	1.63(1.66)	1.63(1.46)	38(90)	1.63
6	6.0	14	9.1	2.08	2.09	2.00	50	1.63
9	6.0	14	7.0	1.58	1.54	1.65	94	1.19
10	6.0	14	7.0	1.76(1.89)	1.83(1.70)	1.80(2.27)	38(90)	1.19

** assumed; # due to a sideways force from a blast anomaly, no data were taken;
* assumed by interpolation; () are camera data; † shaded cylinder

TABLE NO. 2

$C_D(M,L/D)$ FOR FINITE L/D CALCULATED FROM DIAL PACK DATA AND INFINITE L/D FROM THE OPEN LITERATURE

Flow Mach No.	C_D Values from DIAL PACK-finite L/D					$C_D(M,\infty)$ from Fig. 1	Ratio Average $C_D(M,L/D)$ / $C_D(M,\infty)$
	Cylinder No:				Average C_D ± S.D.		
	4	5	6	7			
0.60	-	-	0.7	0.7	0.7	1.5	0.5
0.55	0.7	0.9	0.7	1.0	0.83 ± 0.15	1.4	0.6
0.50	0.7	0.8	1.0	1.3	0.95 ± 0.26	1.1	0.85
Avge (0.50 - 0.60)							0.65 ± 0.18
0.45	0.6	0.6	1.2	1.4	0.95 ± 0.41	0.5	1.9
0.40	0.5	0.5	1.0	---	0.67 ± 0.29	0.3	2.2
0.30	0.4	0.5	---	---	0.45 ± 0.07	0.3	1.5
Avge (0.30 - 0.45)							1.9 ± 0.35

Note: (1) For DIAL PACK cylinders 4 - 7 and for $M \geq 0.30$ we have $R > 6.5 \times 10^5$ so that the flow conditions are always with supercritical Reynolds numbers.

(2) The data are rough. The purpose of the table is to estimate the two average quantities in the last column; i.e., for $M > M_{C1}$ and $M < M_{C1}$ with M_{C1} = the first critical Mach number = 0.48.

TABLE NO. 3

SUMMARY OF L/D RATIO EFFECT VERSUS MACH AND REYNOLDS NUMBERS

From previous steady and unsteady flow experiments,

$$\eta,\ \eta',\ \eta'' = \frac{C_D(L/D = \text{finite})}{C_D(L/D = \text{infinite})} \quad \text{where}$$

η, η' and η'' are all the above same ratio for different flow conditions defined as:

$$\eta = \frac{C_D(\text{finite } L/D,\ \text{steady flow})}{C_D(\text{infinite } L/D,\ \text{steady flow})}\ ;\ \eta' = \frac{\text{"unsteady"}}{\text{"steady"}}\ ;\ \eta'' = \frac{\text{"unsteady"}}{\text{"unsteady}}\ .$$

$$\text{We also define } \phi = \frac{\eta'}{\eta} = \frac{C_D(\text{finite } L/D,\ \text{unsteady})}{C_D(\text{finite } L/D,\ \text{steady})}\ .$$

- Finite L/D means L/D in the range 5-20 over which C_D does not change very much.
- Different regions of M and R values are denoted by Roman numerals I-VI. Only regions I-III are of interest to us.
- References are given in brackets (X) and listed below.

References for Table No. 3

A - Martin et al. (1967)
B - Martin et al. (1965)
C - Mellsen (1971) - (STP 382) DIAL PACK results analyzed by Hill
D - Mellsen and Naylor (1969) shock tube work
E - Delaney and Sorenson (1953), analyzed by Hill
F - Welsh (1953) - some analyzed by Hill
G - Gowen and Perkins (1953)
H - Naylor and Mellsen (1973) Summary of PRAIRIE FLAT and DIAL PACK
I - Long and Laidlaw (1973) from the Lattice Mast II report - a direct comparison of Naylor's $C_D(\infty)$ values with Mellsen's C_D(finite); analyzed by Hill
J - Hoerner (1958)

Table No. 3 (Cont'd)

Summary of L/D Ratio Effect Versus Mach and Reynolds Numbers

Mach No., M	$R = 0$ to R_c	$R > R_c$
above $M_{c_2} \doteq 0.9$	VI $\eta \doteq 1$ (F) $\eta = 0.95$ to 1.00 for L/D = 1-8 (G)	V $\eta \doteq 1$ (F)
$M_{c_1} = 0.48$ to $M_{c_2} \doteq 0.9$	IV $\eta \doteq \frac{2}{3}$ (F)	III $\eta \doteq 0.5 - 0.6$ (F) $\eta' = 0.65 \pm 0.2$ (C) $\eta'' = 0.8 \pm 0.1$ (I) $\left.\begin{array}{l} C_D(\infty) = 1.5 \pm 0.1 \text{ (A\&D, unsteady)} \\ C_D(L/D) = 0.7 \text{ (H, unsteady)} \end{array}\right\} \eta'' = 0.5$ η'' avge $= \frac{0.8 + 0.5}{2} = 0.65$ $\phi = 1.2 \pm 0.3$
$M = 0$ to $M_{c_1} = 0.48$	II $\eta \doteq \frac{2}{3}$ (J) $C_D(\infty) = 1.2$ (H, unsteady)	I $\eta \doteq 1.0 \pm 0.2$ (E) $\eta' = 1.9 \pm 0.4$ (C) $\eta'' = 1.0 \pm 0.4$ (I) $\eta'' > 1$ and $\doteq 2$ (B, approx,) η'' avge $= \frac{2 + 1}{2} \doteq 1.5$ $C_D \doteq 0.5$ (H, unsteady) $\phi = 1.9 \pm 0.5$

$M = 0$, $R = 0$

$R_c \doteq (3\text{-}5) \times 10^5$

Reynolds No., R

TABLE NO. 4

SELECTION OF CYLINDERS

Cylinder Number	Over-pressure level (psi)	END PLATE Extended by number of diameters	Length L (ft.)	Diameter D (in.)	L/D	Purpose (see text)
1	20	.83	7.5	18	5	- table (120+ms) - overlap - diffraction
2	20	1	5	3.5	17	- table - end effects - overlap (70 ms) - diffraction - test
3	10	0	7.5	18	5	- table (100 ms) - end effects - unsteady - overlap
4	7	0	4	9.5	5	- support VHF mast(70 ms) - table - end effects - unsteady
5	7	1	4	9.5	5	- support VHF mast(70 ms) - table - end effect - unsteady - diffraction
6	10	0	5	3.5	17	- support lattice mast (50 ms) - end effects - unsteady - overlap - test
7	10	2	5	3.5	17	- support lattice mast and whip antenna (50+ ms) - end effects - unsteady - overlap - diffraction - test

TABLE NO. 5

CONTRIBUTIONS OF EACH CYLINDER TO THE GOALS

GOAL		CYLINDER NOS.
1. Support present projects	mast	6, 7
	VHF/UHF	4, 5
	whip	2, 6, 7
2. Table of data to support future masts for diffraction phase and $C_D(t)$	$M<M_c$	3, 4, 5
	$M>M_c$	1, 2
3. End Effects: finite L/D	$M>M_c$	2
vs infinite	$M<M_c$	3, 4, 5, 6, 7
4. Unsteady vs steady flow	$M>M_c$	3 vs ref.M
	$M<M_c$	4, 5, 6, 7 vs ref.I
5. With unsteady flow, overlap $M>M_c$ with $M<M_c$		1 with 3 2 with 6 and 7
6. Scientific study of diffraction for infinite length ($R>R_c$)	$M>M_c$	1, 2
	$M<M_c$	5, 7
Other		
7. Test needed diameter of end plate		2, 6, 7
8. Brand new regions of measurement		1, 3
9. Some overlap with previous work (DRES and open literature)		2, 4, 5, 6, 7

TABLE NO. 6

VALUES OF DYNAMIC PRESSURE USED IN CYLINDER MOTION ESTIMATES

Over-pressure (psi)	Dynamic Pressure, q(psi)					Reference
	Time Period (ms)					Values taken at mid point of time interval
	0 - 20	20 - 40	40 - 60	60 - 80	80 - 100	
20	6.51	3.24	1.57	0.73	---	Taken equal to 20.5 psi results from Dial Pack cylinder #7
10	2.00	1.27	0.77	0.46	0.25	Taken as average of Mixed Company #4 (9.1 psi) and Dial Pack #2 (11 psi)
7	1.2	0.80	0.54	0.35	0.22	Taken from Mixed Company #10 at 7.0 psi

UNCLASSIFIED

TABLE NO. 7

CALCULATED CYLINDER MOTION

Cylinder Number	CYLINDER SPECIFICATIONS						CALCULATED MOTION					
	Peak Over-pressure (psi)	Length L (in.)	Diameter D (in.)	Area A=LxD (in^2)	Weight (lb_M)	End Plate Diameter (in.)	Transit Time (ms)	C_D Value Chosen	Speed after diffraction (ft/s)	Leaving Transducer Speed (ft/s)	Leaving Transducer Time (ms)	End Plate Drag / Cylinder Drag calc. (%)
1	20	90	18	1620	266.0	48	.90	1.3 0.7	8.4	46	35	4.2
2	20	60	3.5	210	63.3	10.5	.18	0.5 0.5	1.25	23	75	1.6
3	10	90	18	1620	162.3	NA	1.07	0.6	7.7	25	80	0.4
4	7	48	9.5	460	37.4	NA	.60	0.5	2.0	14	160	0.4
5	7	48	9.5	460	60.0	28.5	.60	0.5	2.0	9	200	8.9
6	10	60	3.5	210	20.6	NA	.21	0.5	2.5	19	120	0.5
7	10	60	3.5	210	21.8	17.5	.21	0.5	2.5	19	120	7.3

UNCLASSIFIED

TABLE NO. 8

CALCULATIONS FOR BLAST RESISTANT CYLINDER DESIGN

Cylinder Number	Diameter	Support Disc Spacing ℓ	Wall Thickness t	Over-pressure	Shock Front Transit Time, T.T.	Diffraction Phase Drag Force		Pressure Drag Phase		Uniform Pressure for Elastic Buckling	Design Safety Factor for Diffraction †*
	(in.)	(in.)	(in.)	(psi)	(ms)	Impulse (psi-ms)	Max. Pressure $= \frac{\text{Impulse}}{2\ \text{T.T.}}$ (psi)	Max. Accel. (ft/s^2)	Max. Pressure (psi)	(psi)	
1	18	15	.162 (gauge 6)	20	.90	43	23.8	1690	8.5	235	9.9
2**	3.5	NA	NA	20	.18	13.7	38	815	8.5	NA	NA
3	18	15	.162	10	1.07	24	11.3	350	1.2	235	21
4††	9.5	12	.125	10	.56	12	10.8	470	1.2	395	37
5††	9.5	12	.125	10	.56	12	10.8	283	1.0	395	37
6	3.5	15	.125	10	.21	7.6	19.0	740	1.2	1267	67
7	3.5	15	.125	10	.21	7.6	19.0	330	1.0	1267	67

** Solid Aluminum, so the collapse formulae do not apply.

* $\left(\text{Design safety factor for diffraction}\right) = \frac{(\text{Uniform Pressure for Elastic Buckling})}{(\text{Max. diffraction Pressure})}$

† Does not take into account rigidity introduced by the welded centre rod.

†† Designed to withstand 10 psi overpressure; tested at 7 psi peak overpressure.

AD-A065 914 DEFENCE RESEARCH ESTABLISHMENT SUFFIELD RALSTON (ALBERTA) F/G 18/3
FREE-FLIGHT MEASUREMENT OF THE DRAG FORCES ON CYLINDERS IN EVEN--ETC(U)
FEB 79 A W GIBB, D A HILL
UNCLASSIFIED DRES-TP-453 NL

2 OF 2
AD A065914

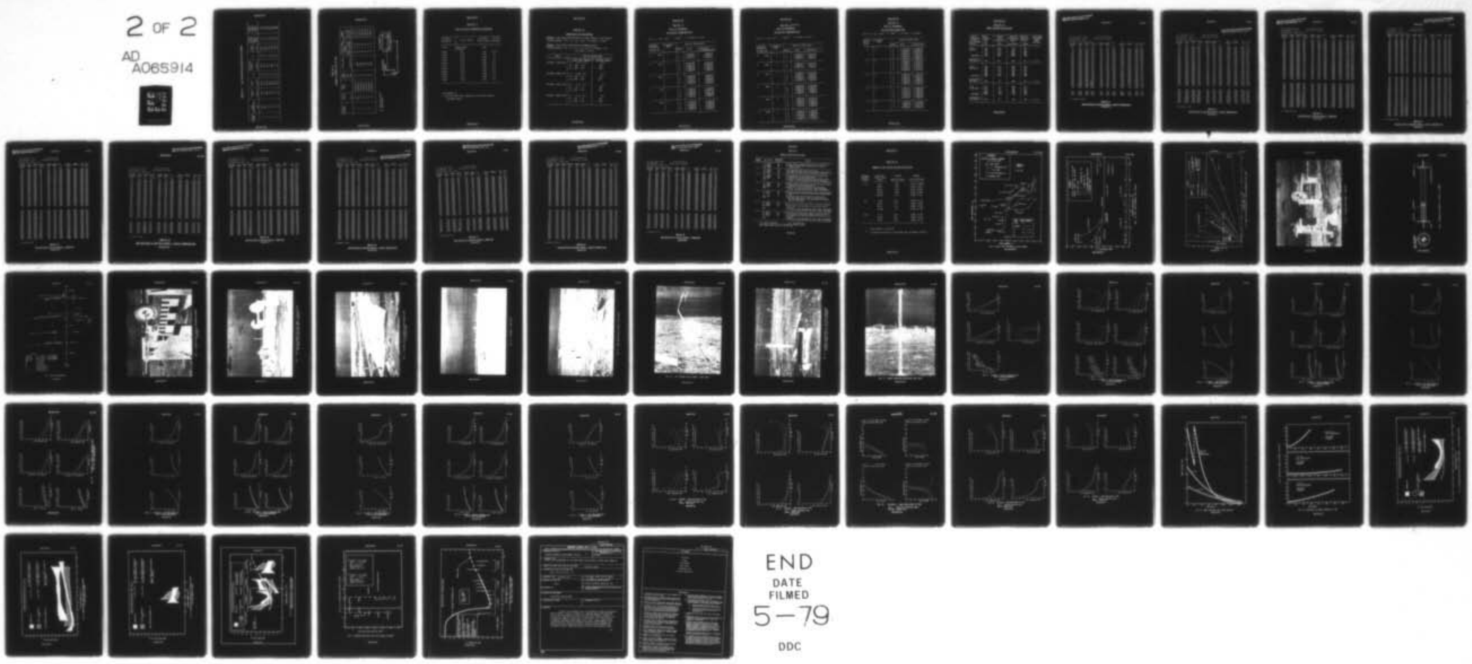

END
DATE
FILMED
5-79
DDC

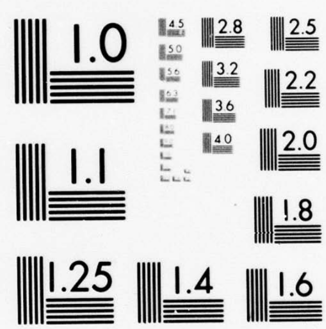

MICROCOPY RESOLUTION TEST CHART
NATIONAL BUREAU OF STANDARDS-1963-A

TABLE NO. 9 SIZE, WEIGHT AND LOCATION OF TEST CYLINDERS

Cylinder Number	Peak Overpressure (psi)	Diameter D (inches)	Length L (inches)	L/D	End Plate Diameter E (inches)	E/D	Total Weight (lbs)	Height of Axis Above Ground (feet)	Distance from Ground Zero (feet)
1	20.1	18.0	90.0	5.0	48.0	2.67	266.7	6.0	739
2	20.1	3.5	60.0	17.1	10.5	3.0	63.3	5.0	739
3	9.7	18.0	90.0	5.0	18.0	1.0	162.3	6.0	964
4	6.7	9.5	48.0	5.1	9.5	1.0	37.4	5.0	1139
5	6.7	9.5	48.0	5.1	28.5	3.0	60.0	5.0	1139
6	9.7	3.5	60.0	17.1	3.5	1.0	20.6	5.0	964
7	9.7	3.5	60.0	17.5	17.5	5.0	21.8	5.0	964

TABLE NO. 10

SUMMARY OF CAMERAS USED IN TRIAL

Cylinder Location	Over-pressure (psi)	Camera Type	Focal Length of Lens (mm)	Framing Rate (frames/sec)	Field of View in plane of Photo-marker		Camera Position	
					Width (inches)	Height (inches)	a** (ft)	w** (ft)
1	20.1	Photosonic	13	--	85	53	4.79	15.6
2	20.1	Photosonic	13	1090*	35	22	2.11	7.6
3	9.7	Photosonic	13	1130	40	25	2.38	9.5
4	6.7	Photosonic	50	1000	16	10	1.50	10.6
5	6.7	Photosonic	50	990	16	10	1.63	10.6
6	9.7	Photosonic	50	941	16	10	1.42	11.0
7	9.7	Photosonic	50	1090	16	10	1.50	11.0

* Rate not constant
** See diagram

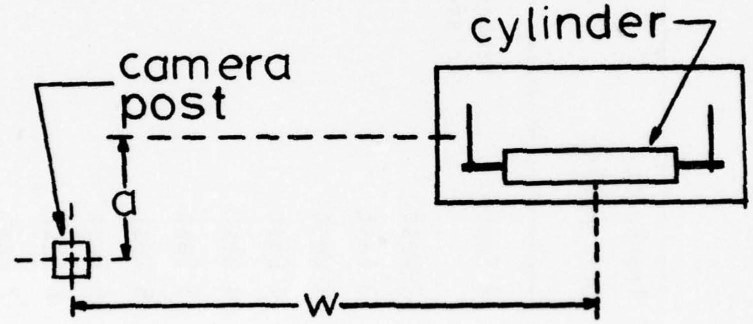

TABLE NO. 11

CHECK OF VELOCITY TRANSDUCER CALIBRATION*

Transducer Designation	$\int_0^T v(t)dt$ (inches)	X_o (inches) (±0.06 inches)	Per cent Difference
2 East	Broken magnet - no signal	9.65	--
2 West	12.7	9.65	31.6 **
3 East	10.34	9.65	7.2
3 West	9.76	9.65	1.1
4 East	10.23	9.86	3.8
4 West	9.75	9.68	0.1
5 East	10.17	9.80	3.7
5 West	9.90	9.84	0.6
6 East	9.94	9.60	3.5
6 West	9.73	9.60	1.4
7 East	9.77	9.60	1.8
7 West	9.68	9.65	0.3

* See Appendix D

** Poor v(t) data (poor signal/noise, large oscillations, truncated record)

TABLE NO. 12

COMPARISON OF FITTING METHODS

METHOD A - Mean Square Minimization by (Linear) Theory of Least Squares

Fitting Function: $v(t) = a_1 + a_2t + a_3t^2$, v in ft/sec, t in sec.

METHOD B - Mean Square Minimization by Parameter Search

Fitting Function: $v(t) = a_1 + a_2t + a_3t + a_4e^{-a_5t}\sin(2\pi a_6t + a_7)$,
v in ft/sec, t in sec.

DATA	BEST-FIT COEFFICIENTS	
	A. Linear Least Squares	B. Parameter Search
Cylinder 3 (East End)	a_1 = 9.0 ± 1.0	6.9
	a_2 = 224 ± 45	308
	a_3 = -962 ±412	-1583
Cylinder 3 (West End)	a_1 = 8.00± 0.8	6.5
	a_2 = 262 ± 35	325
	a_3 =-1350 ±318	-1817
Cylinder 4 (East End)	a_1 = 4.5 ± 0.3	4.0
	a_2 = 93 ± 9	108
	a_3 = -342 ± 43	-367
Cylinder 4 (West End)	a_1 = 4.3 ± 0.2	4.0
	a_2 = 112 ± 6	119
	a_3 = -420 ± 34	-408

TABLE NO. 13

BEST-FIT POLYNOMIALS

FOR VELOCITY TRANSDUCER DATA

$v(t) = a_1 + a_2t + a_3t^2 + \text{---} + a_nt^{n-1}$, v in ft/sec, t in sec.

Transducer Designation: Cylinder	Transducer Designation: End	Polynomial Order	Best-Fit Coefficients: Number	Value	Uncertainty (1 Std Deviation)
2	West	2	1	8.3904×10^0	1.0016×10^0
			2	7.0125×10^2	5.4556×10^1
			3	-5.3077×10^3	6.0782×10^2
3	East	4	1	8.6017×10^0	2.0015×10^0
			2	3.0837×10^2	2.5543×10^2
			3	-5.0942×10^3	9.7309×10^3
			4	6.7784×10^4	1.3828×10^5
			5	-3.5039×10^5	6.5335×10^5
3	West	4	1	8.2889×10^0	1.5603×10^0
			2	2.7845×10^2	1.9723×10^2
			3	-4.1275×10^3	7.4484×10^3
			4	6.3368×10^4	1.0497×10^5
			5	-3.8457×10^5	4.9172×10^5
4	East	4	1	4.1260×10^0	0.5768×10^0
			2	1.1047×10^2	0.4570×10^2
			3	-3.2360×10^2	10.667×10^2
			4	-3.3886×10^3	9.2508×10^3
			5	1.7292×10^4	2.6663×10^4
4	West	4	1	3.5314×10^0	0.3704×10^0
			2	1.8431×10^2	0.3103×10^2
			3	-2.1854×10^3	0.7650×10^3
			4	1.5365×10^4	0.6972×10^4
			5	-4.3843×10^4	2.1055×10^4

TABLE NO. 13 (Cont'd)

BEST-FIT POLYNOMIALS

FOR VELOCITY TRANSDUCER DATA

$v(t) = a_1 + a_2t + a_3t^2 + \text{---} + a_n t^{n-1}$, v in ft/sec, t in sec.

Transducer Designation Cylinder	End	Polynomial Order	Best-Fit Coefficients Number	Value	Uncertainty
5	East	2	1	2.7445×10^{0}	3.8581×10^{-1}
			2	1.0981×10^{2}	1.5367×10^{1}
			3	-4.8908×10^{2}	1.2920×10^{2}
5	West	2	1	2.3405×10^{0}	2.9415×10^{-1}
			2	1.4965×10^{2}	1.3521×10^{1}
			3	-6.3441×10^{2}	1.3136×10^{2}
6	East	4	1	1.9525×10^{0}	0.2717×10^{0}
			2	2.5509×10^{2}	0.2378×10^{2}
			3	-2.8499×10^{3}	0.6169×10^{3}
			4	2.0936×10^{4}	0.5970×10^{4}
			5	-6.1043×10^{4}	1.9212×10^{4}
6	West	4	1	2.0853×10^{0}	0.3312×10^{0}
			2	2.8674×10^{2}	0.3252×10^{2}
			3	-2.5961×10^{3}	0.9472×10^{3}
			4	1.5990×10^{4}	1.0289×10^{4}
			5	-4.3328×10^{4}	3.7195×10^{4}
7	East	4	1	2.2995×10^{0}	0.3017×10^{0}
			2	2.5942×10^{2}	0.2672×10^{2}
			3	-2.6452×10^{3}	0.6995×10^{3}
			4	1.4874×10^{4}	0.6795×10^{4}
			5	-3.3221×10^{4}	2.1900×10^{4}
7	West	4	1	2.5874×10^{0}	0.3463×10^{0}
			2	2.5647×10^{2}	0.3235×10^{2}
			3	-2.3679×10^{3}	0.8945×10^{3}
			4	1.3172×10^{4}	0.9193×10^{4}
			5	-3.2238×10^{4}	3.1373×10^{4}

TABLE NO. 14

BEST-FIT POLYNOMIALS

FOR HIGH-SPEED CAMERA DATA

$x(t) = a_1 + a_2t + a_3t^2 + \text{------} + a_nt^{n-1}$, x in feet, t in seconds

Cylinder Designation	Polynomial Order	Best-Fit Coefficients		
		Number	Value	Uncertainty
3	5	1	-2.1168×10^{-2}	0.2699×10^{-2}
		2	8.8515×10^{0}	0.5018×10^{0}
		3	1.7282×10^{2}	0.2874×10^{2}
		4	-2.3930×10^{3}	0.6772×10^{3}
		5	2.3814×10^{4}	0.6960×10^{4}
		6	-8.7640×10^{4}	2.5890×10^{4}
4	5	1	1.1682×10^{-4}	7.1695×10^{-4}
		2	2.6309×10^{0}	0.1075×10^{0}
		3	1.0103×10^{2}	0.0496×10^{2}
		4	-5.5793×10^{2}	0.9418×10^{2}
		5	1.2340×10^{3}	0.7795×10^{3}
		6	-8.0000×10^{0}	2.3327×10^{3}
5	5	1	-1.9645×10^{-3}	1.7078×10^{-3}
		2	1.4761×10^{0}	0.2673×10^{0}
		3	8.5265×10^{1}	1.2886×10^{1}
		4	-4.3162×10^{2}	2.5558×10^{2}
		5	1.5490×10^{3}	2.2105×10^{3}
		6	-3.5520×10^{3}	6.9140×10^{3}
6	5	1	-2.559×10^{-3}	1.4469×10^{-3}
		2	5.4772×10^{-1}	2.7658×10^{-1}
		3	2.0469×10^{2}	0.1525×10^{2}
		4	-2.3431×10^{3}	0.3582×10^{3}
		5	1.9516×10^{4}	0.3671×10^{4}
		6	-6.7472×10^{4}	1.3609×10^{4}
7	3	1	-1.1862×10^{-2}	0.1723×10^{-2}
		2	3.3434×10^{0}	0.1541×10^{0}
		3	1.0242×10^{2}	0.0371×10^{2}
		4	-2.7622×10^{2}	0.2531×10^{2}

TABLE NO. 15

IMPACT PRESSURE CALCULATIONS

Nominal Overpressure Location (and distance from GZ)	Gauge Distance from GZ (ft)	Measured Peak Overpressure P_o (psi)	Measured Overpressure Impulse I (psi-msec)	Measured Positive Duration t_+ (msec)	Calculated Friedlander Decay Constant
20 psi (739 ft)	735	20.6	723	127	
	735	18.6	787	168	
	725	21.5	1610	286	
	714	22.2	1046	203	
Averages—>	727	20.7	1041	196	
Corrected to 739 feet——>	739	20.1	1029	201 ——>	2.22
10 psi (964 feet)	940	10.4	904	238	
	950	10.5	889	229	
	965	9.8	835	225	
	950	10.1	862	227	
	953	9.8	847	230	
Averages—>	952	10.1	867	230	
Corrected to 964 feet——>	964	9.7	855	233 ——>	0.83
7 psi (1139 feet)	1125	7.0	694	216	
	1135	6.7	584	212	
	1115	7.2	881	304	
	1125	6.8	700	242	
Averages—>	1125	6.9	715	244	
Corrected to 1139 feet——>	1139	6.7	708	249 ——>	0.51

NO 2 3.5 IN DIAM 20.1 PSI 10.5 IN DIAM END PLATES

PEAK OVERPRESSURE 20.1 PSI POSITIVE DURATION 190.0 MSEC

FRIEDLANDER DECAY CONSTANT = 2.23

TIME AFTER SHOCK FRONT ARRIVAL (MSEC)	DRAG PRESSURE PD (PSI)	ABSOLUTE ERROR** (PSI)	RELATIVE ERROR** (PERCENT)	DYNAMIC PRESSURE Q (PSI)	IMPACT PRESSURE QI (PSI)	RATIO (QI/Q)	DRAG COEFFICIENT CD (PD/QI)	ABSOLUTE ERROR**	FLOW MACH NO. M	REYNOLDS NO. R (X10-5)
2.0	6.364	1.783	28.0	8.81	9.72	1.103	0.654	0.183	0.628	13.87
4.0	6.166	1.707	27.6	8.23	9.08	1.103	0.678	0.187	0.614	13.47
6.0	5.967	1.631	27.3	7.68	8.48	1.103	0.703	0.192	0.599	13.09
8.0	5.768	1.555	26.9	7.17	7.91	1.103	0.728	0.196	0.585	12.71
10.0	5.570	1.480	26.5	6.69	7.39	1.103	0.753	0.200	0.570	12.34
12.0	5.371	1.404	26.1	6.24	6.89	1.103	0.778	0.203	0.556	11.98
14.0	5.172	1.330	25.7	5.82	6.43	1.103	0.803	0.206	0.543	11.63
16.0	4.973	1.255	25.2	5.43	5.99	1.103	0.828	0.209	0.529	11.29
18.0	4.775	1.181	24.7	5.06	5.59	1.103	0.853	0.211	0.516	10.95
20.0	4.576	1.108	24.2	4.72	5.21	1.103	0.877	0.212	0.503	10.63
22.0	4.377	1.036	23.6	4.40	4.85	1.103	0.901	0.213	0.490	10.31
24.0	4.179	0.964	23.0	4.10	4.52	1.103	0.923	0.213	0.477	9.99
26.0	3.980	0.894	22.4	3.81	4.21	1.103	0.944	0.212	0.465	9.69
28.0	3.781	0.826	21.8	3.55	3.92	1.103	0.963	0.210	0.452	9.39
30.0	3.582	0.760	21.2	3.30	3.65	1.103	0.980	0.208	0.440	9.10
32.0	3.384	0.696	20.5	3.07	3.39	1.103	0.995	0.204	0.428	8.82
34.0	3.185	0.636	19.9	2.86	3.16	1.103	1.007	0.201	0.417	8.54
36.0	2.986	0.582	19.4	2.66	2.93	1.103	1.016	0.198	0.405	8.27
38.0	2.787	0.534	19.1	2.47	2.73	1.103	1.020	0.195	0.394	8.00
40.0	2.589	0.495	19.1	2.29	2.53	1.103	1.020	0.195	0.383	7.75
42.0	2.390	0.467	19.5	2.13	2.35	1.103	1.013	0.198	0.372	7.50
44.0	2.191	0.452	20.6	1.98	2.18	1.103	1.000	0.206	0.361	7.25
46.0	1.993	0.451	22.6	1.84	2.03	1.103	0.980	0.221	0.351	7.01
48.0	1.794	0.462	25.7	1.70	1.88	1.103	0.951	0.245	0.341	6.78
50.0	1.595	0.483	30.2	1.58	1.74	1.103	0.912	0.276	0.331	6.55
52.0	1.396	0.513	36.7	1.46	1.62	1.103	0.861	0.316	0.321	6.33
54.0	1.198	0.550	45.9	1.36	1.50	1.103	0.797	0.366	0.311	6.12
56.0	0.999	0.590	59.0	1.26	1.39	1.103	0.718	0.424	0.301	5.91
58.0	0.800	0.635	79.3	1.16	1.28	1.103	0.621	0.492	0.292	5.70
60.0	0.602	0.682	113.2	1.08	1.19	1.103	0.504	0.572	0.283	5.50
62.0	0.403	0.731	181.3	0.99	1.10	1.103	0.365	0.662	0.274	5.31
64.0	0.204	0.782	383.3	0.92	1.01	1.103	0.200	0.767	0.265	5.12
66.0	0.005	0.833	16660.0	0.85	0.94	1.103	0.005	0.884	0.257	4.94
68.0	-0.192	0.886	-461.4	0.78	0.87	1.103	-0.220	1.018	0.248	4.76
70.0	-0.391	0.940	-240.4	0.72	0.80	1.103	-0.486	1.170	0.240	4.59
72.0	-0.590	0.994	-168.4	0.67	0.74	1.103	-0.796	1.341	0.232	4.42
74.0	-0.789	1.048	-132.8	0.61	0.68	1.103	-1.154	1.533	0.224	4.25
76.0	-0.987	1.103	-111.7	0.57	0.62	1.103	-1.567	1.751	0.216	4.09
78.0	-1.186	1.159	-97.7	0.52	0.57	1.103	-2.045	1.998	0.209	3.94
80.0	-1.385	1.215	-87.7	0.48	0.53	1.103	-2.594	2.276	0.201	3.79
82.0	-1.583	1.271	-80.2	0.44	0.49	1.103	-3.224	2.589	0.194	3.64

** 3 STANDARD DEVIATIONS

TABLE NO. 16

DRAG COEFFICIENT VS TIME FOR CYLINDER 2 - VELOCITY TRANSDUCER DATA

THIS PAGE IS BEST QUALITY PRACTICABLE
FROM COPY FURNISHED TO DDC

NO 3 18.0 IN DIAM 9.7 PSI 18.0 IN DIAM END PLATES

PEAK OVERPRESSURE 9.7 PSI POSITIVE DURATION 233.0 MSEC

FRIEDLANDER DECAY CONSTANT = 0.83

TIME AFTER SHOCK FRONT ARRIVAL (MSEC)	DRAG PRESSURE PD (PSI)	ABSOLUTE ERROR** (PSI)	RELATIVE ERROR** (PERCENT)	DYNAMIC PRESSURE Q (PSI)	IMPACT PRESSURE QI (PSI)	RATIO (QI/Q)	DRAG COEFFICIENT CD (PD/QI)	ABSOLUTE ERROR**	FLOW MACH NO. M	REYNOLDS NO. R (X10-5)
2.0	0.847	1.281	151.1	2.35	2.45	1.039	0.345	0.522	0.391	42.66
4.0	0.798	1.091	136.6	2.28	2.37	1.039	0.336	0.459	0.386	42.06
6.0	0.754	0.920	122.0	2.21	2.30	1.039	0.327	0.400	0.382	41.46
8.0	0.714	0.767	107.4	2.14	2.22	1.039	0.320	0.344	0.377	40.87
10.0	0.678	0.630	93.0	2.07	2.15	1.039	0.314	0.292	0.372	40.29
12.0	0.645	0.512	79.4	2.01	2.08	1.039	0.308	0.245	0.367	39.70
14.0	0.616	0.412	66.9	1.94	2.02	1.039	0.304	0.204	0.363	39.13
16.0	0.590	0.332	56.2	1.88	1.95	1.039	0.301	0.169	0.358	38.56
18.0	0.568	0.272	47.9	1.82	1.89	1.039	0.299	0.143	0.353	37.99
20.0	0.547	0.235	43.0	1.76	1.83	1.039	0.298	0.128	0.349	37.43
22.0	0.530	0.220	41.5	1.70	1.77	1.039	0.299	0.124	0.344	36.87
24.0	0.515	0.220	42.7	1.65	1.71	1.039	0.300	0.128	0.339	36.32
26.0	0.503	0.229	45.5	1.59	1.65	1.039	0.303	0.138	0.335	35.77
28.0	0.492	0.239	48.5	1.54	1.60	1.039	0.307	0.149	0.330	35.22
30.0	0.484	0.248	51.3	1.49	1.55	1.039	0.312	0.160	0.326	34.69
32.0	0.476	0.253	53.2	1.44	1.49	1.039	0.317	0.169	0.321	34.15
34.0	0.469	0.255	54.2	1.39	1.44	1.039	0.324	0.176	0.317	33.62
36.0	0.465	0.252	54.1	1.34	1.39	1.039	0.332	0.180	0.312	33.10
38.0	0.461	0.245	53.1	1.30	1.35	1.039	0.341	0.181	0.308	32.57
40.0	0.457	0.234	51.2	1.25	1.30	1.039	0.350	0.179	0.304	32.06
42.0	0.454	0.221	48.7	1.21	1.26	1.039	0.360	0.175	0.299	31.55
44.0	0.451	0.207	45.9	1.17	1.21	1.039	0.371	0.170	0.295	31.04
46.0	0.448	0.192	42.8	1.12	1.17	1.039	0.381	0.163	0.291	30.54
48.0	0.445	0.178	39.9	1.09	1.13	1.039	0.393	0.157	0.286	30.04
50.0	0.441	0.167	37.8	1.05	1.09	1.039	0.404	0.153	0.282	29.54
52.0	0.437	0.160	36.6	1.01	1.05	1.039	0.415	0.152	0.278	29.05
54.0	0.433	0.159	36.7	0.97	1.01	1.039	0.426	0.156	0.274	28.57
56.0	0.426	0.163	38.4	0.94	0.97	1.039	0.435	0.167	0.270	28.09
58.0	0.419	0.173	41.3	0.90	0.94	1.039	0.443	0.183	0.265	27.61
60.0	0.410	0.185	45.1	0.87	0.90	1.039	0.451	0.203	0.261	27.14
62.0	0.399	0.198	49.7	0.84	0.87	1.039	0.455	0.227	0.257	26.67
64.0	0.385	0.212	55.0	0.81	0.84	1.039	0.457	0.251	0.253	26.20
66.0	0.370	0.224	60.6	0.78	0.81	1.039	0.455	0.276	0.249	25.74
68.0	0.353	0.233	66.2	0.75	0.78	1.039	0.451	0.299	0.245	25.29
70.0	0.332	0.239	72.0	0.72	0.75	1.039	0.442	0.318	0.241	24.84
72.0	0.309	0.241	78.2	0.69	0.72	1.039	0.427	0.334	0.237	24.39
74.0	0.282	0.240	85.0	0.66	0.69	1.039	0.406	0.345	0.233	23.95
76.0	0.252	0.234	93.0	0.64	0.66	1.039	0.377	0.351	0.229	23.51
78.0	0.219	0.226	103.2	0.61	0.64	1.039	0.341	0.352	0.225	23.07
80.0	0.181	0.218	120.5	0.59	0.61	1.039	0.293	0.353	0.221	22.64
82.0	0.138	0.213	153.6	0.56	0.59	1.039	0.234	0.360	0.218	22.21
84.0	0.091	0.218	239.6	0.54	0.56	1.039	0.160	0.383	0.214	21.79
86.0	0.038	0.239	614.4	0.52	0.54	1.039	0.071	0.438	0.210	21.37
88.0	-0.018	0.279	-1473.3	0.50	0.52	1.039	-0.036	0.533	0.206	20.96
90.0	-0.080	0.340	-424.1	0.48	0.50	1.039	-0.159	0.677	0.202	20.55
92.0	-0.146	0.420	-286.4	0.46	0.48	1.039	-0.305	0.873	0.199	20.14
94.0	-0.217	0.519	-238.6	0.44	0.46	1.039	-0.472	1.126	0.195	19.73
96.0	-0.293	0.635	-216.5	0.42	0.44	1.039	-0.665	1.440	0.191	19.34
98.0	-0.376	0.769	-204.3	0.40	0.42	1.039	-0.890	1.820	0.188	18.94
100.0	-0.464	0.920	-198.1	0.38	0.40	1.039	-1.148	2.276	0.184	18.55

** 3 STANDARD DEVIATIONS

TABLE NO. 17

DRAG COEFFICIENT VS TIME FOR CYLINDER 3 - VELOCITY TRANSDUCER DATA

NO 3 18.0 IN DIAM 9.7 PSI 18.0 IN DIAM END PLATES

PEAK OVERPRESSURE 9.7 PSI POSITIVE DURATION [illegible]33.0 MSEC

FRIEDLANDER DECAY CONSTANT = 0.83

TIME AFTER SHOCK FRONT ARRIVAL (MSEC)	DRAG PRESSURE PD (PSI)	ABSOLUTE ERROR** (PSI)	RELATIVE ERROR** (PERCENT)	DYNAMIC PRESSURE Q (PSI)	IMPACT PRESSURE QI (PSI)	RATIO (QI/Q)	DRAG COEFFICIENT CD (PD/QI)	ABSOLUTE ERROR**	FLOW MACH NO. M	REYNOLDS NO. R (X10-5)
2.0	0.602	0.163	27.0	2.35	2.45	1.039	0.245	0.066	0.391	42.66
4.0	0.592	0.157	26.5	2.28	2.37	1.039	0.249	0.066	0.386	42.06
6.0	0.582	0.151	25.9	2.21	2.30	1.039	0.252	0.065	0.382	41.46
8.0	0.571	0.146	25.5	2.14	2.22	1.039	0.256	0.065	0.377	40.87
10.0	0.561	0.140	24.9	2.07	2.15	1.039	0.259	0.064	0.372	40.29
12.0	0.550	0.134	24.3	2.01	2.08	1.039	0.263	0.064	0.367	39.70
14.0	0.540	0.129	23.8	1.94	2.02	1.039	0.266	0.063	0.363	39.13
16.0	0.530	0.123	23.2	1.88	1.95	1.039	0.270	0.062	0.358	38.56
18.0	0.519	0.118	22.7	1.82	1.89	1.039	0.273	0.062	0.353	37.99
20.0	0.509	0.112	22.0	1.76	1.83	1.039	0.277	0.061	0.349	37.43
22.0	0.498	0.107	21.4	1.70	1.77	1.039	0.280	0.060	0.344	36.87
24.0	0.488	0.101	20.6	1.65	1.71	1.039	0.284	0.058	0.339	36.32
26.0	0.478	0.096	20.0	1.59	1.65	1.039	0.288	0.057	0.335	35.77
28.0	0.467	0.090	19.2	1.54	1.60	1.039	0.291	0.056	0.330	35.22
30.0	0.457	0.085	18.5	1.49	1.55	1.039	0.294	0.054	0.326	34.69
32.0	0.446	0.080	17.9	1.44	1.49	1.039	0.297	0.053	0.321	34.15
34.0	0.436	0.075	17.2	1.39	1.44	1.039	0.301	0.051	0.317	33.62
36.0	0.426	0.071	16.6	1.34	1.39	1.039	0.304	0.050	0.312	33.10
38.0	0.415	0.066	15.9	1.30	1.35	1.039	0.307	0.048	0.308	32.57
40.0	0.405	0.062	15.3	1.25	1.30	1.039	0.310	0.047	0.304	32.06
42.0	0.394	0.058	14.7	1.21	1.26	1.039	0.312	0.046	0.299	31.55
44.0	0.384	0.055	14.3	1.17	1.21	1.039	0.315	0.045	0.295	31.04
46.0	0.374	0.053	14.1	1.12	1.17	1.039	0.318	0.045	0.291	30.54
48.0	0.363	0.051	14.0	1.09	1.13	1.039	0.320	0.045	0.286	30.04
50.0	0.353	0.050	14.1	1.05	1.09	1.039	0.323	0.045	0.282	29.54
52.0	0.342	0.050	14.6	1.01	1.05	1.039	0.324	0.047	0.278	29.05
54.0	0.332	0.051	15.3	0.97	1.01	1.039	0.326	0.050	0.274	28.57
56.0	0.322	0.052	16.1	0.94	0.97	1.039	0.328	0.053	0.270	28.09
58.0	0.311	0.054	17.3	0.90	0.94	1.039	0.329	0.057	0.265	27.61
60.0	0.301	0.057	18.9	0.87	0.90	1.039	0.330	0.062	0.261	27.14
62.0	0.290	0.060	20.6	0.84	0.87	1.039	0.331	0.068	0.257	26.67
64.0	0.280	0.063	22.5	0.81	0.84	1.039	0.331	0.074	0.253	26.20
66.0	0.270	0.067	24.8	0.78	0.81	1.039	0.332	0.082	0.249	25.74
68.0	0.259	0.071	27.4	0.75	0.78	1.039	0.331	0.090	0.245	25.29
70.0	0.249	0.075	30.1	0.72	0.75	1.039	0.331	0.099	0.241	24.84
72.0	0.238	0.079	33.1	0.69	0.72	1.039	0.329	0.109	0.237	24.39
74.0	0.228	0.083	36.4	0.66	0.69	1.039	0.327	0.119	0.233	23.95
76.0	0.218	0.088	40.3	0.64	0.66	1.039	0.326	0.131	0.229	23.51
78.0	0.207	0.092	44.4	0.61	0.64	1.039	0.322	0.143	0.225	23.07
80.0	0.197	0.096	48.7	0.59	0.61	1.039	0.319	0.155	0.221	22.64
82.0	0.186	0.101	54.3	0.56	0.59	1.039	0.313	0.170	0.218	22.21
84.0	0.176	0.105	59.6	0.54	0.56	1.039	0.309	0.184	0.214	21.79
86.0	0.166	0.110	66.2	0.52	0.54	1.039	0.304	0.201	0.210	21.37
88.0	0.155	0.115	74.1	0.50	0.52	1.039	0.296	0.219	0.206	20.96
90.0	0.145	0.119	82.0	0.48	0.50	1.039	0.288	0.237	0.202	20.55
92.0	0.134	0.124	92.5	0.46	0.48	1.039	0.278	0.257	0.199	20.14
94.0	0.124	0.128	103.2	0.44	0.46	1.039	0.269	0.277	0.195	19.73
96.0	0.114	0.133	116.6	0.42	0.44	1.039	0.258	0.301	0.191	19.34
98.0	0.057	0.081	142.1	0.40	0.42	1.039	0.134	0.191	0.188	18.94
100.0	0.049	0.084	171.4	0.38	0.40	1.039	0.121	0.207	0.184	18.55
102.0	0.041	0.087	212.1	0.37	0.38	1.039	0.106	0.225	0.181	18.16
104.0	0.033	0.090	272.7	0.35	0.36	1.039	0.089	0.243	0.177	17.78
106.0	0.025	0.093	372.0	0.33	0.35	1.039	0.070	0.263	0.173	17.40
108.0	0.017	0.096	564.7	0.32	0.33	1.039	0.050	0.284	0.170	17.02
110.0	0.009	0.099	1100.0	0.30	0.32	1.039	0.027	0.307	0.166	16.65
112.0	0.001	0.103	10300.0	0.29	0.30	1.039	0.003	0.335	0.163	16.28
114.0	-0.667	0.220	-32.9	0.28	0.29	1.039	-2.277	0.751	0.160	15.91
116.0	-0.644	0.199	-30.9	0.26	0.27	1.039	-2.307	0.712	0.156	15.55
118.0	-0.636	0.171	-26.8	0.25	0.26	1.039	-2.392	0.643	0.153	15.19
120.0	-0.645	0.164	-25.4	0.24	0.25	1.039	-2.548	0.648	0.149	14.84

** 3 STANDARD DEVIATIONS

TABLE NO. 18

DRAG COEFFICIENT VS TIME FOR CYLINDER 3 - CAMERA DATA

NO 4 9.5 IN DIAM 6.7 PSI 9.5 IN DIAM END PLATES

PEAK OVERPRESSURE 6.7 PSI POSITIVE DURATION 249.0 MSEC

FRIEDLANDER DECAY CONSTANT = 0.51

TIME AFTER SHOCK FRONT ARRIVAL (MSEC)	DRAG PRESSURE PD (PSI)	ABSOLUTE ERROR** (PSI)	RELATIVE ERROR** (PERCENT)	DYNAMIC PRESSURE Q (PSI)	IMPACT PRESSURE QI (PSI)	RATIO (QI/Q)	DRAG COEFFICIENT CD (PD/QI)	ABSOLUTE ERROR**	FLOW MACH NO. M	REYNOLDS NO. R (X10-5)
2.0	0.390	0.192	49.3	1.16	1.19	1.022	0.326	0.161	0.296	16.53
4.0	0.376	0.175	46.6	1.14	1.16	1.022	0.322	0.150	0.293	16.34
6.0	0.361	0.159	44.0	1.11	1.13	1.022	0.317	0.139	0.290	16.16
8.0	0.347	0.143	41.1	1.08	1.11	1.022	0.313	0.128	0.287	15.97
10.0	0.334	0.128	38.4	1.05	1.08	1.022	0.309	0.118	0.284	15.79
12.0	0.321	0.115	35.7	1.03	1.05	1.022	0.304	0.108	0.281	15.61
14.0	0.309	0.102	33.1	1.00	1.03	1.022	0.300	0.099	0.278	15.43
16.0	0.297	0.091	30.7	0.98	1.00	1.022	0.295	0.090	0.275	15.25
18.0	0.285	0.080	28.0	0.95	0.97	1.022	0.291	0.081	0.272	15.07
20.0	0.274	0.071	25.9	0.93	0.95	1.022	0.287	0.074	0.269	14.89
22.0	0.263	0.062	23.5	0.90	0.92	1.022	0.283	0.066	0.266	14.71
24.0	0.253	0.054	21.6	0.88	0.90	1.022	0.279	0.060	0.263	14.54
26.0	0.243	0.048	20.0	0.86	0.88	1.022	0.275	0.055	0.261	14.36
28.0	0.233	0.043	18.7	0.84	0.85	1.022	0.271	0.050	0.258	14.19
30.0	0.223	0.040	17.9	0.81	0.83	1.022	0.267	0.047	0.255	14.01
32.0	0.215	0.037	17.4	0.79	0.81	1.022	0.264	0.046	0.252	13.84
34.0	0.206	0.036	17.6	0.77	0.79	1.022	0.260	0.045	0.249	13.67
36.0	0.198	0.036	18.2	0.75	0.77	1.022	0.257	0.046	0.246	13.50
38.0	0.191	0.036	18.8	0.73	0.75	1.022	0.253	0.047	0.243	13.33
40.0	0.183	0.036	19.9	0.71	0.73	1.022	0.251	0.050	0.241	13.16
42.0	0.177	0.037	21.1	0.69	0.71	1.022	0.248	0.052	0.238	12.99
44.0	0.170	0.037	22.1	0.67	0.69	1.022	0.246	0.054	0.235	12.83
46.0	0.164	0.038	23.5	0.65	0.67	1.022	0.243	0.057	0.232	12.66
48.0	0.158	0.039	24.8	0.64	0.65	1.022	0.241	0.060	0.229	12.49
50.0	0.152	0.039	26.0	0.62	0.63	1.022	0.238	0.062	0.227	12.33
52.0	0.146	0.039	27.0	0.60	0.61	1.022	0.237	0.064	0.224	12.17
54.0	0.141	0.039	27.7	0.58	0.60	1.022	0.235	0.065	0.221	12.00
56.0	0.137	0.039	28.4	0.57	0.58	1.022	0.234	0.066	0.218	11.84
58.0	0.131	0.038	29.2	0.55	0.56	1.022	0.232	0.067	0.216	11.68
60.0	0.126	0.037	29.7	0.53	0.55	1.022	0.230	0.068	0.213	11.52
62.0	0.123	0.036	29.6	0.52	0.53	1.022	0.230	0.068	0.210	11.36
64.0	0.119	0.035	29.7	0.50	0.51	1.022	0.229	0.068	0.207	11.20
66.0	0.114	0.034	29.6	0.49	0.50	1.022	0.227	0.067	0.205	11.05
68.0	0.111	0.033	29.6	0.47	0.48	1.022	0.228	0.067	0.202	10.89
70.0	0.108	0.031	29.2	0.46	0.47	1.022	0.227	0.066	0.199	10.73
72.0	0.105	0.030	28.6	0.44	0.45	1.022	0.228	0.065	0.197	10.58
74.0	0.101	0.029	28.6	0.43	0.44	1.022	0.227	0.065	0.194	10.42
76.0	0.098	0.027	27.9	0.42	0.43	1.022	0.228	0.063	0.191	10.27
78.0	0.095	0.026	27.8	0.40	0.41	1.022	0.228	0.063	0.189	10.12
80.0	0.092	0.025	27.7	0.39	0.40	1.022	0.228	0.063	0.186	9.97
82.0	0.089	0.024	27.7	0.38	0.39	1.022	0.227	0.063	0.184	9.82
84.0	0.086	0.024	28.3	0.37	0.38	1.022	0.228	0.064	0.181	9.67
86.0	0.083	0.024	29.1	0.36	0.36	1.022	0.227	0.066	0.178	9.52
88.0	0.080	0.024	31.0	0.34	0.35	1.022	0.225	0.070	0.176	9.37
90.0	0.077	0.025	32.8	0.33	0.34	1.022	0.225	0.073	0.173	9.22
92.0	0.074	0.026	35.0	0.32	0.33	1.022	0.224	0.078	0.171	9.08
94.0	0.072	0.026	37.2	0.31	0.32	1.022	0.224	0.083	0.168	8.93
96.0	0.068	0.028	40.9	0.30	0.31	1.022	0.220	0.090	0.165	8.79
98.0	0.066	0.029	43.6	0.29	0.30	1.022	0.221	0.096	0.163	8.64
100.0	0.063	0.029	46.7	0.28	0.29	1.022	0.219	0.102	0.160	8.50
102.0	0.061	0.030	49.8	0.27	0.28	1.022	0.220	0.109	0.158	8.36
104.0	0.059	0.032	54.1	0.26	0.27	1.022	0.219	0.119	0.155	8.22
106.0	0.056	0.032	56.9	0.25	0.26	1.022	0.218	0.124	0.153	8.07
108.0	0.055	0.033	60.4	0.24	0.25	1.022	0.219	0.132	0.150	7.94
110.0	0.052	0.034	65.0	0.23	0.24	1.022	0.216	0.140	0.148	7.80
112.0	0.049	0.034	69.2	0.22	0.23	1.022	0.212	0.146	0.145	7.66
114.0	0.047	0.034	72.4	0.22	0.22	1.022	0.211	0.153	0.143	7.52
116.0	0.044	0.034	75.8	0.21	0.21	1.022	0.207	0.157	0.140	7.38
118.0	0.041	0.034	81.1	0.20	0.20	1.022	0.201	0.163	0.138	7.25
120.0	0.039	0.033	84.3	0.19	0.20	1.022	0.197	0.167	0.136	7.11
122.0	0.036	0.032	90.5	0.18	0.19	1.022	0.188	0.170	0.133	6.98
124.0	0.033	0.032	97.3	0.18	0.18	1.022	0.178	0.173	0.131	6.85
126.0	0.029	0.032	107.3	0.17	0.17	1.022	0.167	0.180	0.128	6.71
128.0	0.025	0.031	121.1	0.16	0.17	1.022	0.152	0.184	0.126	6.58
130.0	0.021	0.031	144.6	0.16	0.16	1.022	0.134	0.194	0.124	6.45
132.0	0.017	0.032	183.2	0.15	0.15	1.022	0.112	0.206	0.121	6.32
134.0	0.013	0.033	239.3	0.14	0.15	1.022	0.092	0.222	0.119	6.19
136.0	0.010	0.035	346.7	0.14	0.14	1.022	0.071	0.246	0.116	6.06
138.0	0.007	0.038	511.2	0.13	0.13	1.022	0.054	0.280	0.114	5.94
140.0	0.004	0.042	872.3	0.12	0.13	1.022	0.037	0.323	0.112	5.81
142.0	0.001	0.047	2390.7	0.12	0.12	1.022	0.015	0.375	0.109	5.68
144.0	-0.000	0.053	-15129.2	0.11	0.12	1.022	-0.002	0.446	0.107	5.56
146.0	-0.003	0.060	-1743.3	0.11	0.11	1.022	-0.030	0.526	0.105	5.43
148.0	-0.007	0.068	-916.9	0.10	0.10	1.022	-0.068	0.626	0.102	5.31
150.0	-0.011	0.077	-705.8	0.10	0.10	1.022	-0.105	0.745	0.100	5.19
152.0	-0.015	0.088	-584.6	0.09	0.09	1.022	-0.151	0.886	0.098	5.06
154.0	-0.019	0.098	-504.1	0.09	0.09	1.022	-0.207	1.047	0.096	4.94
156.0	-0.024	0.110	-458.3	0.08	0.08	1.022	-0.269	1.236	0.093	4.82
158.0	-0.030	0.123	-408.5	0.08	0.08	1.022	-0.355	1.454	0.091	4.70

** 3 STANDARD DEVIATIONS

TABLE NO. 19

DRAG COEFFICIENT VS TIME FOR CYLINDER 4 - VELOCITY TRANSDUCER DATA

NO 4 9.5 IN DIAM 6.7 PSI 9.5 IN DIAM END PLATES

PEAK OVERPRESSURE 6.7 PSI POSITIVE DURATION 249.0 MSEC

FRIEDLANDER DECAY CONSTANT = 0.51

TIME AFTER SHOCK FRONT ARRIVAL (MSEC)	DRAG PRESSURE PD (PSI)	ABSOLUTE ERROR** (PSI)	RELATIVE ERROR** (PERCENT)	DYNAMIC PRESSURE Q (PSI)	IMPACT PRESSURE QI (PSI)	RATIO (QI/Q)	DRAG COEFFICIENT CD (PD/QI)	ABSOLUTE ERROR**	FLOW MACH NO. M	REYNOLDS NO. R (X10-5)
2.0	0.498	0.067	13.4	1.16	1.19	1.022	0.416	0.056	0.296	16.53
4.0	0.482	0.060	12.4	1.14	1.16	1.022	0.413	0.051	0.293	16.34
6.0	0.465	0.052	11.1	1.11	1.13	1.022	0.408	0.045	0.290	16.16
8.0	0.449	0.046	10.2	1.08	1.11	1.022	0.404	0.041	0.287	15.97
10.0	0.434	0.040	9.2	1.05	1.08	1.022	0.400	0.036	0.284	15.79
12.0	0.418	0.034	8.1	1.03	1.05	1.022	0.395	0.032	0.281	15.61
14.0	0.403	0.029	7.1	1.00	1.03	1.022	0.391	0.028	0.278	15.43
16.0	0.388	0.024	6.1	0.98	1.00	1.022	0.386	0.023	0.275	15.25
18.0	0.374	0.020	5.3	0.95	0.97	1.022	0.382	0.020	0.272	15.07
20.0	0.360	0.017	4.7	0.93	0.95	1.022	0.377	0.017	0.269	14.89
22.0	0.346	0.013	3.7	0.90	0.92	1.022	0.372	0.013	0.266	14.71
24.0	0.332	0.011	3.3	0.88	0.90	1.022	0.366	0.012	0.263	14.54
26.0	0.319	0.009	2.8	0.86	0.88	1.022	0.361	0.010	0.261	14.36
28.0	0.306	0.007	2.2	0.84	0.85	1.022	0.355	0.008	0.258	14.19
30.0	0.293	0.006	2.0	0.81	0.83	1.022	0.349	0.007	0.255	14.01
32.0	0.281	0.006	2.1	0.79	0.81	1.022	0.344	0.007	0.252	13.84
34.0	0.268	0.006	2.2	0.77	0.79	1.022	0.337	0.007	0.249	13.67
36.0	0.257	0.007	2.7	0.75	0.77	1.022	0.332	0.009	0.246	13.50
38.0	0.245	0.007	2.8	0.73	0.75	1.022	0.325	0.009	0.243	13.33
40.0	0.234	0.007	2.9	0.71	0.73	1.022	0.319	0.009	0.241	13.16
42.0	0.223	0.008	3.5	0.69	0.71	1.022	0.313	0.011	0.238	12.99
44.0	0.212	0.008	3.7	0.67	0.69	1.022	0.306	0.011	0.235	12.83
46.0	0.202	0.008	3.9	0.65	0.67	1.022	0.299	0.011	0.232	12.66
48.0	0.192	0.008	4.1	0.64	0.65	1.022	0.293	0.012	0.229	12.49
50.0	0.182	0.007	3.8	0.62	0.63	1.022	0.285	0.010	0.227	12.33
52.0	0.173	0.007	4.0	0.60	0.61	1.022	0.279	0.011	0.224	12.17
54.0	0.164	0.006	3.6	0.58	0.60	1.022	0.272	0.009	0.221	12.00
56.0	0.155	0.006	3.8	0.57	0.58	1.022	0.265	0.010	0.218	11.84
58.0	0.147	0.005	3.4	0.55	0.56	1.022	0.259	0.008	0.216	11.68
60.0	0.139	0.005	3.5	0.53	0.55	1.022	0.252	0.009	0.213	11.52
62.0	0.131	0.005	3.8	0.52	0.53	1.022	0.244	0.009	0.210	11.36
64.0	0.123	0.004	3.2	0.50	0.51	1.022	0.236	0.007	0.207	11.20
66.0	0.116	0.004	3.4	0.49	0.50	1.022	0.230	0.007	0.205	11.05
68.0	0.109	0.004	3.6	0.47	0.48	1.022	0.222	0.008	0.202	10.89
70.0	0.102	0.004	3.9	0.46	0.47	1.022	0.215	0.008	0.199	10.73
72.0	0.096	0.005	5.2	0.44	0.45	1.022	0.208	0.010	0.197	10.58
74.0	0.090	0.005	5.5	0.43	0.44	1.022	0.201	0.011	0.194	10.42
76.0	0.084	0.006	7.1	0.42	0.43	1.022	0.194	0.013	0.191	10.27
78.0	0.079	0.006	7.5	0.40	0.41	1.022	0.188	0.014	0.189	10.12
80.0	0.073	0.007	9.5	0.39	0.40	1.022	0.179	0.017	0.186	9.97
82.0	0.069	0.007	10.1	0.38	0.39	1.022	0.175	0.017	0.184	9.82
84.0	0.064	0.007	10.9	0.37	0.38	1.022	0.168	0.018	0.181	9.67
86.0	0.060	0.008	13.3	0.36	0.36	1.022	0.162	0.021	0.178	9.52
88.0	0.056	0.008	14.2	0.34	0.35	1.022	0.157	0.022	0.176	9.37
90.0	0.052	0.008	15.3	0.33	0.34	1.022	0.150	0.023	0.173	9.22
92.0	0.049	0.008	16.3	0.32	0.33	1.022	0.147	0.024	0.171	9.08
94.0	0.046	0.007	15.2	0.31	0.32	1.022	0.142	0.021	0.168	8.93
96.0	0.043	0.007	16.2	0.30	0.31	1.022	0.138	0.022	0.165	8.79
98.0	0.041	0.007	17.0	0.29	0.30	1.022	0.136	0.023	0.163	8.64
100.0	0.038	0.006	15.7	0.28	0.29	1.022	0.130	0.020	0.160	8.50
102.0	0.037	0.006	16.2	0.27	0.28	1.022	0.132	0.021	0.158	8.36
104.0	0.035	0.007	20.0	0.26	0.27	1.022	0.129	0.025	0.155	8.22
106.0	0.034	0.008	23.5	0.25	0.26	1.022	0.130	0.030	0.153	8.07
108.0	0.033	0.010	30.3	0.24	0.25	1.022	0.131	0.039	0.150	7.94
110.0	0.032	0.012	37.5	0.23	0.24	1.022	0.131	0.049	0.148	7.80
112.0	0.032	0.015	46.8	0.22	0.23	1.022	0.136	0.064	0.145	7.66
114.0	0.032	0.018	56.2	0.22	0.22	1.022	0.142	0.080	0.143	7.52
116.0	0.032	0.022	68.7	0.21	0.21	1.022	0.147	0.101	0.140	7.38
118.0	0.033	0.027	81.8	0.20	0.20	1.022	0.158	0.129	0.138	7.25
120.0	0.033	0.031	93.9	0.19	0.20	1.022	0.164	0.154	0.136	7.11
122.0	0.035	0.037	105.7	0.18	0.19	1.022	0.181	0.192	0.133	6.98
124.0	0.036	0.043	119.4	0.18	0.18	1.022	0.194	0.232	0.131	6.85
126.0	0.038	0.049	128.9	0.17	0.17	1.022	0.213	0.275	0.128	6.71
128.0	0.040	0.056	140.0	0.16	0.17	1.022	0.234	0.328	0.126	6.58
130.0	0.042	0.063	150.0	0.16	0.16	1.022	0.256	0.385	0.124	6.45
132.0	0.045	0.071	157.7	0.15	0.15	1.022	0.286	0.452	0.121	6.32

** 3 STANDARD DEVIATIONS

TABLE NO. 20

DRAG COEFFICIENT VS TIME FOR CYLINDER 4 - CAMERA DATA

THIS PAGE IS BEST QUALITY PRACTICABLE
FROM COPY FURNISHED TO DDC

NO 5 9.5 IN DIAM 6.7 PSI 28.5 IN DIAM END PLATES

PEAK OVERPRESSURE 6.7 PSI POSITIVE DURATION 249.0 MSEC

FRIEDLANDER DECAY CONSTANT = 0.51

TIME AFTER SHOCK FRONT ARRIVAL (MSEC)	DRAG PRESSURE PD (PSI)	ABSOLUTE ERROR** (PSI)	RELATIVE ERROR** (PERCENT)	DYNAMIC PRESSURE Q (PSI)	IMPACT PRESSURE QI (PSI)	RATIO (QI/Q)	DRAG COEFFICIENT CD (PD/QI)	ABSOLUTE ERROR**	FLOW MACH NO. M	REYNOLDS NO. R (X10-5)
2.0	0.527	0.139	26.3	1.16	1.19	1.022	0.441	0.116	0.296	16.53
4.0	0.519	0.134	25.8	1.14	1.16	1.022	0.444	0.115	0.293	16.34
6.0	0.509	0.129	25.3	1.11	1.13	1.022	0.447	0.113	0.290	16.16
8.0	0.500	0.124	24.9	1.08	1.11	1.022	0.451	0.112	0.287	15.97
10.0	0.491	0.120	24.4	1.05	1.08	1.022	0.453	0.110	0.284	15.79
12.0	0.482	0.115	23.9	1.03	1.05	1.022	0.456	0.109	0.281	15.61
14.0	0.473	0.110	23.3	1.00	1.03	1.022	0.460	0.107	0.278	15.43
16.0	0.465	0.106	22.8	0.98	1.00	1.022	0.463	0.105	0.275	15.25
18.0	0.455	0.101	22.2	0.95	0.97	1.022	0.465	0.103	0.272	15.07
20.0	0.447	0.097	21.7	0.93	0.95	1.022	0.468	0.101	0.269	14.89
22.0	0.438	0.092	21.0	0.90	0.92	1.022	0.471	0.099	0.266	14.71
24.0	0.429	0.088	20.5	0.88	0.90	1.022	0.474	0.097	0.263	14.54
26.0	0.420	0.083	19.7	0.86	0.88	1.022	0.476	0.094	0.261	14.36
28.0	0.411	0.078	19.1	0.84	0.85	1.022	0.478	0.091	0.258	14.19
30.0	0.403	0.074	18.5	0.81	0.83	1.022	0.481	0.089	0.255	14.01
32.0	0.393	0.070	17.8	0.79	0.81	1.022	0.483	0.086	0.252	13.84
34.0	0.385	0.066	17.1	0.77	0.79	1.022	0.485	0.083	0.249	13.67
36.0	0.376	0.062	16.5	0.75	0.77	1.022	0.486	0.080	0.246	13.50
38.0	0.367	0.058	15.9	0.73	0.75	1.022	0.488	0.077	0.243	13.33
40.0	0.357	0.054	15.2	0.71	0.73	1.022	0.489	0.074	0.241	13.16
42.0	0.348	0.051	14.6	0.69	0.71	1.022	0.490	0.071	0.238	12.99
44.0	0.338	0.048	14.3	0.67	0.69	1.022	0.489	0.070	0.235	12.83
46.0	0.328	0.045	13.9	0.65	0.67	1.022	0.487	0.068	0.232	12.66
48.0	0.317	0.043	13.8	0.64	0.65	1.022	0.484	0.066	0.229	12.49
50.0	0.306	0.042	13.8	0.62	0.63	1.022	0.480	0.066	0.227	12.33
52.0	0.294	0.041	14.0	0.60	0.61	1.022	0.475	0.066	0.224	12.17
54.0	0.282	0.041	14.5	0.58	0.60	1.022	0.469	0.068	0.221	12.00
56.0	0.270	0.040	15.1	0.57	0.58	1.022	0.462	0.070	0.218	11.84
58.0	0.258	0.041	15.9	0.55	0.56	1.022	0.455	0.072	0.216	11.68
60.0	0.247	0.042	17.2	0.53	0.55	1.022	0.449	0.077	0.213	11.52
62.0	0.237	0.043	18.5	0.52	0.53	1.022	0.443	0.082	0.210	11.36
64.0	0.226	0.045	20.1	0.50	0.51	1.022	0.435	0.087	0.207	11.20
66.0	0.217	0.048	22.1	0.49	0.50	1.022	0.431	0.095	0.205	11.05
68.0	0.207	0.050	24.4	0.47	0.48	1.022	0.424	0.103	0.202	10.89
70.0	0.198	0.053	27.0	0.46	0.47	1.022	0.419	0.113	0.199	10.73
72.0	0.189	0.056	29.8	0.44	0.45	1.022	0.411	0.122	0.197	10.58
74.0	0.181	0.060	33.1	0.43	0.44	1.022	0.406	0.134	0.194	10.42
76.0	0.172	0.063	36.6	0.42	0.43	1.022	0.399	0.146	0.191	10.27
78.0	0.163	0.067	41.0	0.40	0.41	1.022	0.390	0.160	0.189	10.12
80.0	0.155	0.070	45.5	0.39	0.40	1.022	0.382	0.174	0.186	9.97
82.0	0.146	0.074	50.7	0.38	0.39	1.022	0.372	0.188	0.184	9.82
84.0	0.137	0.078	56.7	0.37	0.38	1.022	0.361	0.205	0.181	9.67
86.0	0.128	0.081	63.5	0.36	0.36	1.022	0.350	0.222	0.178	9.52
88.0	0.120	0.085	71.5	0.34	0.35	1.022	0.337	0.241	0.176	9.37
90.0	0.111	0.089	80.6	0.33	0.34	1.022	0.323	0.260	0.173	9.22
92.0	0.102	0.093	91.6	0.32	0.33	1.022	0.306	0.281	0.171	9.08
94.0	0.093	0.097	104.1	0.31	0.32	1.022	0.291	0.303	0.168	8.93
96.0	0.084	0.101	119.4	0.30	0.31	1.022	0.273	0.326	0.165	8.79

** 3 STANDARD DEVIATIONS

TABLE NO. 21

DRAG COEFFICIENT VS TIME FOR CYLINDER 5 - VELOCITY TRANSDUCER DATA

NO 5 9.5 IN DIAM 6.7 PSI 28.5 IN DIAM END PLATES

PEAK OVERPRESSURE 6.7 PSI POSITIVE DURATION 249.0 MSEC

FRIEDLANDER DECAY CONSTANT = 0.51

TIME AFTER SHOCK FRONT ARRIVAL (MSEC)	DRAG PRESSURE PD (PSI)	ABSOLUTE ERROR (PSI)	RELATIVE ERROR (PERCENT)	DYNAMIC PRESSURE Q (PSI)	IMPACT PRESSURE QI (PSI)	RATIO (QI/Q)	DRAG COEFFICIENT CD (PD/QI)	ABSOLUTE ERROR	FLOW MACH NO. M	REYNOLDS NO. R (X10-5)
2.0	0.677	0.280	41.3	1.16	1.19	1.022	0.566	0.234	0.296	16.53
4.0	0.657	0.247	37.5	1.14	1.16	1.022	0.563	0.211	0.293	16.34
6.0	0.637	0.216	33.9	1.11	1.13	1.022	0.559	0.189	0.290	16.16
8.0	0.618	0.188	30.4	1.08	1.11	1.022	0.556	0.169	0.287	15.97
10.0	0.600	0.162	26.9	1.05	1.08	1.022	0.553	0.149	0.284	15.79
12.0	0.581	0.138	23.7	1.03	1.05	1.022	0.549	0.130	0.281	15.61
14.0	0.564	0.116	20.5	1.00	1.03	1.022	0.547	0.112	0.278	15.43
16.0	0.547	0.097	17.7	0.98	1.00	1.022	0.544	0.096	0.275	15.25
18.0	0.530	0.080	15.0	0.95	0.97	1.022	0.541	0.081	0.272	15.07
20.0	0.514	0.064	12.4	0.93	0.95	1.022	0.538	0.067	0.269	14.89
22.0	0.499	0.052	10.4	0.90	0.92	1.022	0.536	0.055	0.266	14.71
24.0	0.484	0.041	8.4	0.88	0.90	1.022	0.534	0.045	0.263	14.54
26.0	0.469	0.034	7.2	0.86	0.88	1.022	0.531	0.038	0.261	14.36
28.0	0.455	0.029	6.3	0.84	0.85	1.022	0.529	0.033	0.258	14.19
30.0	0.441	0.028	6.3	0.81	0.83	1.022	0.526	0.033	0.255	14.01
32.0	0.427	0.028	6.5	0.79	0.81	1.022	0.523	0.034	0.252	13.84
34.0	0.414	0.029	7.0	0.77	0.79	1.022	0.521	0.036	0.249	13.67
36.0	0.401	0.031	7.7	0.75	0.77	1.022	0.518	0.040	0.246	13.50
38.0	0.389	0.032	8.2	0.73	0.75	1.022	0.517	0.042	0.243	13.33
40.0	0.377	0.033	8.7	0.71	0.73	1.022	0.515	0.045	0.241	13.16
42.0	0.365	0.034	9.3	0.69	0.71	1.022	0.512	0.047	0.238	12.99
44.0	0.354	0.034	9.6	0.67	0.69	1.022	0.511	0.049	0.235	12.83
46.0	0.343	0.033	9.6	0.65	0.67	1.022	0.509	0.048	0.232	12.66
48.0	0.332	0.032	9.6	0.64	0.65	1.022	0.506	0.048	0.229	12.49
50.0	0.322	0.030	9.3	0.62	0.63	1.022	0.505	0.047	0.227	12.33
52.0	0.312	0.028	8.9	0.60	0.61	1.022	0.504	0.045	0.224	12.17
54.0	0.302	0.026	8.6	0.58	0.60	1.022	0.502	0.043	0.221	12.00
56.0	0.292	0.024	8.2	0.57	0.58	1.022	0.499	0.041	0.218	11.84
58.0	0.282	0.022	7.8	0.55	0.56	1.022	0.496	0.038	0.216	11.68
60.0	0.273	0.020	7.3	0.53	0.55	1.022	0.495	0.036	0.213	11.52
62.0	0.264	0.019	7.1	0.52	0.53	1.022	0.493	0.035	0.210	11.36
64.0	0.255	0.019	7.4	0.50	0.51	1.022	0.491	0.036	0.207	11.20
66.0	0.246	0.019	7.7	0.49	0.50	1.022	0.488	0.037	0.205	11.05
68.0	0.237	0.021	8.8	0.47	0.48	1.022	0.484	0.042	0.202	10.89
70.0	0.229	0.022	9.6	0.46	0.47	1.022	0.482	0.046	0.199	10.73
72.0	0.220	0.025	11.3	0.44	0.45	1.022	0.478	0.054	0.197	10.58
74.0	0.212	0.027	12.7	0.43	0.44	1.022	0.475	0.060	0.194	10.42
76.0	0.204	0.029	14.2	0.42	0.43	1.022	0.472	0.067	0.191	10.27
78.0	0.196	0.031	15.8	0.40	0.41	1.022	0.468	0.074	0.189	10.12
80.0	0.188	0.032	17.0	0.39	0.40	1.022	0.463	0.078	0.186	9.97
82.0	0.180	0.033	18.3	0.38	0.39	1.022	0.458	0.083	0.184	9.82
84.0	0.172	0.034	19.7	0.37	0.38	1.022	0.452	0.089	0.181	9.67
86.0	0.164	0.034	20.7	0.36	0.36	1.022	0.445	0.092	0.178	9.52
88.0	0.156	0.033	21.1	0.34	0.35	1.022	0.437	0.092	0.176	9.37
90.0	0.148	0.032	21.6	0.33	0.34	1.022	0.429	0.092	0.173	9.22
92.0	0.140	0.030	21.4	0.32	0.33	1.022	0.420	0.090	0.171	9.08
94.0	0.132	0.029	21.9	0.31	0.32	1.022	0.409	0.090	0.168	8.93
96.0	0.124	0.028	22.5	0.30	0.31	1.022	0.398	0.089	0.165	8.79
98.0	0.116	0.028	24.1	0.29	0.30	1.022	0.385	0.093	0.163	8.64
100.0	0.108	0.031	28.7	0.28	0.29	1.022	0.371	0.106	0.160	8.50
102.0	0.09[illegible]	0.036	36.3	0.27	0.28	1.022	0.353	0.128	0.158	8.36
104.0	0.091	0.045	49.4	0.26	0.27	1.022	0.336	0.166	0.155	8.22
106.0	0.083	0.056	67.4	0.25	0.26	1.022	0.318	0.214	0.153	8.07
108.0	0.074	0.070	94.5	0.24	0.25	1.022	0.294	0.278	0.150	7.94
110.0	0.065	0.086	132.3	0.23	0.24	1.022	0.268	0.354	0.148	7.80
112.0	0.056	0.104	185.7	0.22	0.23	1.022	0.239	0.445	0.145	7.66
114.0	0.047	0.124	263.8	0.22	0.22	1.022	0.208	0.551	0.143	7.52
116.0	0.038	0.146	384.2	0.21	0.21	1.022	0.175	0.674	0.140	7.38
118.0	0.028	0.171	610.7	0.20	0.20	1.022	0.134	0.820	0.138	7.25
120.0	0.019	0.198	1042.1	0.19	0.20	1.022	0.094	0.988	0.136	7.11
122.0	0.009	0.227	2522.2	0.18	0.19	1.022	0.046	1.178	0.133	6.98
124.0	0.000	0.259	25.9	0.18	0.18	1.022	0.000	1.399	0.131	6.85

TABLE NO. 22

DRAG COEFFICIENT VS TIME FOR CYLINDER 5 - CAMERA DATA

NO 6 3.5 IN DIAM 9.7 PSI 3.5 IN DIAM END PLATES

PEAK OVERPRESSURE 9.7 PSI POSITIVE DURATION 233.0 MSEC

FRIEDLANDER DECAY CONSTANT = 0.83

TIME AFTER SHOCK FRONT ARRIVAL (MSEC)	DRAG PRESSURE PD (PSI)	ABSOLUTE ERROR** (PSI)	RELATIVE ERROR** (PERCENT)	DYNAMIC PRESSURE Q (PSI)	IMPACT PRESSURE QI (PSI)	RATIO (QI/Q)	DRAG COEFFICIENT CD (PD/QI)	ABSOLUTE ERROR**	FLOW MACH NO. M	REYNOLDS NO. R (X10-5)
2.0	0.777	0.184	23.7	2.35	2.45	1.039	0.317	0.075	0.391	8.29
4.0	0.746	0.167	22.3	2.28	2.37	1.039	0.314	0.070	0.386	8.17
6.0	0.717	0.149	20.9	2.21	2.30	1.039	0.311	0.065	0.382	8.06
8.0	0.688	0.134	19.5	2.14	2.22	1.039	0.309	0.060	0.377	7.94
10.0	0.661	0.120	18.1	2.07	2.15	1.039	0.306	0.055	0.372	7.83
12.0	0.636	0.106	16.7	2.01	2.08	1.039	0.304	0.051	0.367	7.72
14.0	0.612	0.094	15.4	1.94	2.02	1.039	0.302	0.046	0.363	7.60
16.0	0.589	0.083	14.1	1.88	1.95	1.039	0.301	0.042	0.358	7.49
18.0	0.567	0.073	12.9	1.82	1.89	1.039	0.299	0.038	0.353	7.38
20.0	0.546	0.064	11.8	1.76	1.83	1.039	0.298	0.035	0.349	7.27
22.0	0.526	0.057	10.8	1.70	1.77	1.039	0.296	0.032	0.344	7.17
24.0	0.506	0.051	10.1	1.65	1.71	1.039	0.295	0.029	0.339	7.06
26.0	0.485	0.046	9.5	1.59	1.65	1.039	0.292	0.028	0.335	6.95
28.0	0.466	0.043	9.3	1.54	1.60	1.039	0.290	0.027	0.330	6.85
30.0	0.448	0.041	9.2	1.49	1.55	1.039	0.289	0.026	0.326	6.74
32.0	0.430	0.040	9.4	1.44	1.49	1.039	0.287	0.027	0.321	6.64
34.0	0.413	0.040	9.7	1.39	1.44	1.039	0.285	0.027	0.317	6.53
36.0	0.399	0.040	10.1	1.34	1.39	1.039	0.285	0.028	0.312	6.43
38.0	0.386	0.040	10.5	1.30	1.35	1.039	0.285	0.030	0.308	6.33
40.0	0.373	0.040	10.8	1.25	1.30	1.039	0.286	0.031	0.304	6.23
42.0	0.362	0.041	11.3	1.21	1.26	1.039	0.287	0.032	0.299	6.13
44.0	0.351	0.041	11.7	1.17	1.21	1.039	0.289	0.033	0.295	6.03
46.0	0.342	0.041	11.9	1.12	1.17	1.039	0.291	0.034	0.291	5.93
48.0	0.333	0.040	12.2	1.09	1.13	1.039	0.294	0.036	0.286	5.84
50.0	0.325	0.040	12.3	1.05	1.09	1.039	0.298	0.036	0.282	5.74
52.0	0.318	0.039	12.3	1.01	1.05	1.039	0.301	0.037	0.278	5.65
54.0	0.310	0.038	12.3	0.97	1.01	1.039	0.305	0.037	0.274	5.55
56.0	0.304	0.037	12.2	0.94	0.97	1.039	0.310	0.038	0.270	5.46
58.0	0.297	0.036	12.1	0.90	0.94	1.039	0.315	0.038	0.265	5.36
60.0	0.292	0.035	11.9	0.87	0.90	1.039	0.321	0.038	0.261	5.27
62.0	0.287	0.033	11.6	0.84	0.87	1.039	0.327	0.038	0.257	5.18
64.0	0.282	0.032	11.5	0.81	0.84	1.039	0.334	0.038	0.253	5.09
66.0	0.276	0.031	11.2	0.78	0.81	1.039	0.340	0.038	0.249	5.00
68.0	0.270	0.030	11.0	0.75	0.78	1.039	0.346	0.038	0.245	4.91
70.0	0.266	0.029	11.0	0.72	0.75	1.039	0.353	0.038	0.241	4.83
72.0	0.260	0.029	11.1	0.69	0.72	1.039	0.360	0.040	0.237	4.74
74.0	0.256	0.028	11.1	0.66	0.69	1.039	0.368	0.041	0.233	4.65
76.0	0.251	0.028	11.3	0.64	0.66	1.039	0.375	0.042	0.229	4.57
78.0	0.247	0.028	11.5	0.61	0.64	1.039	0.385	0.044	0.225	4.48
80.0	0.243	0.029	11.9	0.59	0.61	1.039	0.395	0.047	0.221	4.40
82.0	0.240	0.029	12.2	0.56	0.59	1.039	0.405	0.049	0.218	4.32
84.0	0.237	0.030	12.6	0.54	0.56	1.039	0.417	0.052	0.214	4.23
86.0	0.234	0.031	13.2	0.52	0.54	1.039	0.429	0.056	0.210	4.15
88.0	0.231	0.031	13.7	0.50	0.52	1.039	0.442	0.060	0.206	4.07
90.0	0.229	0.032	14.1	0.48	0.50	1.039	0.456	0.064	0.202	3.99
92.0	0.226	0.033	14.8	0.46	0.48	1.039	0.471	0.069	0.199	3.91
94.0	0.224	0.034	15.2	0.44	0.46	1.039	0.486	0.074	0.195	3.83
96.0	0.221	0.034	15.6	0.42	0.44	1.039	0.502	0.078	0.191	3.76
98.0	0.218	0.035	16.0	0.40	0.42	1.039	0.516	0.082	0.188	3.68
100.0	0.214	0.034	16.2	0.38	0.40	1.039	0.530	0.086	0.184	3.60
102.0	0.211	0.035	16.6	0.37	0.38	1.039	0.545	0.090	0.181	3.53
104.0	0.207	0.034	16.7	0.35	0.36	1.039	0.561	0.094	0.177	3.45
106.0	0.203	0.034	16.9	0.33	0.35	1.039	0.576	0.097	0.173	3.38
108.0	0.199	0.034	17.4	0.32	0.33	1.039	0.590	0.103	0.170	3.31
110.0	0.193	0.034	17.9	0.30	0.32	1.039	0.601	0.108	0.166	3.23
112.0	0.188	0.035	18.6	0.29	0.30	1.039	0.614	0.114	0.163	3.16
114.0	0.182	0.035	19.5	0.28	0.29	1.039	0.622	0.121	0.160	3.09
116.0	0.176	0.036	20.3	0.26	0.27	1.039	0.633	0.129	0.156	3.02
118.0	0.169	0.037	21.8	0.25	0.26	1.039	0.639	0.139	0.153	2.95
120.0	0.163	0.037	22.7	0.24	0.25	1.039	0.646	0.146	0.149	2.88
122.0	0.155	0.038	24.8	0.23	0.24	1.039	0.645	0.160	0.146	2.81
124.0	0.147	0.040	27.1	0.22	0.22	1.039	0.644	0.175	0.143	2.74
126.0	0.138	0.042	30.5	0.20	0.21	1.039	0.636	0.194	0.139	2.68
128.0	0.129	0.046	35.7	0.19	0.20	1.039	0.627	0.224	0.136	2.61
130.0	0.118	0.051	43.2	0.18	0.19	1.039	0.605	0.261	0.133	2.55
132.0	0.107	0.058	53.8	0.17	0.18	1.039	0.580	0.312	0.130	2.48

** 3 STANDARD DEVIATIONS

TABLE NO. 23

DRAG COEFFICIENT VS TIME FOR CYLINDER 6 - VELOCITY TRANSDUCER DATA

NO 6 3.5 IN DIAM 9.7 PSI 3.5 IN DIAM END PLATES

PEAK OVERPRESSURE 9.7 PSI POSITIVE DURATION 233.0 MSEC

FRIEDLANDER DECAY CONSTANT = 0.83

TIME AFTER SHOCK FRONT ARRIVAL (MSEC)	DRAG PRESSURE PD (PSI)	ABSOLUTE ERROR** (PSI)	RELATIVE ERROR** (PERCENT)	DYNAMIC PRESSURE Q (PSI)	IMPACT PRESSURE QI (PSI)	RATIO (QI/Q)	DRAG COEFFICIENT CD (PD/QI)	ABSOLUTE ERROR**	FLOW MACH NO. M	REYNOLDS NO. R (X10-5)
2.0	1.161	0.241	20.7	2.35	2.45	1.039	0.473	0.098	0.391	8.29
4.0	1.084	0.207	19.0	2.28	2.37	1.039	0.456	0.087	0.386	8.17
6.0	1.012	0.176	17.3	2.21	2.30	1.039	0.439	0.076	0.382	8.06
8.0	0.945	0.148	15.6	2.14	2.22	1.039	0.424	0.066	0.377	7.94
10.0	0.883	0.123	13.9	2.07	2.15	1.039	0.409	0.057	0.372	7.83
12.0	0.826	0.100	12.1	2.01	2.08	1.039	0.395	0.047	0.367	7.72
14.0	0.774	0.080	10.3	1.94	2.02	1.039	0.382	0.039	0.363	7.60
16.0	0.725	0.063	8.6	1.88	1.95	1.039	0.370	0.032	0.358	7.49
18.0	0.681	0.049	7.1	1.82	1.89	1.039	0.359	0.025	0.353	7.38
20.0	0.641	0.038	5.9	1.76	1.83	1.039	0.349	0.020	0.349	7.27
22.0	0.604	0.029	4.8	1.70	1.77	1.039	0.340	0.016	0.344	7.17
24.0	0.571	0.025	4.3	1.65	1.71	1.039	0.332	0.014	0.339	7.06
26.0	0.542	0.024	4.4	1.59	1.65	1.039	0.326	0.014	0.335	6.95
28.0	0.515	0.025	4.8	1.54	1.60	1.039	0.321	0.015	0.330	6.85
30.0	0.492	0.026	5.2	1.49	1.55	1.039	0.317	0.016	0.326	6.74
32.0	0.471	0.028	5.9	1.44	1.49	1.039	0.314	0.018	0.321	6.64
34.0	0.452	0.029	6.4	1.39	1.44	1.039	0.312	0.020	0.317	6.53
36.0	0.436	0.029	6.6	1.34	1.39	1.039	0.311	0.020	0.312	6.43
38.0	0.423	0.029	6.8	1.30	1.35	1.039	0.312	0.021	0.308	6.33
40.0	0.411	0.028	6.8	1.25	1.30	1.039	0.314	0.021	0.304	6.23
42.0	0.401	0.026	6.4	1.21	1.26	1.039	0.318	0.020	0.299	6.13
44.0	0.392	0.024	6.1	1.17	1.21	1.039	0.322	0.019	0.295	6.03
46.0	0.385	0.022	5.7	1.12	1.17	1.039	0.327	0.018	0.291	5.93
48.0	0.379	0.020	5.2	1.09	1.13	1.039	0.334	0.017	0.286	5.84
50.0	0.374	0.018	4.8	1.05	1.09	1.039	0.342	0.016	0.282	5.74
52.0	0.370	0.017	4.5	1.01	1.05	1.039	0.351	0.016	0.278	5.65
54.0	0.366	0.016	4.3	0.97	1.01	1.039	0.360	0.015	0.274	5.55
56.0	0.363	0.017	4.6	0.94	0.97	1.039	0.370	0.017	0.270	5.46
58.0	0.359	0.018	5.0	0.90	0.94	1.039	0.380	0.019	0.265	5.36
60.0	0.356	0.021	5.8	0.87	0.90	1.039	0.391	0.023	0.261	5.27
62.0	0.353	0.023	6.5	0.84	0.87	1.039	0.402	0.026	0.257	5.18
64.0	0.349	0.025	7.1	0.81	0.84	1.039	0.413	0.029	0.253	5.09
66.0	0.345	0.027	7.8	0.78	0.81	1.039	0.424	0.033	0.249	5.00
68.0	0.340	0.028	8.2	0.75	0.78	1.039	0.435	0.035	0.245	4.91
70.0	0.333	0.029	8.7	0.72	0.75	1.039	0.442	0.038	0.241	4.83
72.0	0.326	0.029	8.8	0.69	0.72	1.039	0.450	0.040	0.237	4.74
74.0	0.317	0.029	9.1	0.66	0.69	1.039	0.455	0.041	0.233	4.65
76.0	0.307	0.027	8.7	0.64	0.66	1.039	0.459	0.040	0.229	4.57
78.0	0.295	0.026	8.8	0.61	0.64	1.039	0.459	0.040	0.225	4.48
80.0	0.281	0.024	8.5	0.59	0.61	1.039	0.455	0.038	0.221	4.40
82.0	0.264	0.024	9.0	0.56	0.59	1.039	0.445	0.040	0.218	4.32
84.0	0.246	0.026	10.5	0.54	0.56	1.039	0.432	0.045	0.214	4.23
86.0	0.224	0.032	14.2	0.52	0.54	1.039	0.410	0.058	0.210	4.15
88.0	0.200	0.041	20.5	0.50	0.52	1.039	0.382	0.078	0.206	4.07
90.0	0.173	0.053	30.6	0.48	0.50	1.039	0.344	0.105	0.202	3.99
92.0	0.143	0.068	47.5	0.46	0.48	1.039	0.297	0.141	0.199	3.91
94.0	0.110	0.086	78.1	0.44	0.46	1.039	0.238	0.186	0.195	3.83
96.0	0.073	0.107	146.5	0.42	0.44	1.039	0.165	0.242	0.191	3.76
98.0	0.032	0.130	406.2	0.40	0.42	1.039	0.075	0.307	0.188	3.68
100.0	-0.012	0.156	-1300.0	0.38	0.40	1.039	-0.029	0.385	0.184	3.60

** 3 STANDARD DEVIATIONS

TABLE NO. 24

DRAG COEFFICIENT VS TIME FOR CYLINDER 6 - CAMERA DATA

NO 7 3.5 IN DIAM 9.7 PSI 17.5 IN DIAM END PLATES

PEAK OVERPRESSURE 9.7 PSI POSITIVE DURATION 233.0 MSEC

FRIEDLANDER DECAY CONSTANT = 0.83

TIME AFTER SHOCK FRONT ARRIVAL (MSEC)	DRAG PRESSURE PD (PSI)	ABSOLUTE ERROR** (PSI)	RELATIVE ERROR** (PERCENT)	DYNAMIC PRESSURE Q (PSI)	IMPACT PRESSURE QI (PSI)	RATIO (QI/Q)	DRAG COEFFICIENT CD (PD/QI)	ABSOLUTE ERROR**	FLOW MACH NO. M	REYNOLDS NO. R (X10-5)
2.0	0.800	0.207	25.9	2.35	2.45	1.039	0.326	0.084	0.391	8.29
4.0	0.768	0.187	24.3	2.28	2.37	1.039	0.323	0.078	0.386	8.17
6.0	0.739	0.168	22.8	2.21	2.30	1.039	0.321	0.073	0.382	8.06
8.0	0.710	0.150	21.2	2.14	2.22	1.039	0.318	0.067	0.377	7.94
10.0	0.682	0.134	19.7	2.07	2.15	1.039	0.316	0.062	0.372	7.83
12.0	0.655	0.119	18.2	2.01	2.08	1.039	0.313	0.057	0.367	7.72
14.0	0.629	0.105	16.8	1.94	2.02	1.039	0.311	0.052	0.363	7.60
16.0	0.604	0.093	15.4	1.88	1.95	1.039	0.308	0.047	0.358	7.49
18.0	0.581	0.082	14.1	1.82	1.89	1.039	0.306	0.043	0.353	7.38
20.0	0.558	0.072	12.9	1.76	1.83	1.039	0.304	0.039	0.349	7.27
22.0	0.536	0.063	11.9	1.70	1.77	1.039	0.302	0.036	0.344	7.17
24.0	0.514	0.056	11.0	1.65	1.71	1.039	0.300	0.033	0.339	7.06
26.0	0.493	0.051	10.4	1.59	1.65	1.039	0.297	0.031	0.335	6.95
28.0	0.474	0.047	10.0	1.54	1.60	1.039	0.295	0.029	0.330	6.85
30.0	0.455	0.044	9.8	1.49	1.55	1.039	0.293	0.029	0.326	6.74
32.0	0.436	0.043	10.0	1.44	1.49	1.039	0.291	0.029	0.321	6.64
34.0	0.419	0.044	10.5	1.39	1.44	1.039	0.289	0.030	0.317	6.53
36.0	0.402	0.044	10.9	1.34	1.39	1.039	0.287	0.031	0.312	6.43
38.0	0.386	0.044	11.4	1.30	1.35	1.039	0.285	0.032	0.308	6.33
40.0	0.371	0.045	12.1	1.25	1.30	1.039	0.284	0.034	0.304	6.23
42.0	0.357	0.045	12.7	1.21	1.26	1.039	0.283	0.036	0.299	6.13
44.0	0.343	0.045	13.2	1.17	1.21	1.039	0.282	0.037	0.295	6.03
46.0	0.330	0.045	13.8	1.12	1.17	1.039	0.281	0.039	0.291	5.93
48.0	0.317	0.045	14.2	1.09	1.13	1.039	0.280	0.039	0.286	5.84
50.0	0.306	0.044	14.6	1.05	1.09	1.039	0.280	0.041	0.282	5.74
52.0	0.295	0.043	14.8	1.01	1.05	1.039	0.280	0.041	0.278	5.65
54.0	0.284	0.042	14.9	0.97	1.01	1.039	0.279	0.041	0.274	5.55
56.0	0.274	0.041	15.0	0.94	0.97	1.039	0.280	0.042	0.270	5.46
58.0	0.264	0.039	14.9	0.90	0.94	1.039	0.280	0.042	0.265	5.36
60.0	0.255	0.038	14.9	0.87	0.90	1.039	0.281	0.042	0.261	5.27
62.0	0.247	0.036	14.8	0.84	0.87	1.039	0.282	0.041	0.257	5.18
64.0	0.239	0.034	14.5	0.81	0.84	1.039	0.283	0.041	0.253	5.09
66.0	0.231	0.033	14.4	0.78	0.81	1.039	0.285	0.041	0.249	5.00
68.0	0.224	0.032	14.2	0.75	0.78	1.039	0.287	0.040	0.245	4.91
70.0	0.217	0.030	14.0	0.72	0.75	1.039	0.288	0.040	0.241	4.83
72.0	0.210	0.029	14.0	0.69	0.72	1.039	0.290	0.040	0.237	4.74
74.0	0.204	0.028	14.0	0.66	0.69	1.039	0.293	0.041	0.233	4.65
76.0	0.197	0.028	14.3	0.64	0.66	1.039	0.296	0.042	0.229	4.57
78.0	0.191	0.028	14.7	0.61	0.64	1.039	0.297	0.043	0.225	4.48
80.0	0.185	0.028	15.2	0.59	0.61	1.039	0.301	0.045	0.221	4.40
82.0	0.180	0.029	16.2	0.56	0.59	1.039	0.305	0.049	0.218	4.32
84.0	0.175	0.030	17.2	0.54	0.56	1.039	0.309	0.053	0.214	4.23
86.0	0.172	0.030	18.0	0.52	0.54	1.039	0.315	0.056	0.210	4.15
88.0	0.167	0.031	19.0	0.50	0.52	1.039	0.320	0.061	0.206	4.07
90.0	0.163	0.033	20.3	0.48	0.50	1.039	0.326	0.066	0.202	3.99
92.0	0.160	0.034	21.2	0.46	0.48	1.039	0.333	0.070	0.199	3.91
94.0	0.157	0.035	22.6	0.44	0.46	1.039	0.340	0.077	0.195	3.83
96.0	0.153	0.036	23.4	0.42	0.44	1.039	0.347	0.081	0.191	3.76
98.0	0.150	0.036	24.4	0.40	0.42	1.039	0.355	0.087	0.188	3.68
100.0	0.147	0.037	25.3	0.38	0.40	1.039	0.364	0.092	0.184	3.60
102.0	0.144	0.037	25.9	0.37	0.38	1.039	0.373	0.096	0.181	3.53
104.0	0.141	0.037	26.4	0.35	0.36	1.039	0.382	0.101	0.177	3.45
106.0	0.138	0.037	26.8	0.33	0.35	1.039	0.391	0.105	0.173	3.38
108.0	0.135	0.036	26.9	0.32	0.33	1.039	0.401	0.108	0.170	3.31
110.0	0.132	0.035	27.1	0.30	0.32	1.039	0.410	0.111	0.166	3.23
112.0	0.128	0.035	27.6	0.29	0.30	1.039	0.419	0.115	0.163	3.16
114.0	0.125	0.035	27.9	0.28	0.29	1.039	0.430	0.120	0.160	3.09
116.0	0.122	0.035	28.7	0.26	0.27	1.039	0.439	0.126	0.156	3.02
118.0	0.119	0.035	29.6	0.25	0.26	1.039	0.450	0.133	0.153	2.95
120.0	0.116	0.036	31.5	0.24	0.25	1.039	0.461	0.145	0.149	2.88
122.0	0.114	0.038	33.8	0.23	0.24	1.039	0.474	0.160	0.146	2.81
124.0	0.111	0.041	37.0	0.22	0.22	1.039	0.487	0.181	0.143	2.74
126.0	0.109	0.044	40.9	0.20	0.21	1.039	0.503	0.206	0.139	2.68
128.0	0.105	0.049	46.9	0.19	0.20	1.039	0.513	0.240	0.136	2.61
130.0	0.103	0.056	54.4	0.18	0.19	1.039	0.527	0.287	0.133	2.55
132.0	0.099	0.064	64.4	0.17	0.18	1.039	0.537	0.346	0.130	2.48

** 3 STANDARD DEVIATIONS

TABLE NO. 25

DRAG COEFFICIENT VS TIME FOR CYLINDER 7 - VELOCITY TRANSDUCER DATA

NO 7 3.5 IN DIAM 9.7 PSI 17.5 IN DIAM END PLATES

PEAK OVERPRESSURE 9.7 PSI POSITIVE DURATION 233.0 MSEC

FRIEDLANDER DECAY CONSTANT = 0.83

TIME AFTER SHOCK FRONT ARRIVAL (MSEC)	DRAG PRESSURE PD (PSI)	ABSOLUTE ERROR** (PSI)	RELATIVE ERROR** (PERCENT)	DYNAMIC PRESSURE Q (PSI)	IMPACT PRESSURE QI (PSI)	RATIO (QI/Q)	DRAG COEFFICIENT CD (PD/QI)	ABSOLUTE ERROR**	FLOW MACH NO. M	REYNOLDS NO. R (X10-5)
2.0	0.649	0.068	10.4	2.35	2.45	1.039	0.264	0.027	0.391	8.29
4.0	0.639	0.065	10.1	2.28	2.37	1.039	0.269	0.027	0.386	8.17
6.0	0.628	0.063	10.0	2.21	2.30	1.039	0.272	0.027	0.382	8.06
8.0	0.617	0.060	9.7	2.14	2.22	1.039	0.276	0.026	0.377	7.94
10.0	0.607	0.057	9.3	2.07	2.15	1.039	0.281	0.026	0.372	7.83
12.0	0.596	0.054	9.0	2.01	2.08	1.039	0.285	0.025	0.367	7.72
14.0	0.585	0.051	8.7	1.94	2.02	1.039	0.289	0.025	0.363	7.60
16.0	0.575	0.048	8.3	1.88	1.95	1.039	0.293	0.024	0.358	7.49
18.0	0.564	0.045	7.9	1.82	1.89	1.039	0.297	0.023	0.353	7.38
20.0	0.553	0.043	7.7	1.76	1.83	1.039	0.301	0.023	0.349	7.27
22.0	0.542	0.040	7.3	1.70	1.77	1.039	0.305	0.022	0.344	7.17
24.0	0.532	0.037	6.9	1.65	1.71	1.039	0.310	0.021	0.339	7.06
26.0	0.521	0.034	6.5	1.59	1.65	1.039	0.314	0.020	0.335	6.95
28.0	0.510	0.031	6.0	1.54	1.60	1.039	0.317	0.019	0.330	6.85
30.0	0.500	0.029	5.8	1.49	1.55	1.039	0.322	0.018	0.326	6.74
32.0	0.489	0.026	5.3	1.44	1.49	1.039	0.326	0.017	0.321	6.64
34.0	0.478	0.023	4.8	1.39	1.44	1.039	0.330	0.015	0.317	6.53
36.0	0.468	0.021	4.4	1.34	1.39	1.039	0.334	0.015	0.312	6.43
38.0	0.457	0.019	4.1	1.30	1.35	1.039	0.338	0.014	0.308	6.33
40.0	0.446	0.016	3.5	1.25	1.30	1.039	0.341	0.012	0.304	6.23
42.0	0.436	0.014	3.2	1.21	1.26	1.039	0.345	0.011	0.299	6.13
44.0	0.425	0.013	3.0	1.17	1.21	1.039	0.349	0.010	0.295	6.03
46.0	0.414	0.012	2.8	1.12	1.17	1.039	0.352	0.010	0.291	5.93
48.0	0.404	0.011	2.7	1.09	1.13	1.039	0.356	0.009	0.286	5.84
50.0	0.393	0.012	3.0	1.05	1.09	1.039	0.359	0.010	0.282	5.74
52.0	0.382	0.013	3.4	1.01	1.05	1.039	0.362	0.012	0.278	5.65
54.0	0.371	0.014	3.7	0.97	1.01	1.039	0.365	0.013	0.274	5.55
56.0	0.361	0.016	4.4	0.94	0.97	1.039	0.368	0.016	0.270	5.46
58.0	0.350	0.018	5.1	0.90	0.94	1.039	0.370	0.019	0.265	5.36
60.0	0.339	0.021	6.1	0.87	0.90	1.039	0.372	0.023	0.261	5.27
62.0	0.329	0.023	6.9	0.84	0.87	1.039	0.375	0.026	0.257	5.18
64.0	0.318	0.026	8.1	0.81	0.84	1.039	0.376	0.030	0.253	5.09
66.0	0.307	0.028	9.1	0.78	0.81	1.039	0.378	0.034	0.249	5.00
68.0	0.297	0.031	10.4	0.75	0.78	1.039	0.380	0.039	0.245	4.91
70.0	0.286	0.034	11.8	0.72	0.75	1.039	0.380	0.045	0.241	4.83
72.0	0.275	0.036	13.0	0.69	0.72	1.039	0.380	0.049	0.237	4.74
74.0	0.265	0.039	14.7	0.66	0.69	1.039	0.381	0.056	0.233	4.65
76.0	0.254	0.042	16.5	0.64	0.66	1.039	0.380	0.062	0.229	4.57
78.0	0.243	0.045	18.5	0.61	0.64	1.039	0.378	0.070	0.225	4.48
80.0	0.233	0.048	20.6	0.59	0.61	1.039	0.377	0.077	0.221	4.40
82.0	0.222	0.051	22.9	0.56	0.59	1.039	0.374	0.086	0.218	4.32
84.0	0.211	0.053	25.1	0.54	0.56	1.039	0.371	0.093	0.214	4.23
86.0	0.200	0.056	28.0	0.52	0.54	1.039	0.366	0.102	0.210	4.15
88.0	0.190	0.059	31.0	0.50	0.52	1.039	0.363	0.112	0.206	4.07
90.0	0.179	0.062	34.6	0.48	0.50	1.039	0.356	0.123	0.202	3.99
92.0	0.168	0.065	38.6	0.46	0.48	1.039	0.349	0.135	0.199	3.91
94.0	0.158	0.068	43.0	0.44	0.46	1.039	0.342	0.147	0.195	3.83
96.0	0.147	0.071	48.2	0.42	0.44	1.039	0.333	0.160	0.191	3.76
98.0	0.136	0.074	54.4	0.40	0.42	1.039	0.321	0.175	0.188	3.68
100.0	0.126	0.077	61.1	0.38	0.40	1.039	0.311	0.190	0.184	3.60
102.0	0.115	0.079	68.6	0.37	0.38	1.039	0.297	0.204	0.181	3.53
104.0	0.104	0.082	78.8	0.35	0.36	1.039	0.281	0.221	0.177	3.45

** 3 STANDARD DEVIATIONS

TABLE NO. 26

DRAG COEFFICIENT VS TIME FOR CYLINDER 7 - CAMERA DATA

TABLE NO. 27

SUMMARY OF RESULTS FOR EACH CYLINDER

Cylinder Number	Type of Data*	Useful Data Obtained	Remarks
1	V.T. (East)	No	Cylinder failed to undergo free flight due to sidewise blast anomaly at 20 psi peak overpressure location acting on large end plates.
	V.T. (West)	No	
	Cam. (West)	No	
2	V.T. (East)	No	- East magnet broke shortly after shock arrival.
	V.T. (West)	Yes	- Poor signal/noise due to error in circuit controlling sensitivity.
	Cam. (West)	No	- Non-constant film speed; violent displacement of camera post.
3	V.T. (East)	Yes	- Large amplitude 79 Hz oscillations on signal produced large uncertainties in derived drag pressure.
	V.T. (West)	Yes	
	Cam. (West)	Yes	- Oscillations absent; smaller uncertainties than for V.T. data.
	Both -	-	- East-West V.T. results consistent over range of measurement. V.T. and Cam. results consistent over entire range of measurement.
4	V.T. (East)	Yes	- Moderately large 60 Hz oscillations on signals produced increased uncertainties in derived drag pressure.
	V.T. (West)	Yes	
	Cam. (West)	Yes	- Excellent data; only small corrections for camera motion.
	Both -	-	- East-West V.T. results consistent over range of measurement. V.T. and Cam. data consistent over most of range of measurement.
5	V.T. (East)	Yes	- Moderately large 60 Hz oscillations on signals; signals terminated prematurely due to contact of cylinder shaft with photomarker plate.
	V.T. (West)	Yes	
	Cam. (West)	Yes	- Excellent data; only small corrections for camera motion.
	Both -	-	- Linear drag pressure from V.T. data in agreement over most of range with (approximately) linear drag pressure from higher order fit to Cam. data.
6	V.T. (East)	Yes	- Smaller 59 Hz oscillations with irrigular fluctuations superposed.
	V.T. (West)	Yes	
	Cam. (West)	Yes	- Excellent data; larger corrections for camera motion than for Cyl. 4, 5.
	Both -	-	- East-West V.T. results consistent over entire range of measurement. V.T. and Cam. data consistent over most of range of measurement.
7	V.T. (East)	Yes	- Smaller 59 Hz oscillations with irregular fluctations superposed. Uncertainties in drag pressure competitive with Cam. data.
	V.T. (West)	Yes	
	Cam. (West)	Yes	- Large corrections for camera post motion forced linear fit to drag pressure.
	Both -	-	- East-West V.T. results consistent over entire range of measurement. V.T. and Cam. data consistent over most of range of measurement.

* V.T. - Velocity Transducer. Cam. - High-Speed Camera.
(East-West) - refers to end of cylinder where measurement recorded.
Both - Comments refer to both V.T. and Cam. data.

TABLE NO. 28

SUMMARY OF BEST VALUES FOR DRAG COEFFICIENT*

Cylinder Diameter (inches)	Time After Shock Arrival (msec)	Average Reynolds Number	Average Drag Coefficient
3.5	3-25	7.66	0.274 ± 0.054**
	25-50	6.34	0.255 ± 0.042
	50-75	5.14	0.251 ± 0.049
	75-100	4.08	0.282 ± 0.065
	100-125	3.13	0.382 ± 0.148
9.5	3-25	15.5	0.508 ± 0.106
	25-50	13.3	0.482 ± 0.085
	50-75	11.3	0.455 ± 0.106
	75-100	9.4	0.401 ± 0.160
18.0	3-25	39.4	0.420 ± 0.121
	25-50	32.6	0.449 ± 0.099
	50-75	26.5	0.625 ± 0.137

* Data plotted in Figure 28.

** 3 Standard deviations of uncertainty (99% confidence interval)

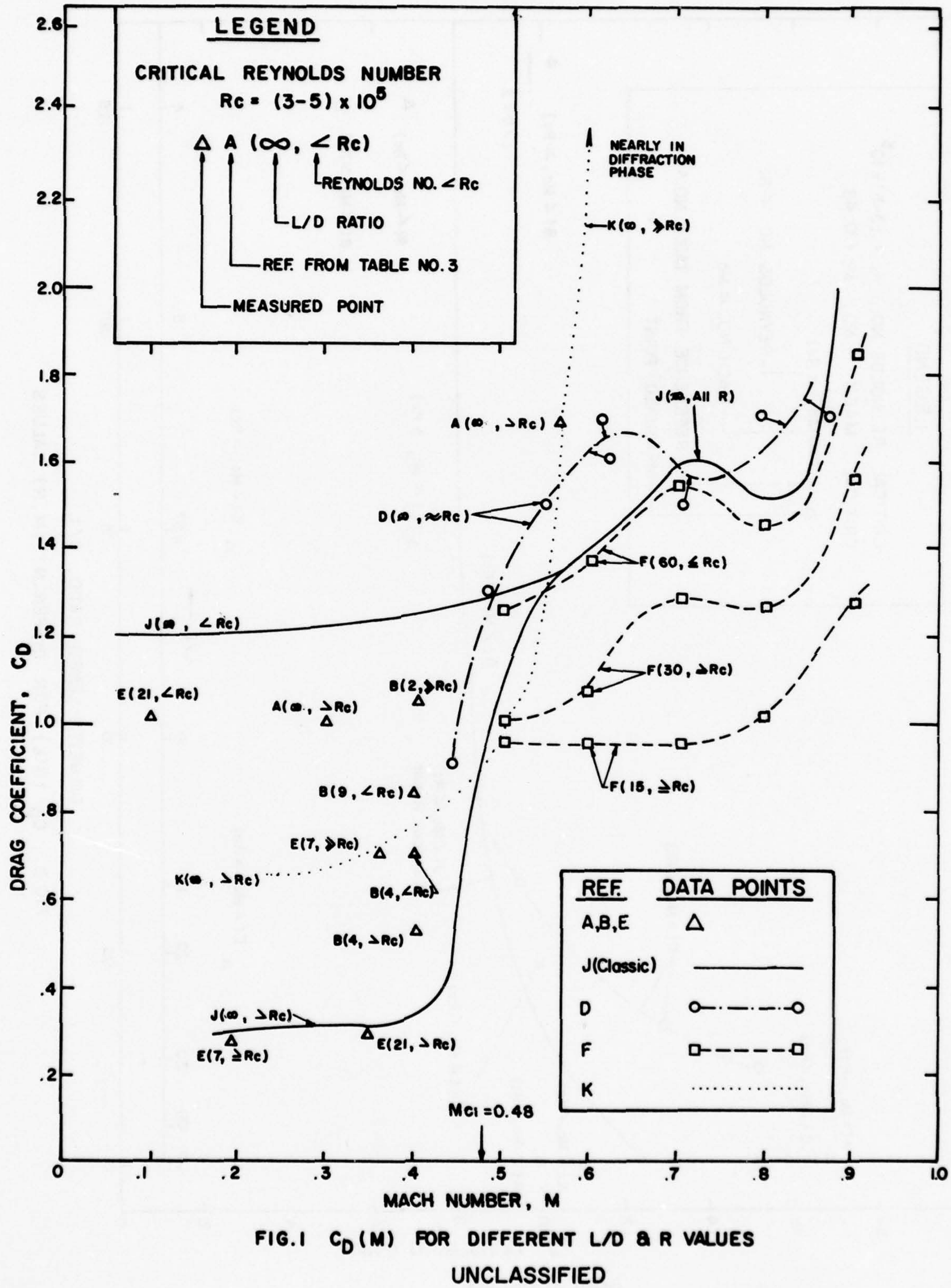

FIG. 1 C_D (M) FOR DIFFERENT L/D & R VALUES

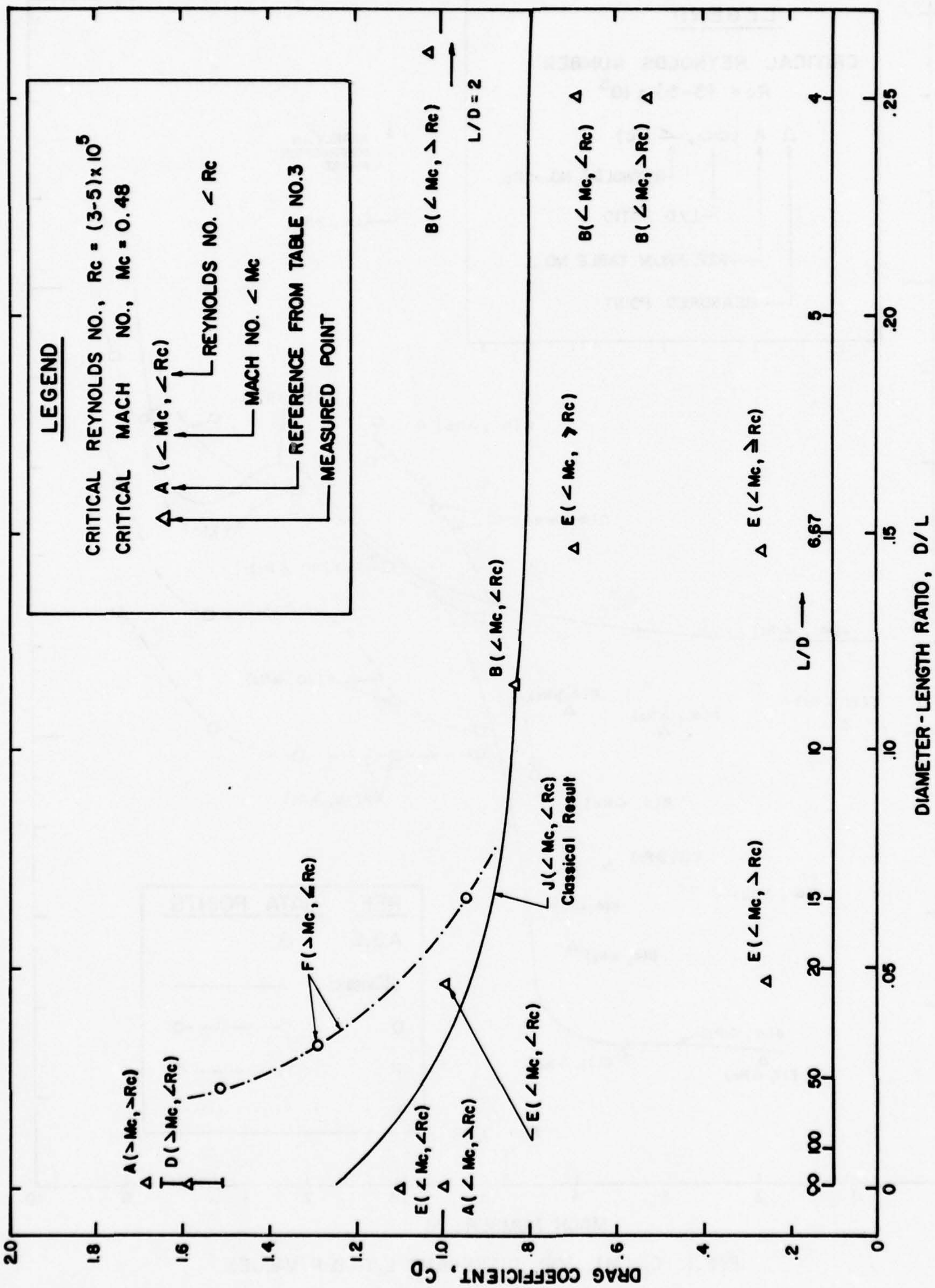

FIG. 2 C_D (D/L) FOR DIFFERENT (M, R) VALUES

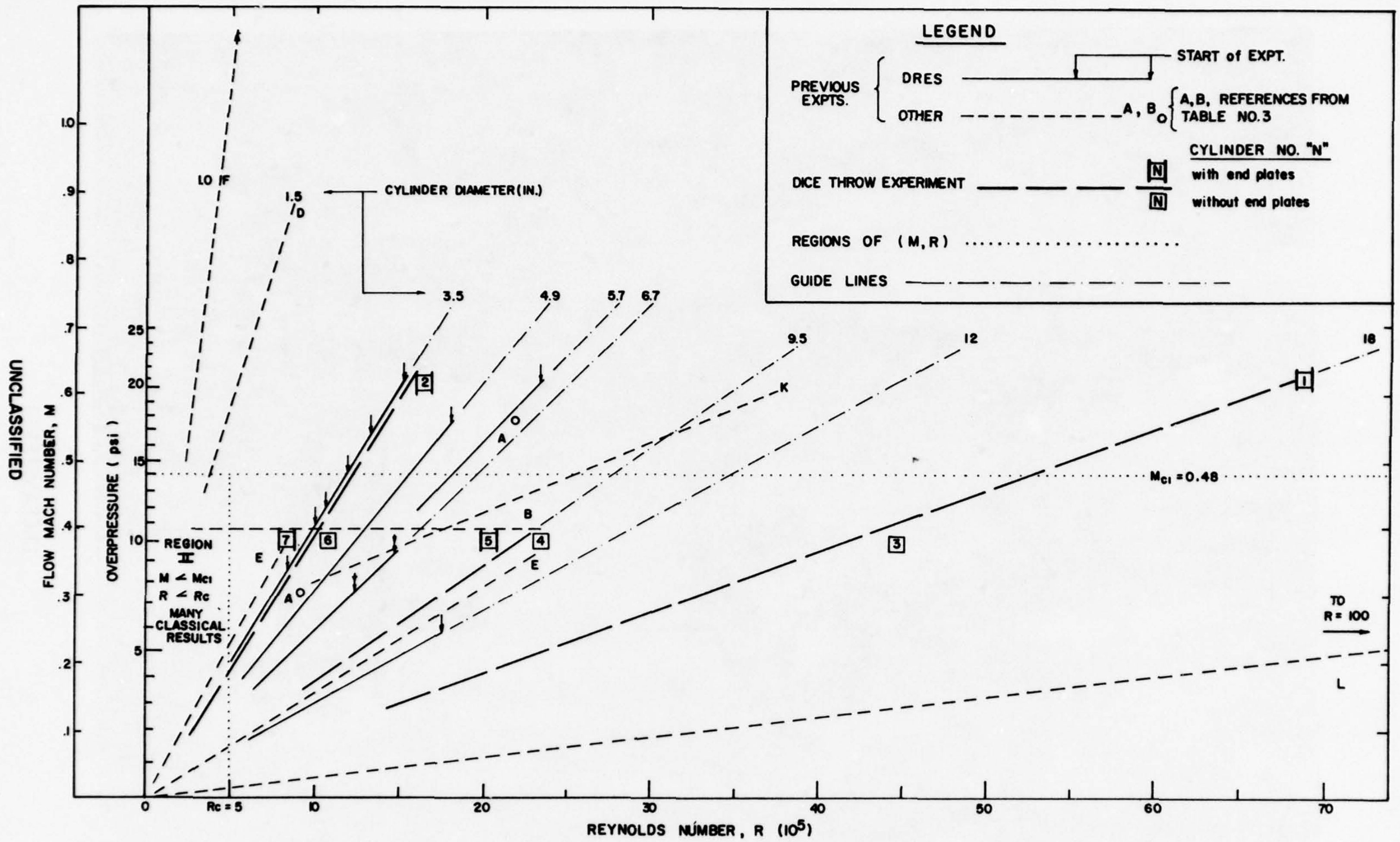

FIG. 3 RANGE OF (M,R) VALUES INCLUDED IN ALL PREVIOUS MEASUREMENTS & IN DICE THROW

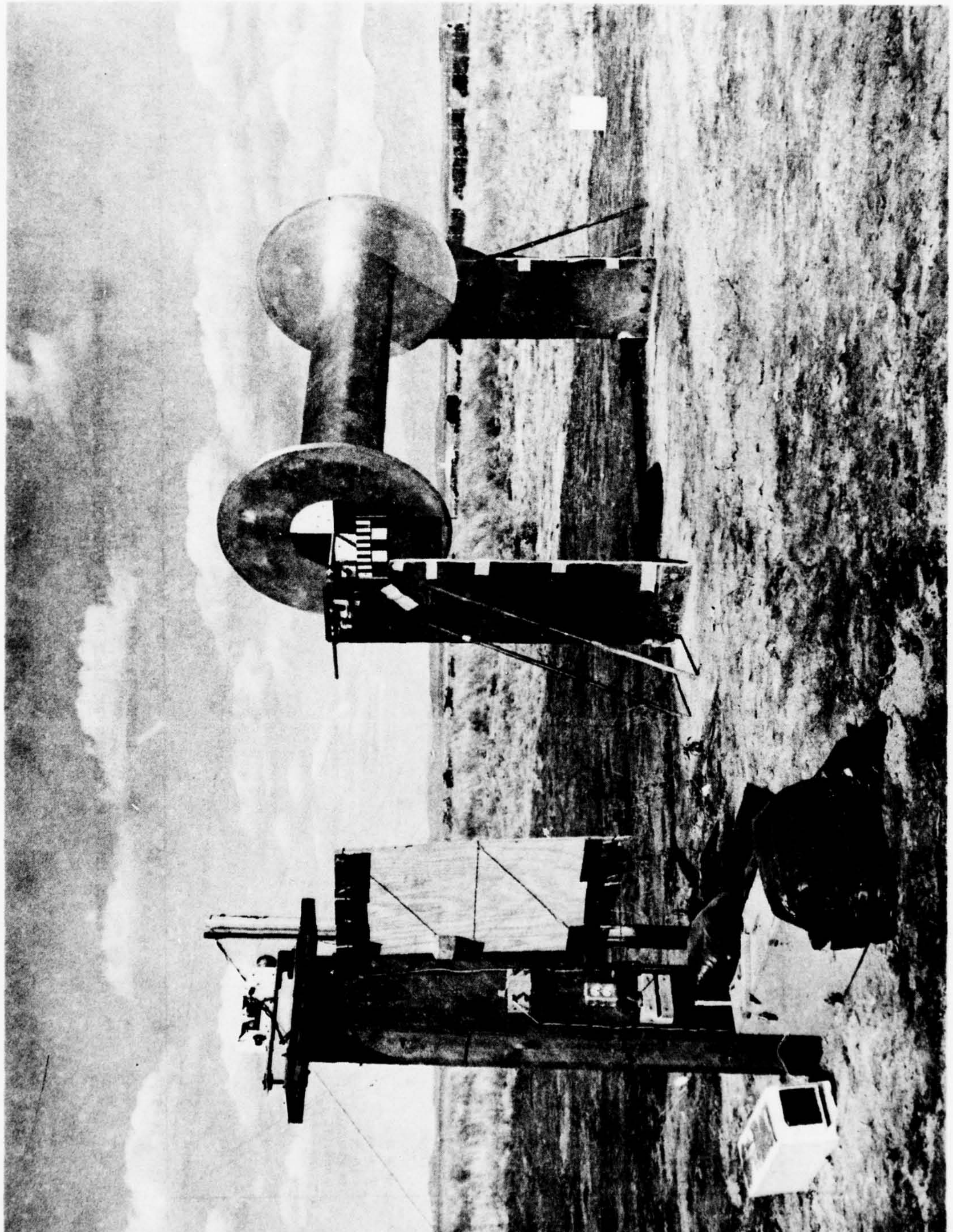

FIG. 4 CYLINDER DRAG ASSEMBLY - LOCATION 1

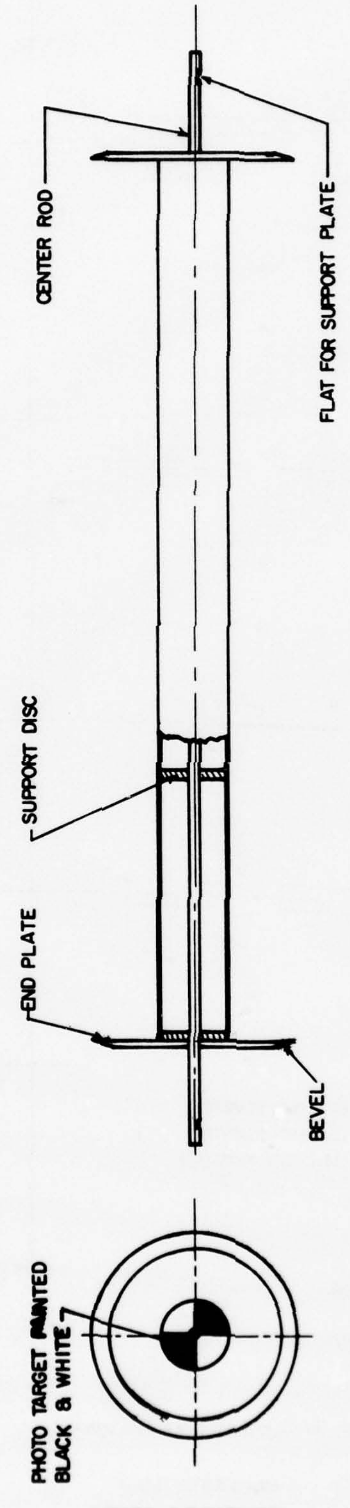

FIG. 5 MECHANICAL DESIGN OF TYPICAL CYLINDER

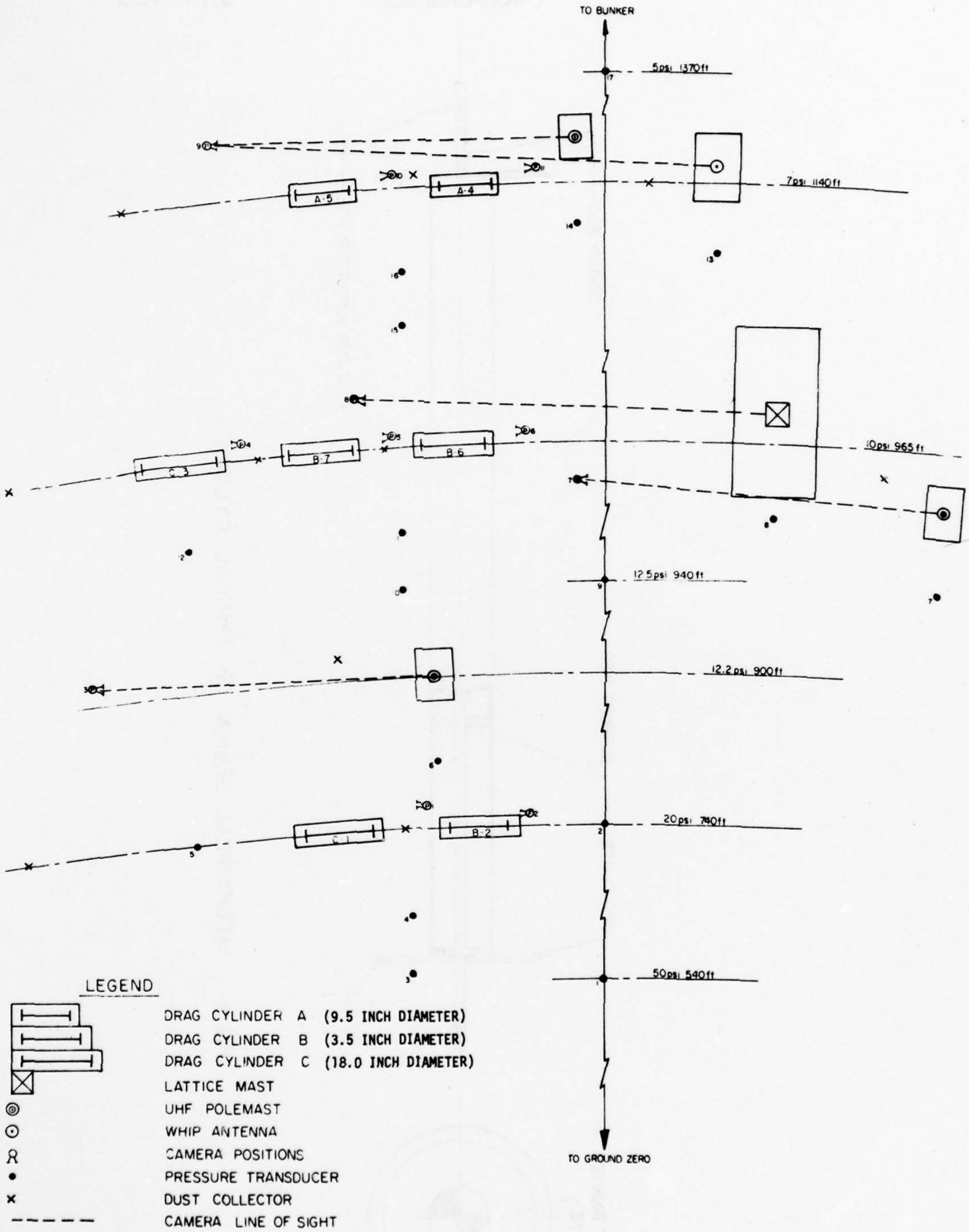

FIG. 6 LAYOUT OF CYLINDER DRAG PROJECT

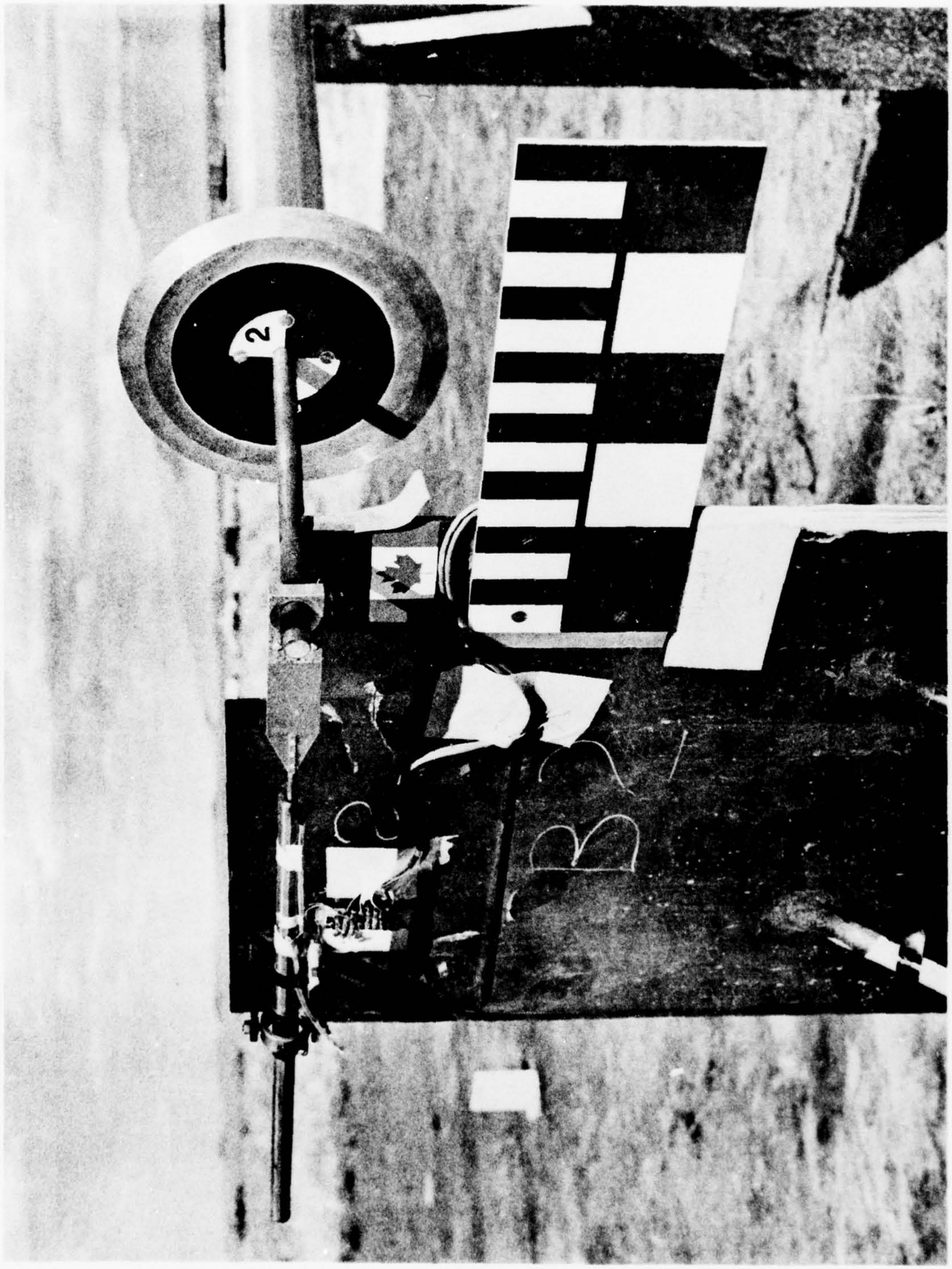

FIG. 7 CLOSE-UP VIEW OF VELOCITY TRANSDUCER ASSEMBLY
LOCATION 2

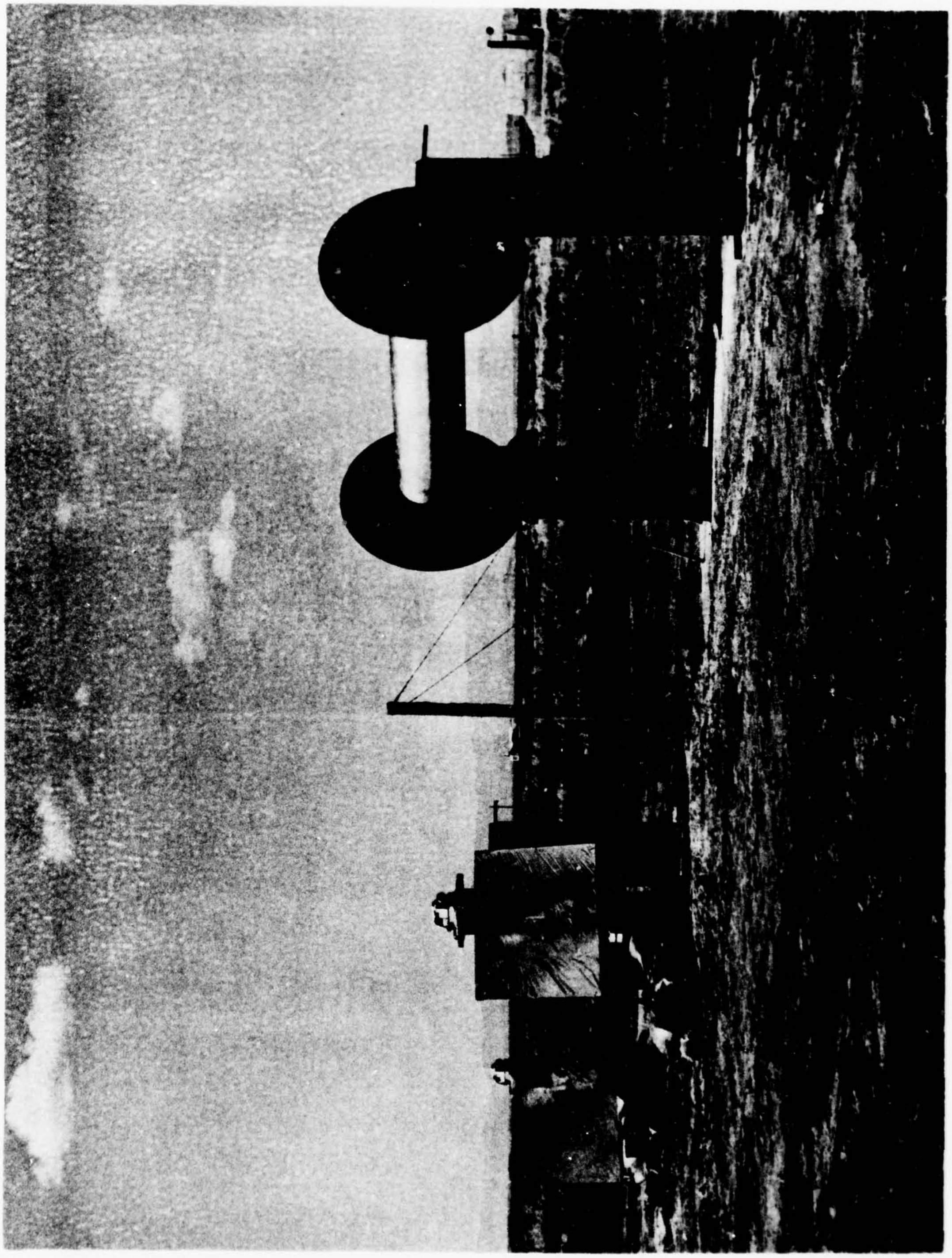

FIG. 8 PRE-SHOT VIEW SHOWING HIGH SPEED CAMERA, LIGHT REFLECTOR, AND GREASY STAKE DUST COLLECTOR - LOCATION 1

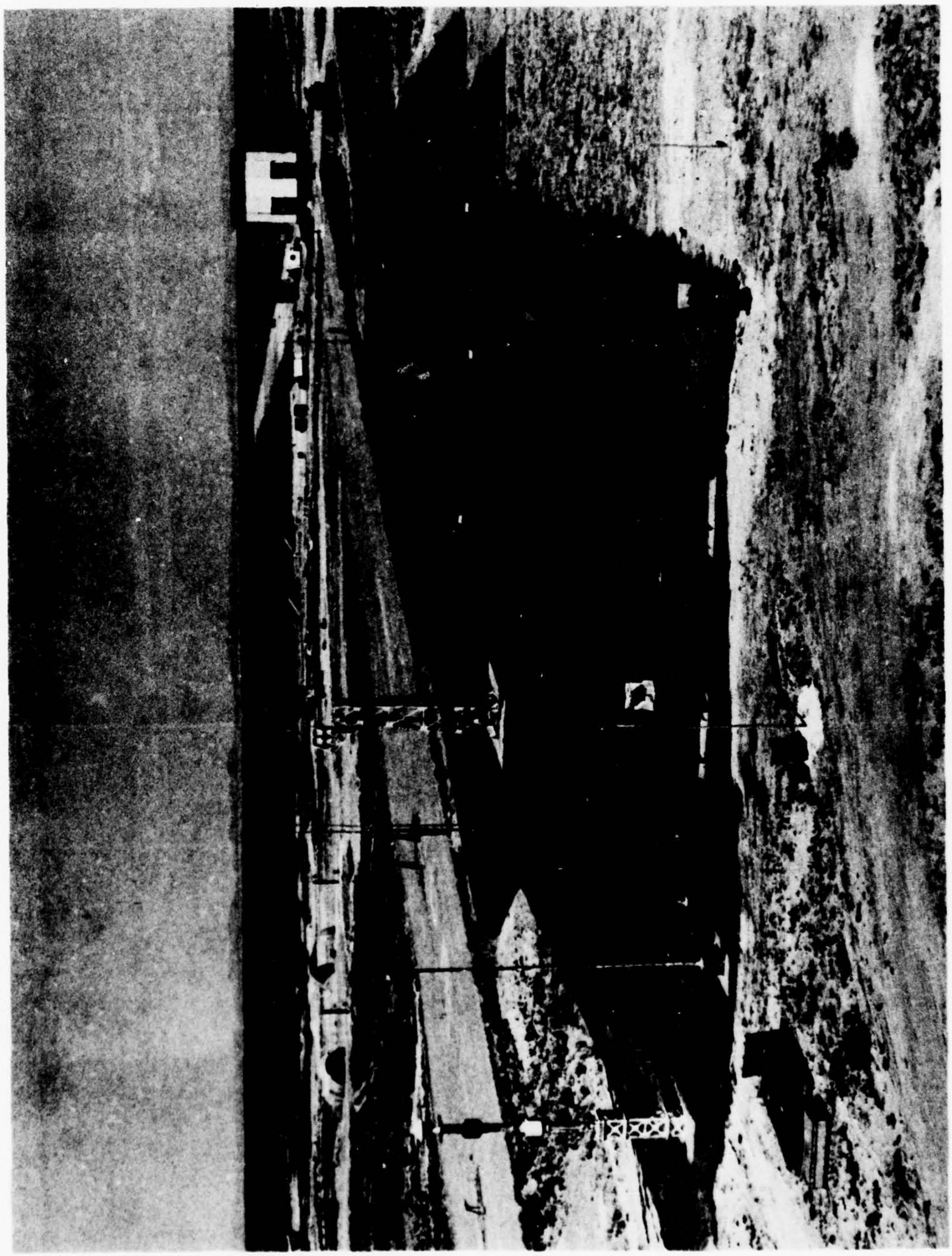

FIG. 9 PRE-SHOT VIEW OF CANADIAN SECTOR SHOWING EXTENT OF TREATED GROUND

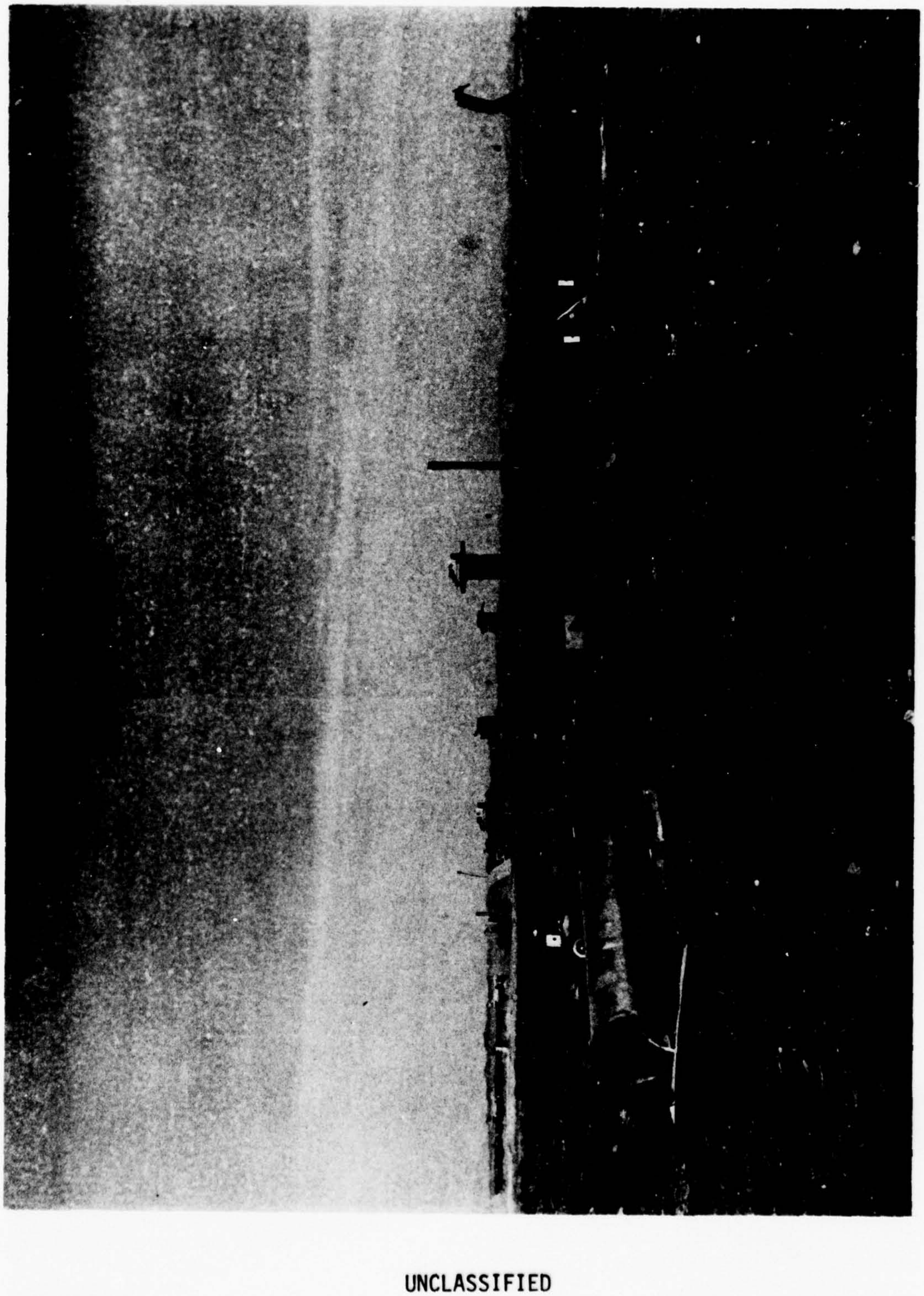

FIG. 10 CYLINDER 1 (POST-SHOT)

FIG. 11 WEST SUPPORT FOR CYLINDER 1 (POST-SHOT)

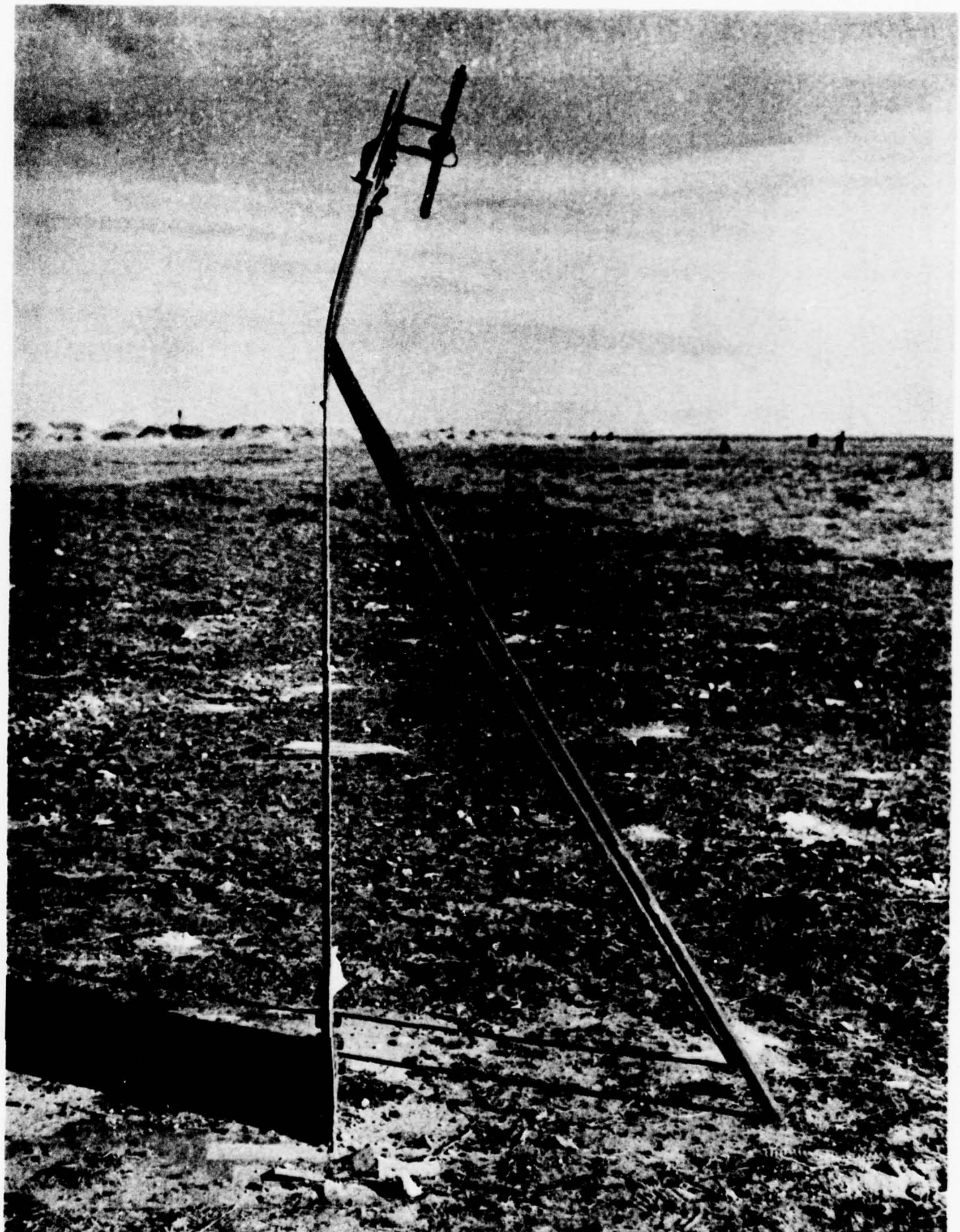

FIG. 12 EAST SUPPORT FOR CYLINDER 1 (POST-SHOT)

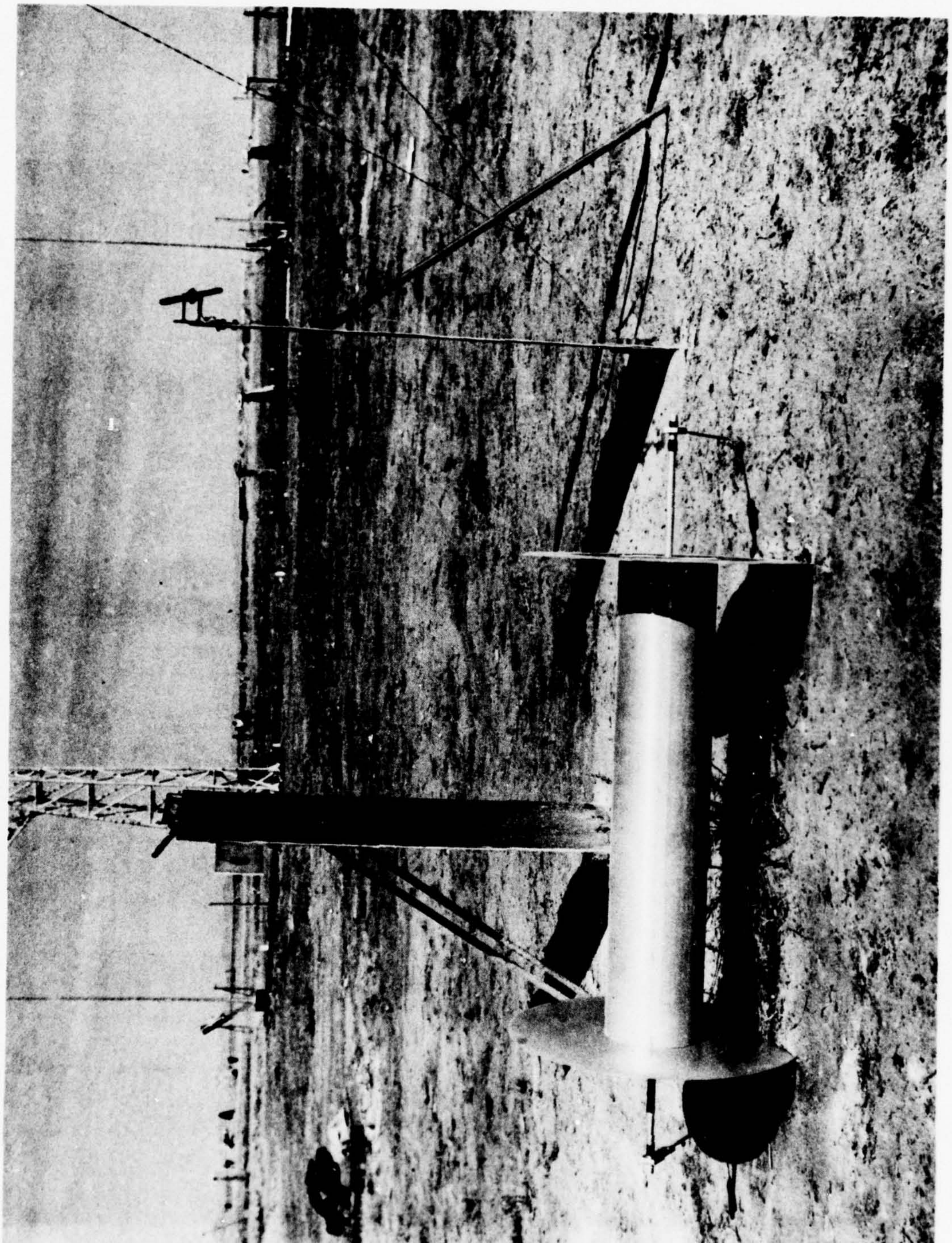

FIG. 13 CYLINDER 5 (POST-SHOT) AT 7 PSI PEAK OVERPRESSURE LOCATION SHOWING EXTENT OF LATERAL DISPLACEMENT

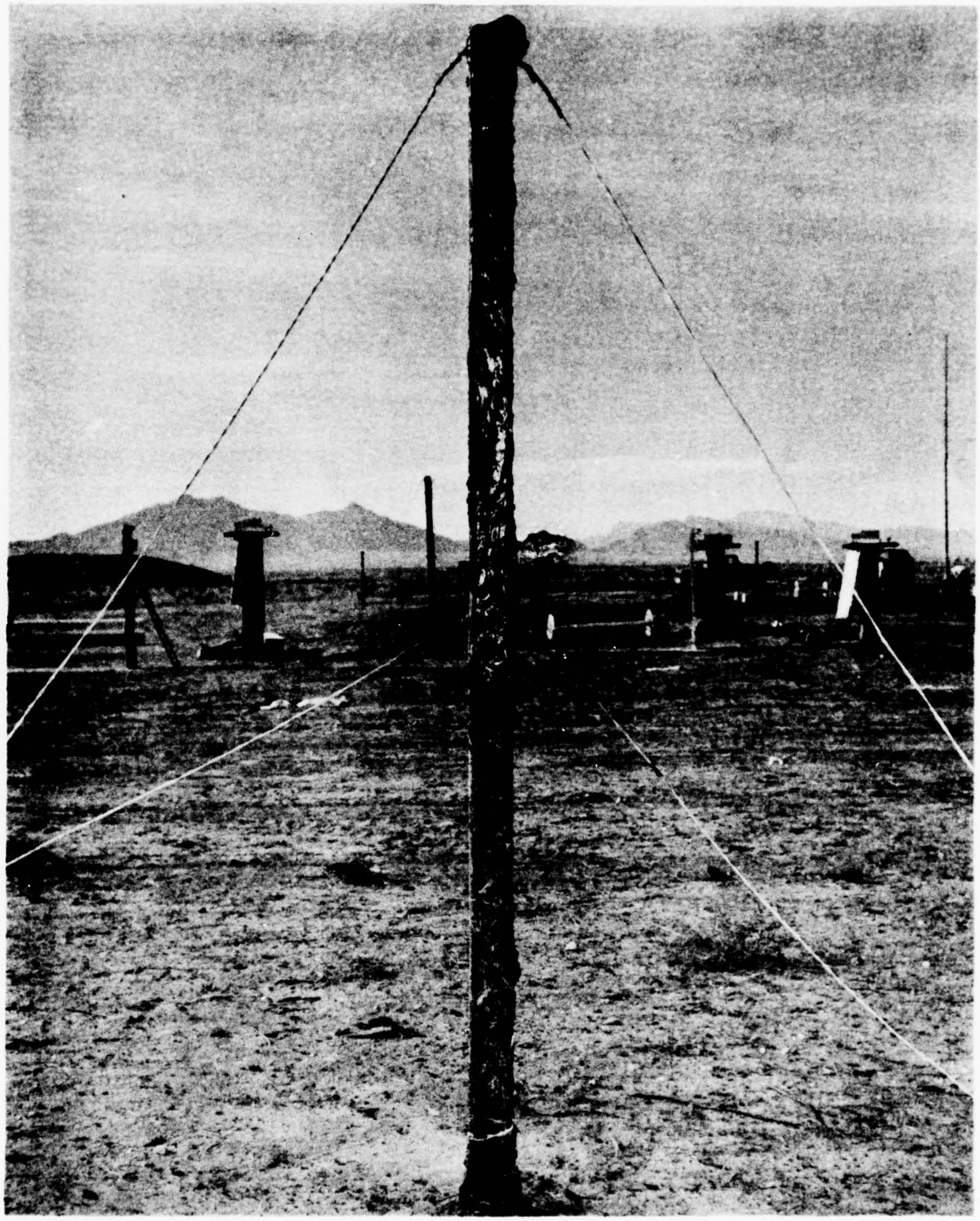

FIG. 14 GREASY STAKE DUST COLLECTOR (POST SHOT)

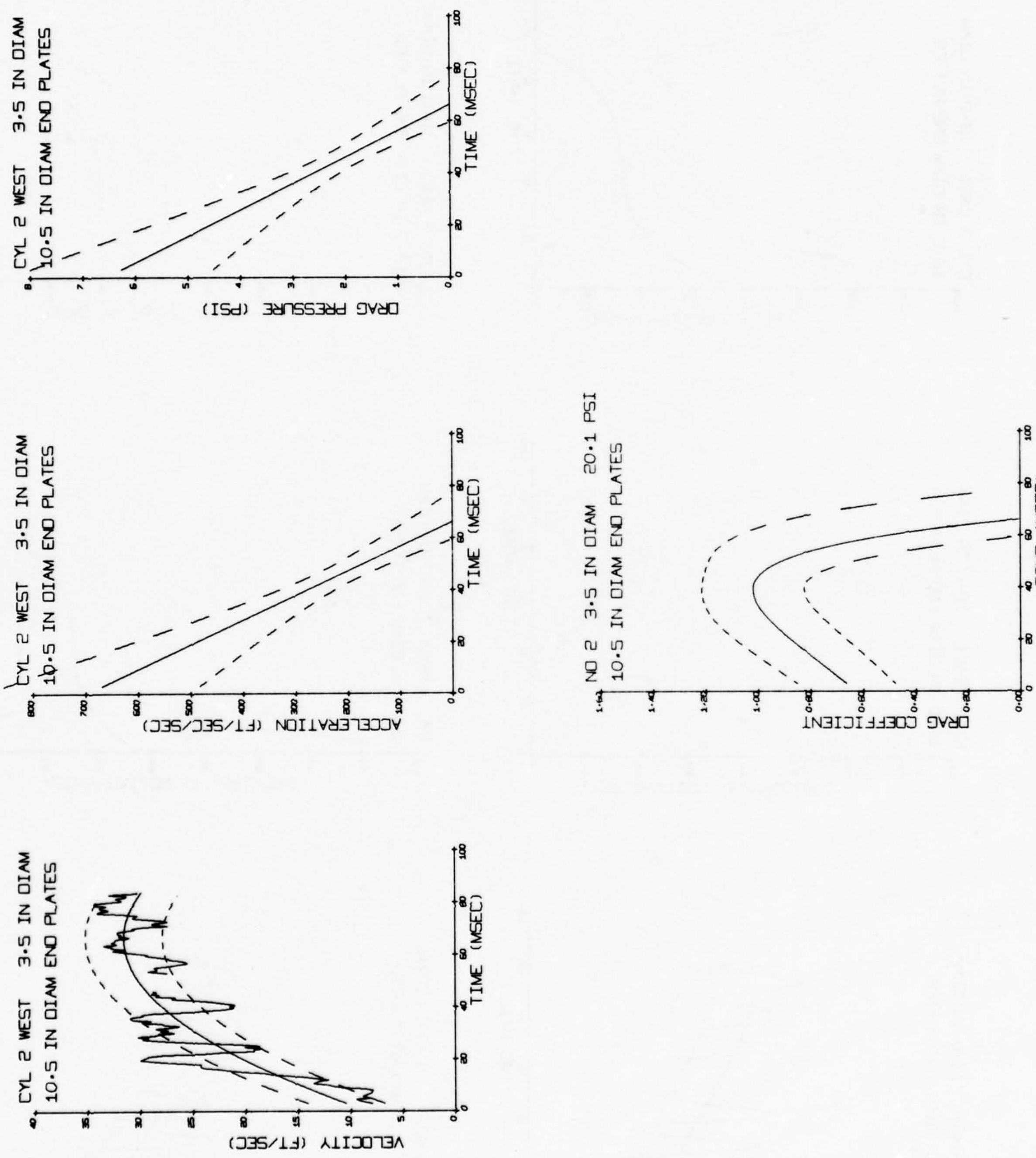

FIG. 15 CYLINDER 2 - VELOCITY TRANSDUCER DATA
(20.1 PSI PEAK OVERPRESSURE)

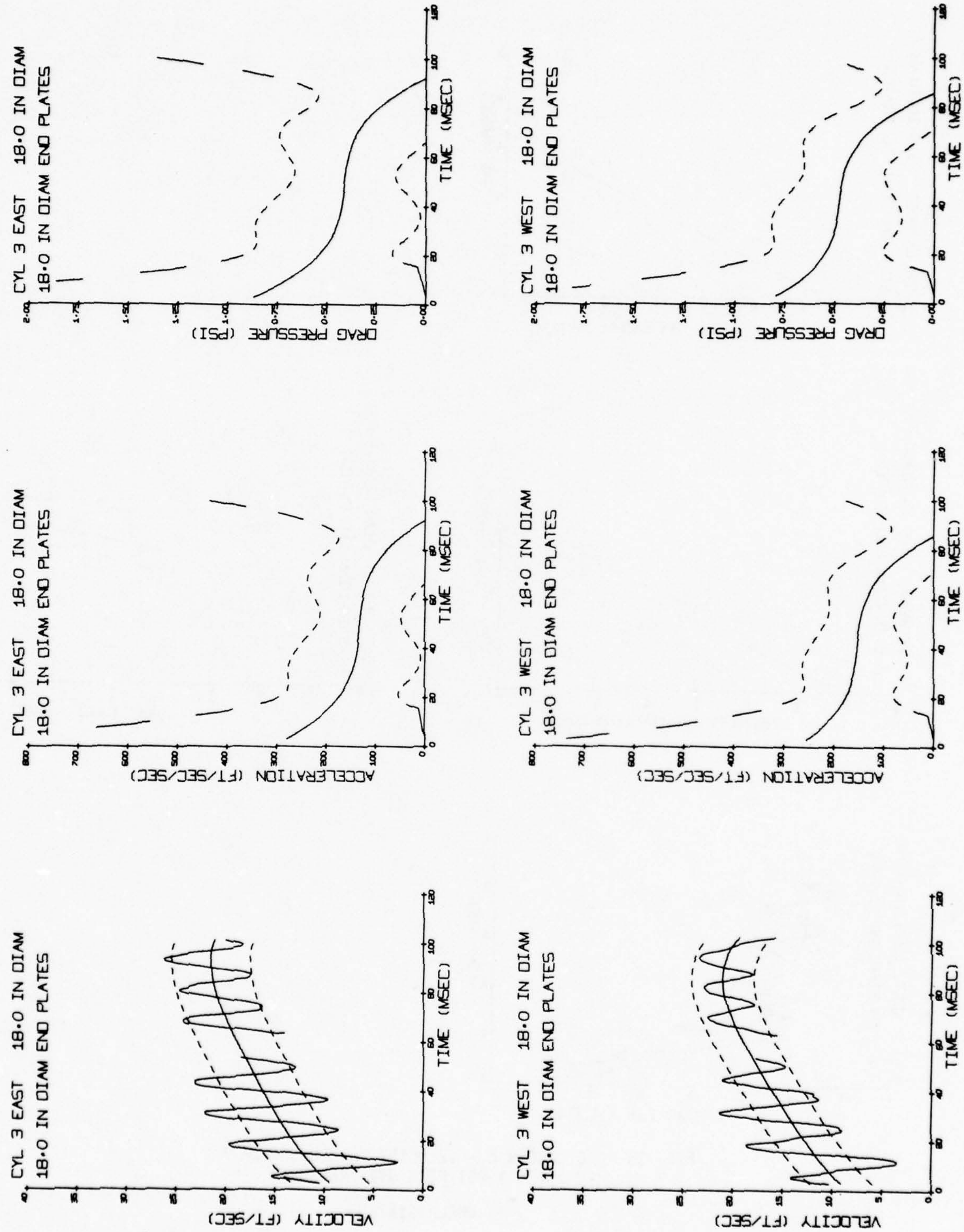

FIG. 16 CYLINDER 3 - VELOCITY TRANSDUCER DATA (9.7 PSI PEAK OVERPRESSURE)

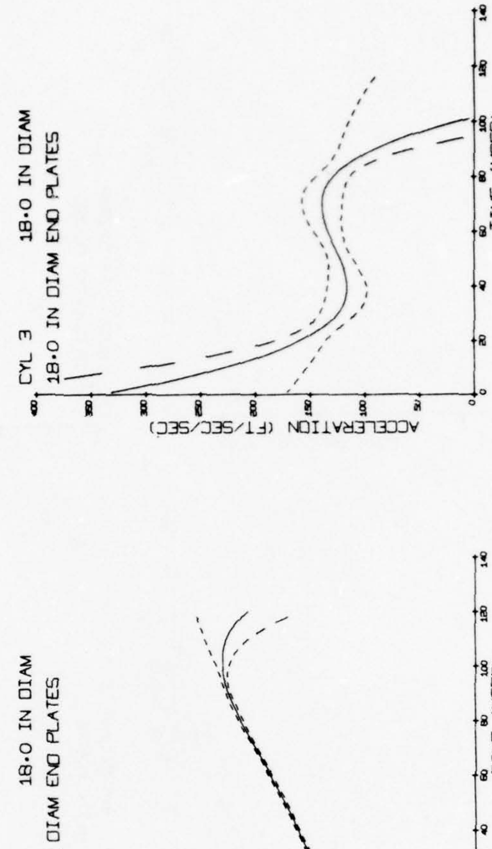

FIG. 17 CYLINDER 3 - HIGH SPEED CAMERA DATA (9.7 PSI PEAK OVERPRESSURE)

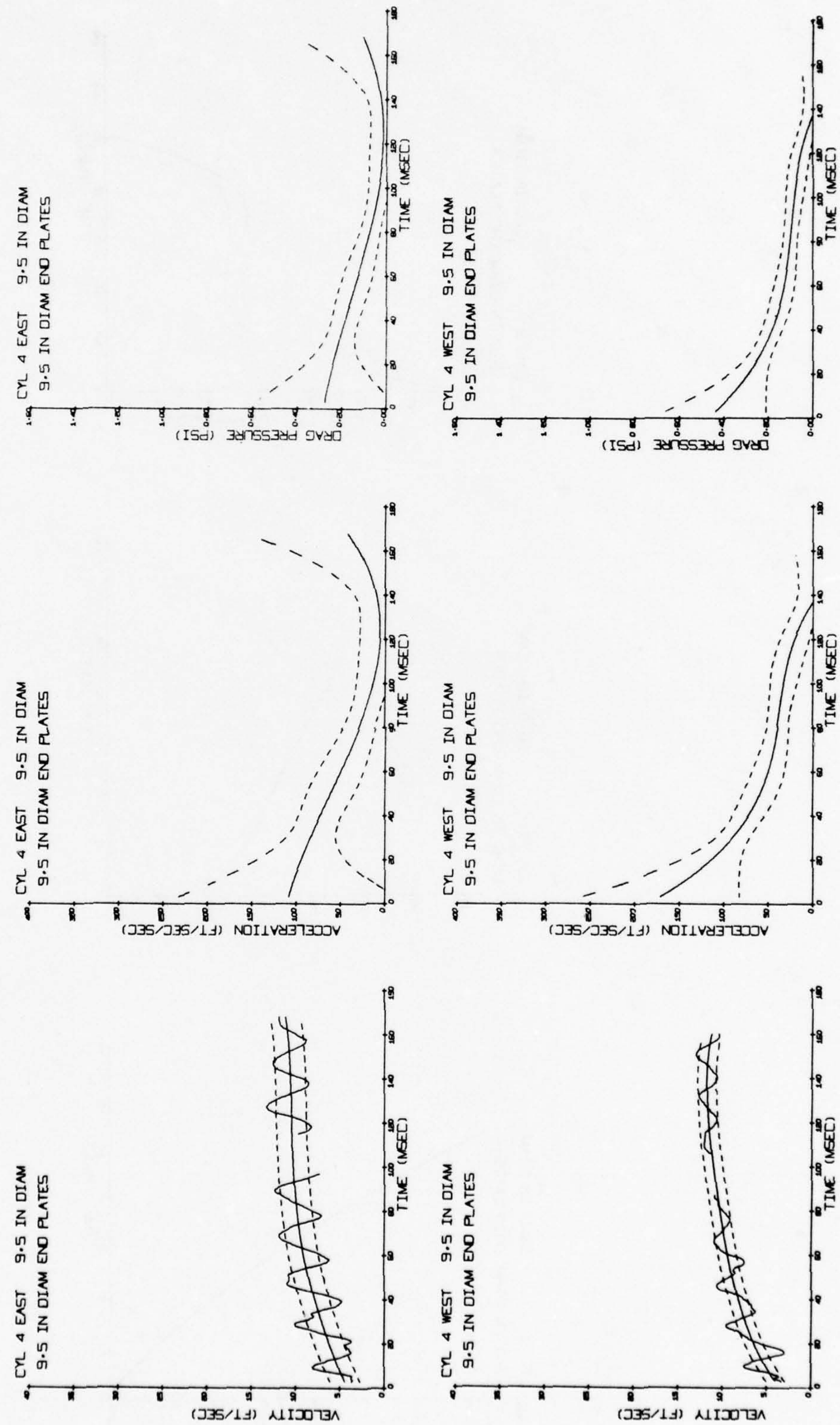

FIG. 18 CYLINDER 4 - VELOCITY TRANSDUCER DATA (6.7 PSI PEAK OVERPRESSURE)

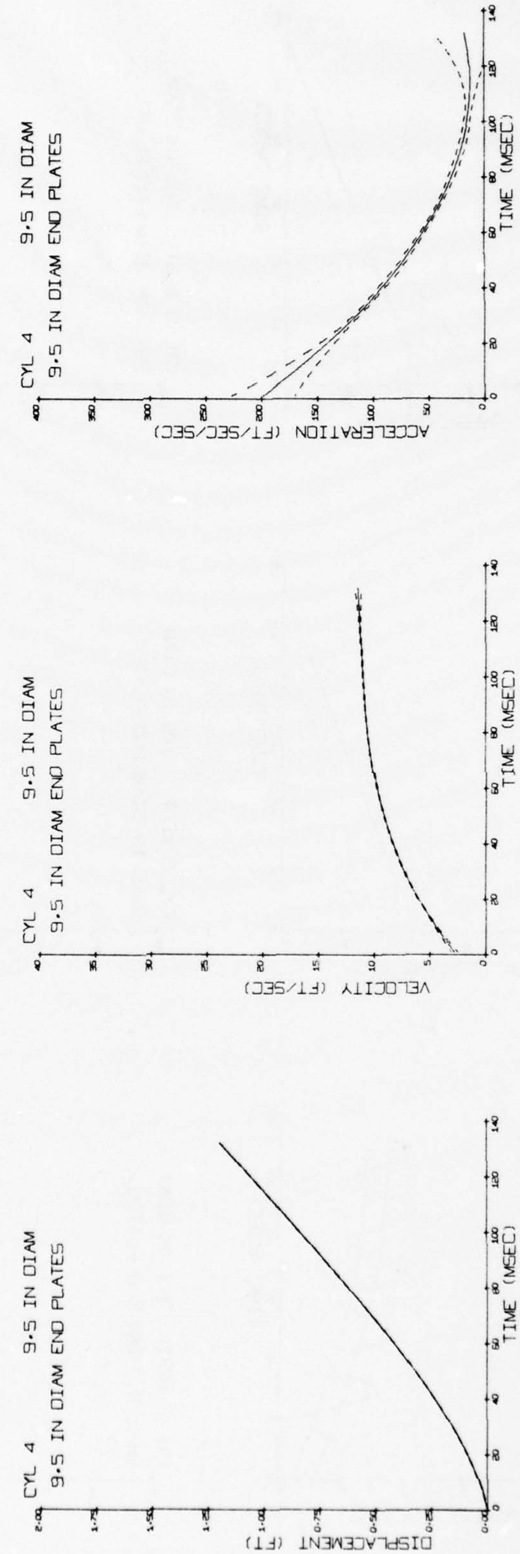

FIG. 19 CYLINDER 4 - HIGH SPEED CAMERA DATA (6.7 PSI PEAK OVERPRESSURE)

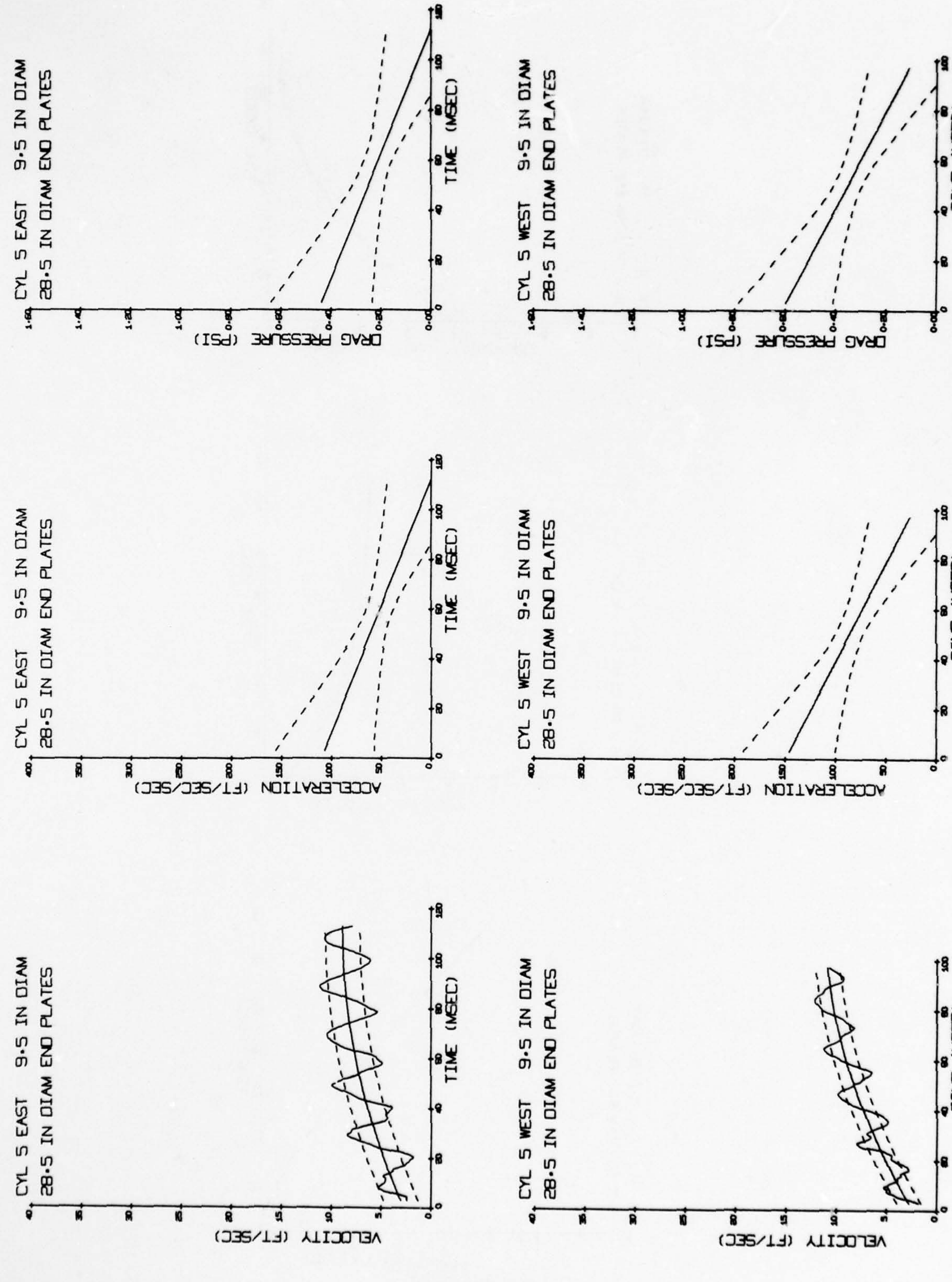

FIG. 20 CYLINDER 5 - VELOCITY TRANSDUCER DATA (6.7 PSI PEAK OVERPRESSURE)

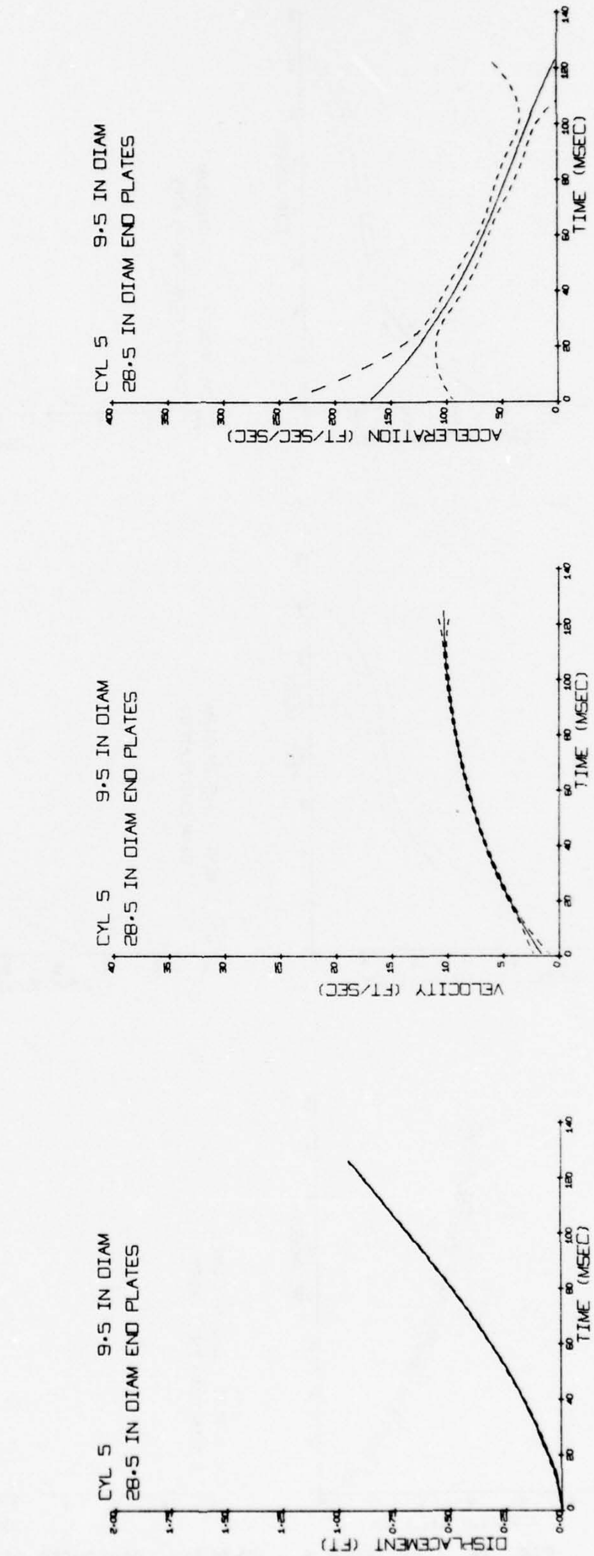

FIG. 21 CYLINDER 5 - HIGH SPEED CAMERA DATA (6.7 PSI PEAK OVERPRESSURE)

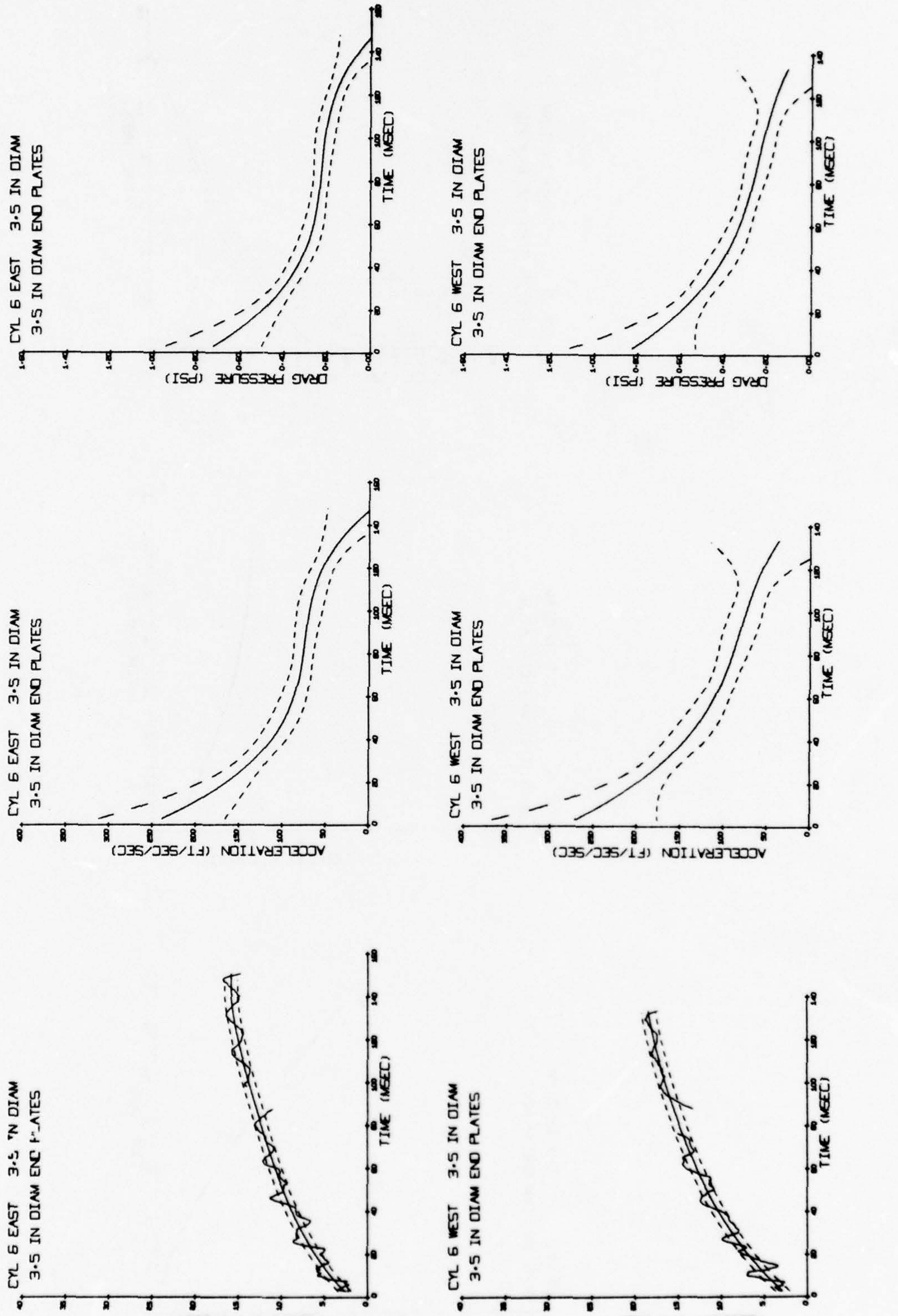

FIG. 22 CYLINDER 6 - VELOCITY TRANSDUCER DATA
(9.7 PSI PEAK OVERPRESSURE)

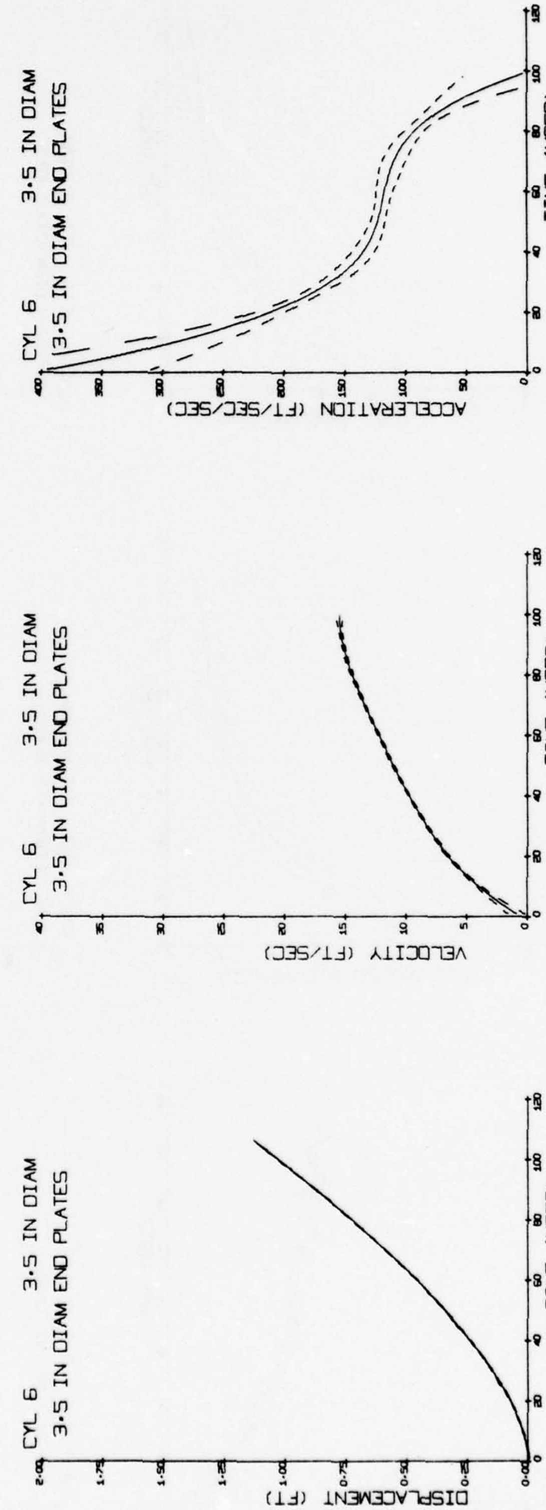

FIG. 23 CYLINDER 6 - HIGH SPEED CAMERA DATA
(9.7 PSI PEAK OVERPRESSURE)

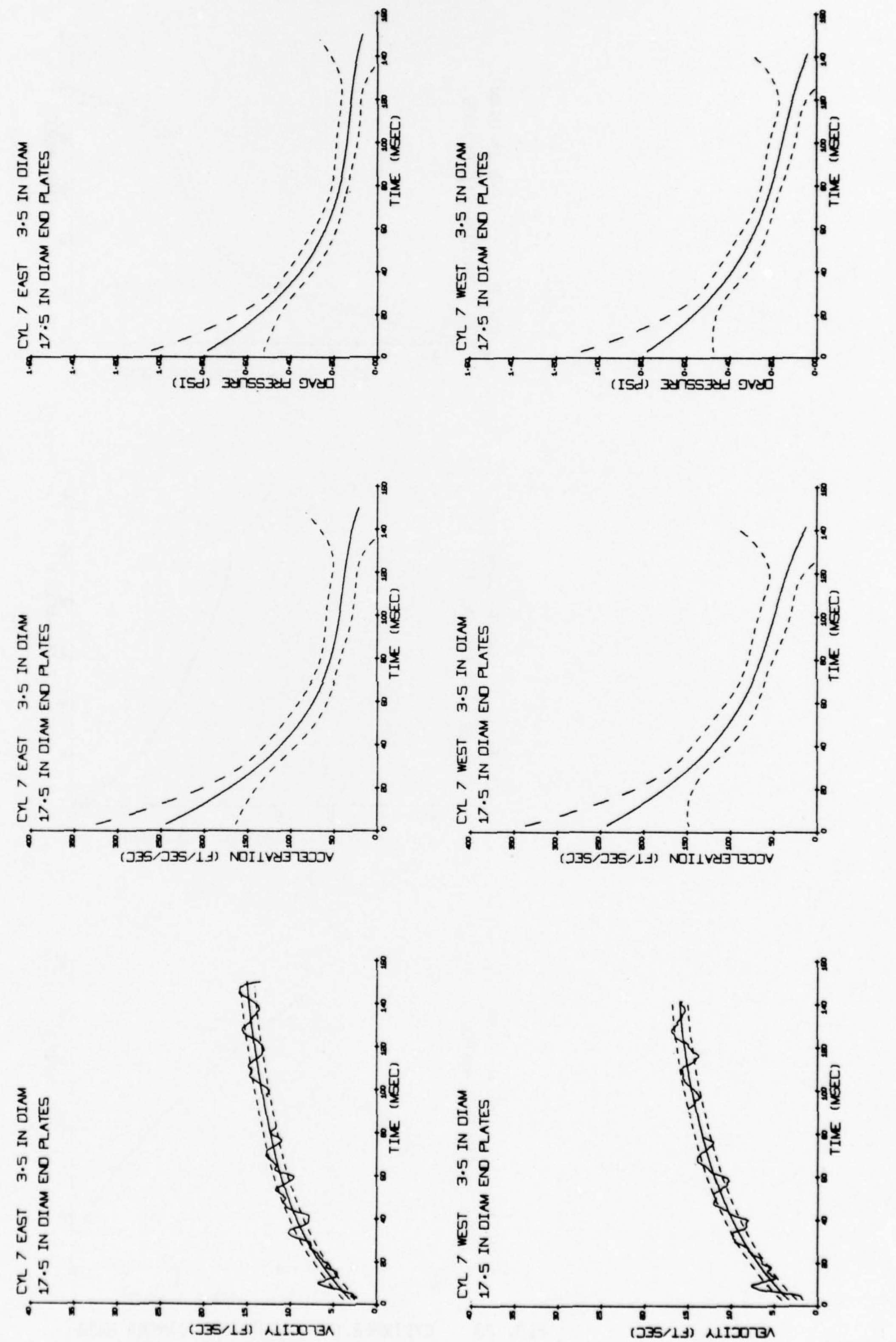

FIG. 24 CYLINDER 7 - VELOCITY TRANSDUCER DATA (9.7 PSI PEAK OVERPRESSURE)

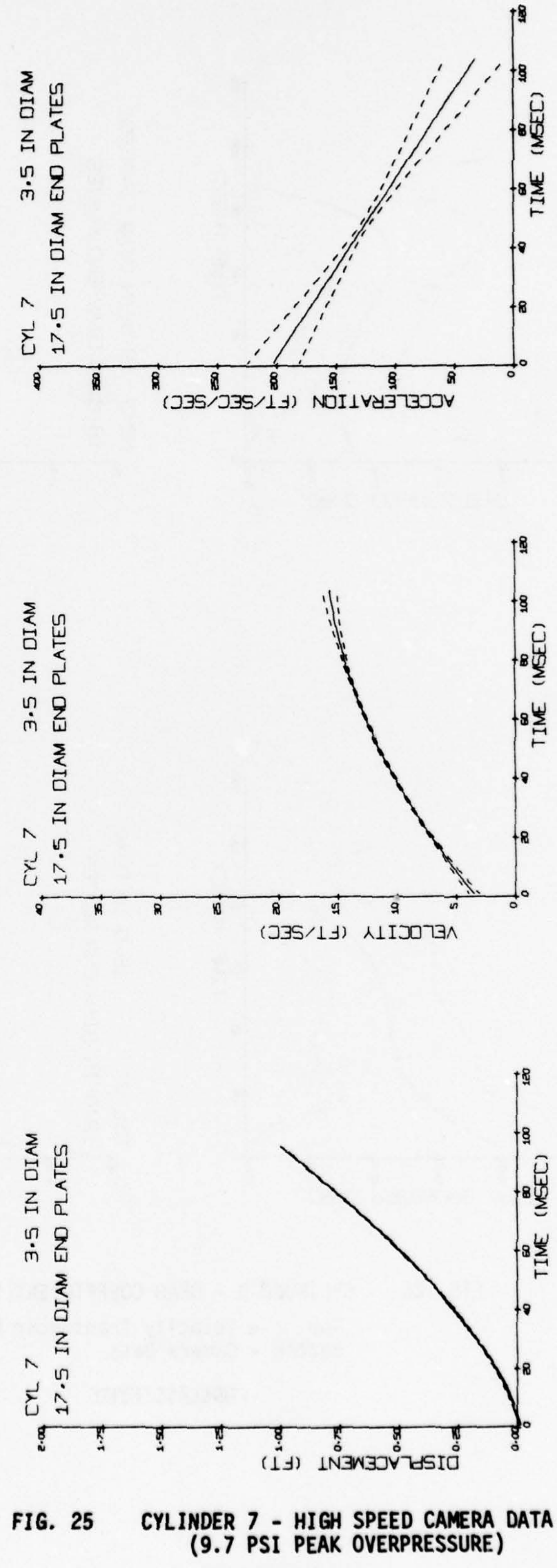

FIG. 25 CYLINDER 7 - HIGH SPEED CAMERA DATA (9.7 PSI PEAK OVERPRESSURE)

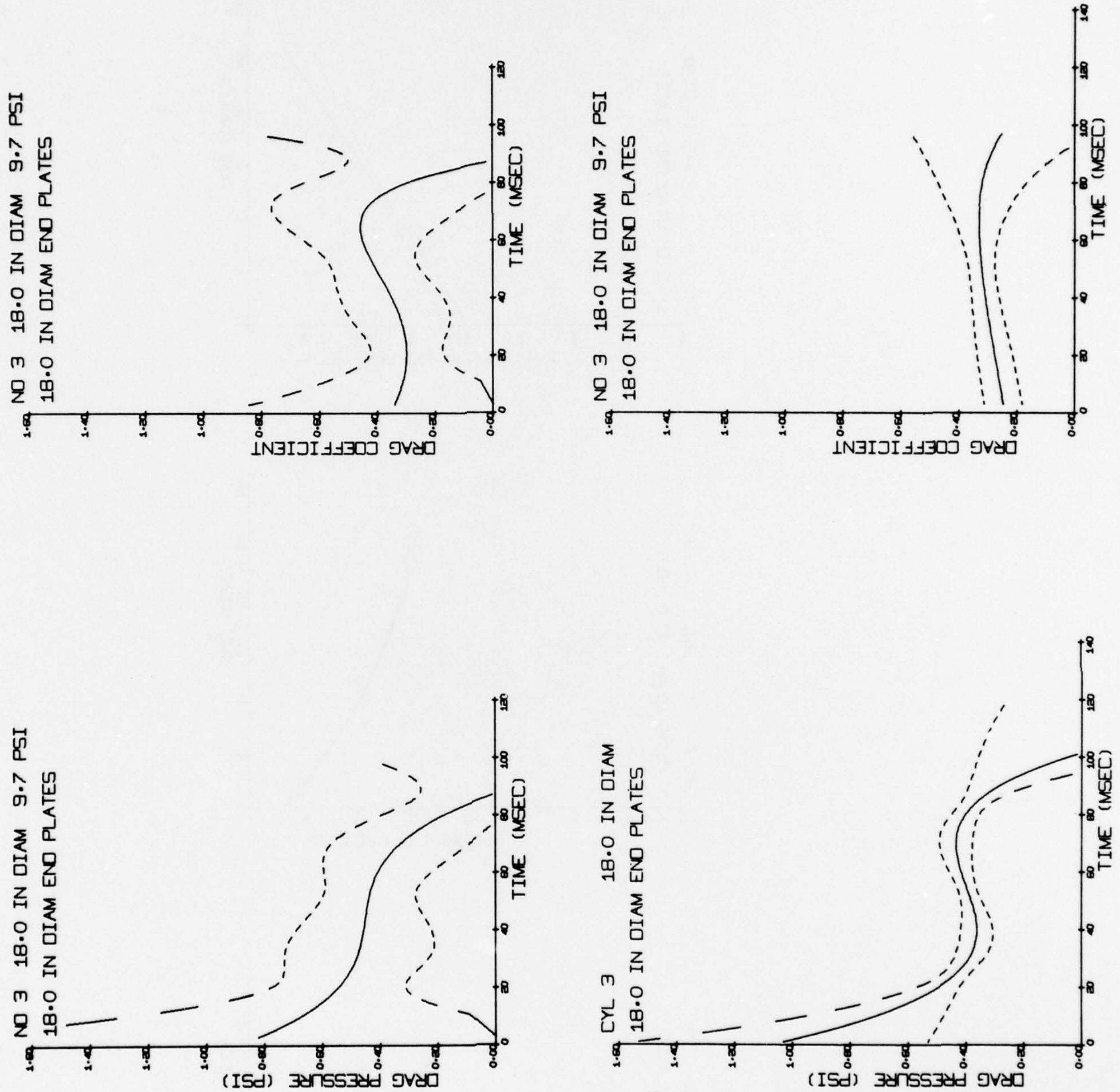

FIG. 26 CYLINDER 3 - DRAG COEFFICIENT VS TIME

Top - Velocity Transducer Data
Bottom - Camera Data

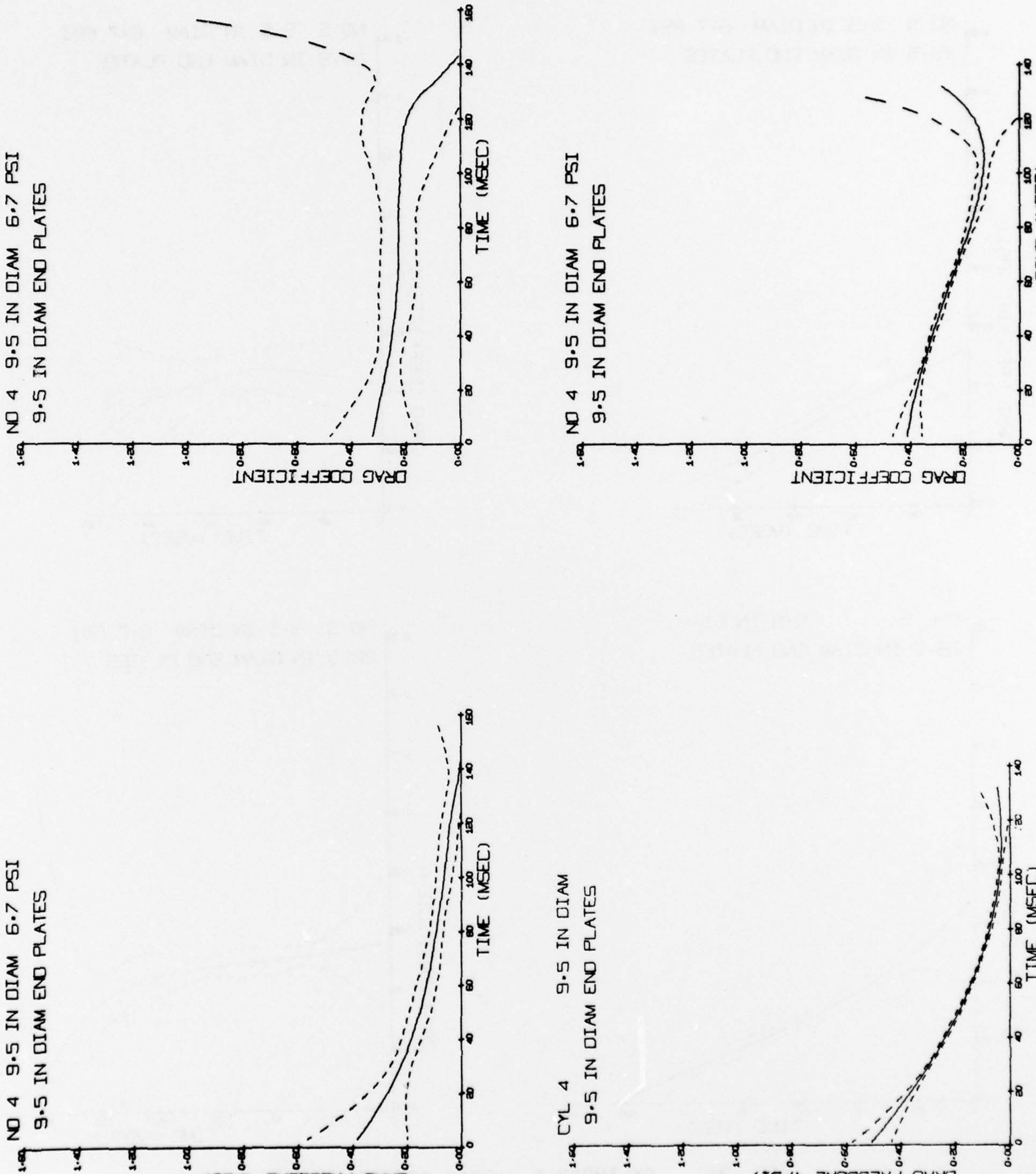

FIG. 27 CYLINDER 4 - DRAG COEFFICIENT VS TIME

Top - Velocity Transducer Data
Bottom - Camera Data

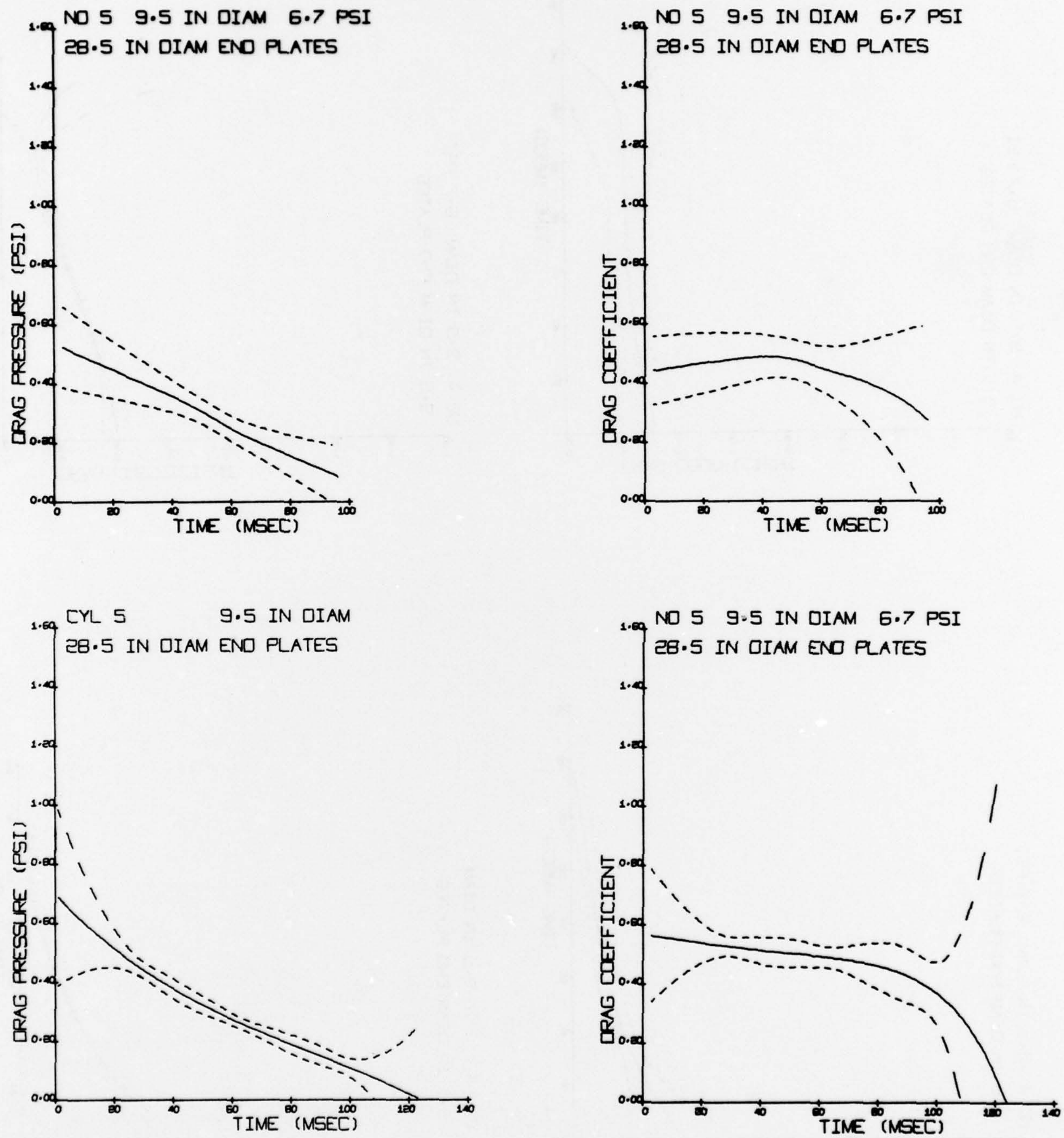

FIG. 28 CYLINDER 5 - DRAG COEFFICIENT VS TIME

Top - Velocity Transducer Data
Bottom - Camera Data

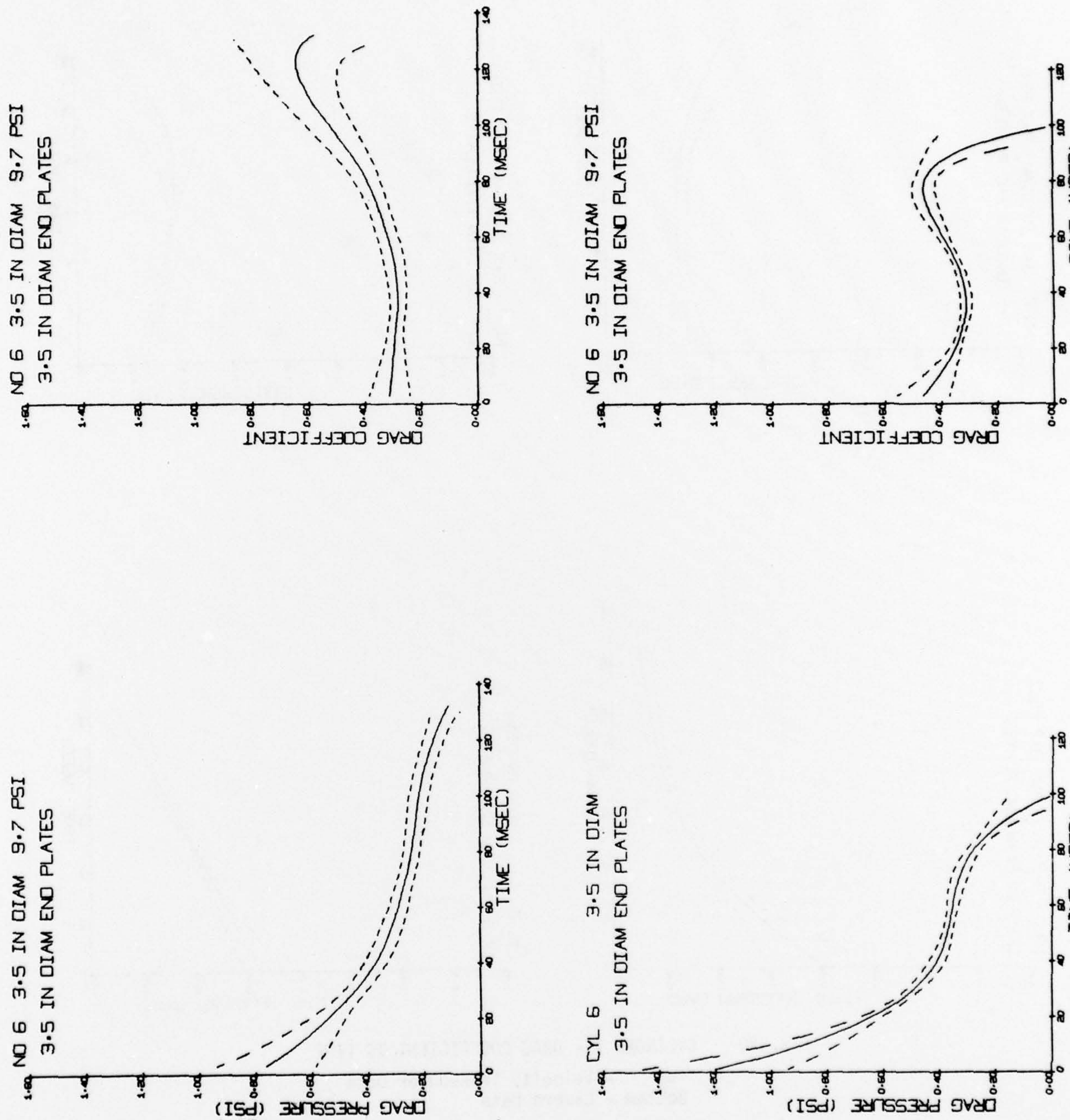

FIG. 29 CYLINDER 6 - DRAG COEFFICIENT VS TIME

Top - Velocity Transducer Data
Bottom - Camera Data

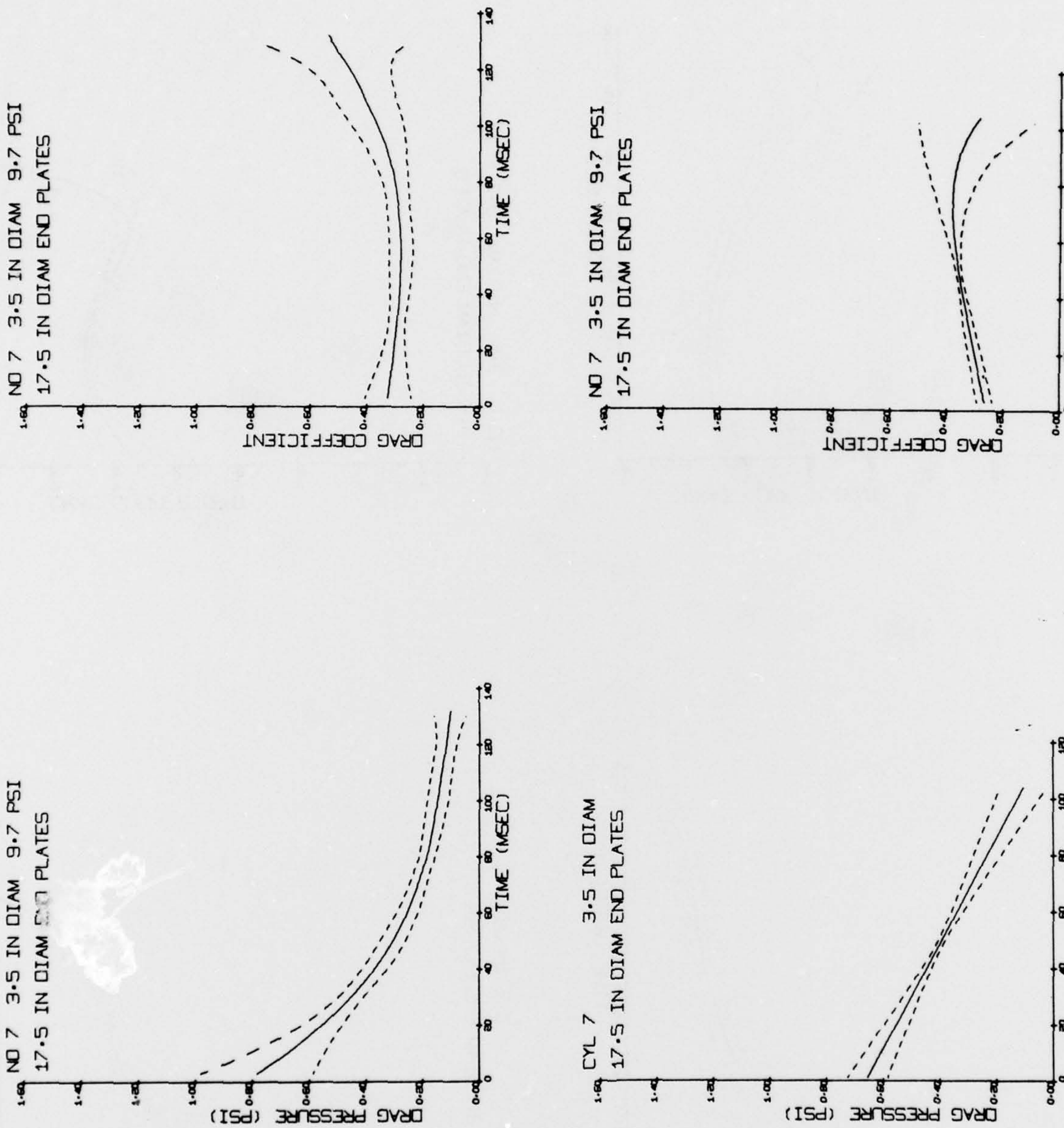

FIG. 30 CYLINDER 7 - DRAG COEFFICIENT VS TIME

Top - Velocity Transducer Data
Bottom - Camera Data

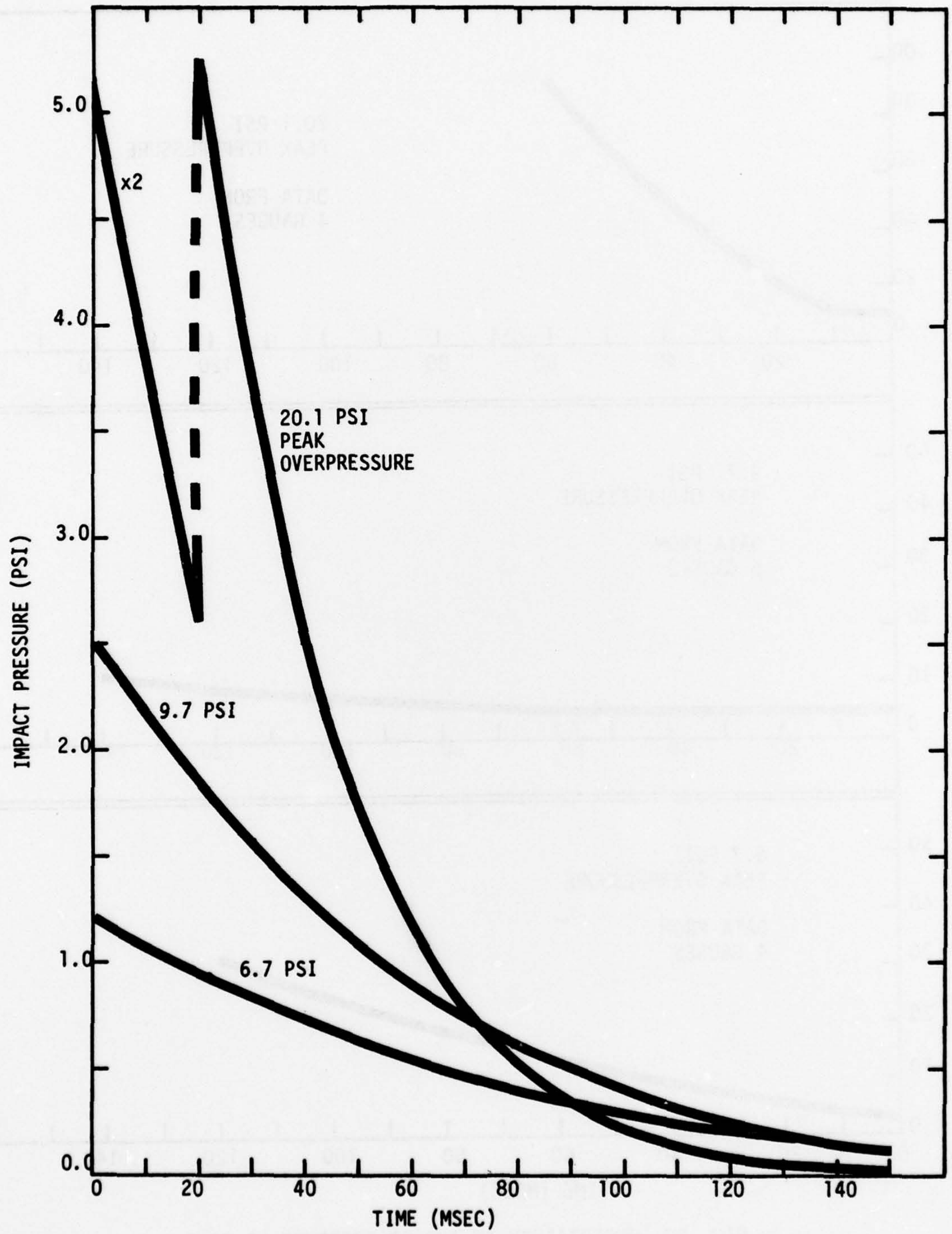

FIG. 31 IMPACT PRESSURES USED IN DATA ANALYSIS

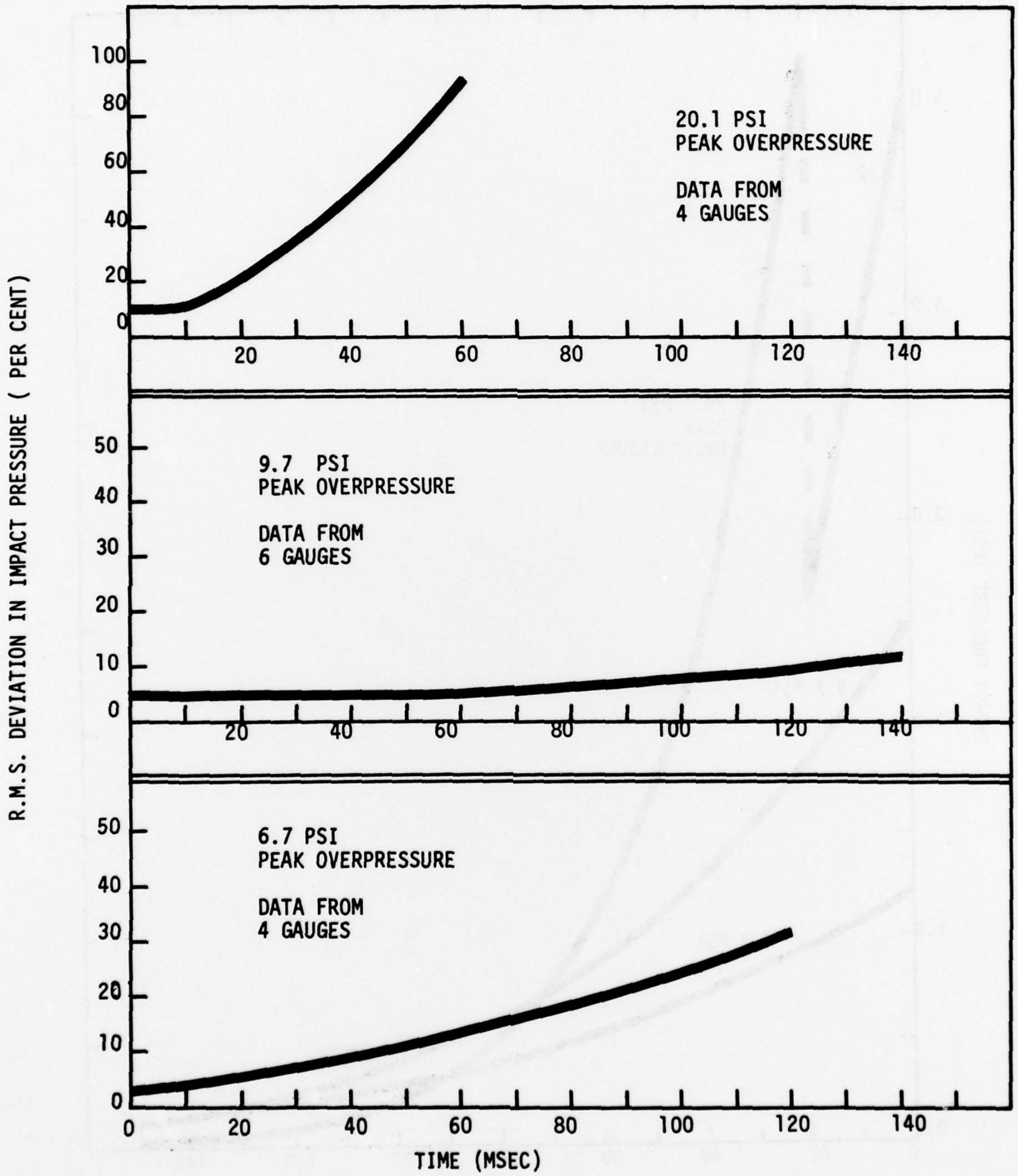

FIG. 32 UNCERTAINTY IN IMPACT PRESSURE VS TIME

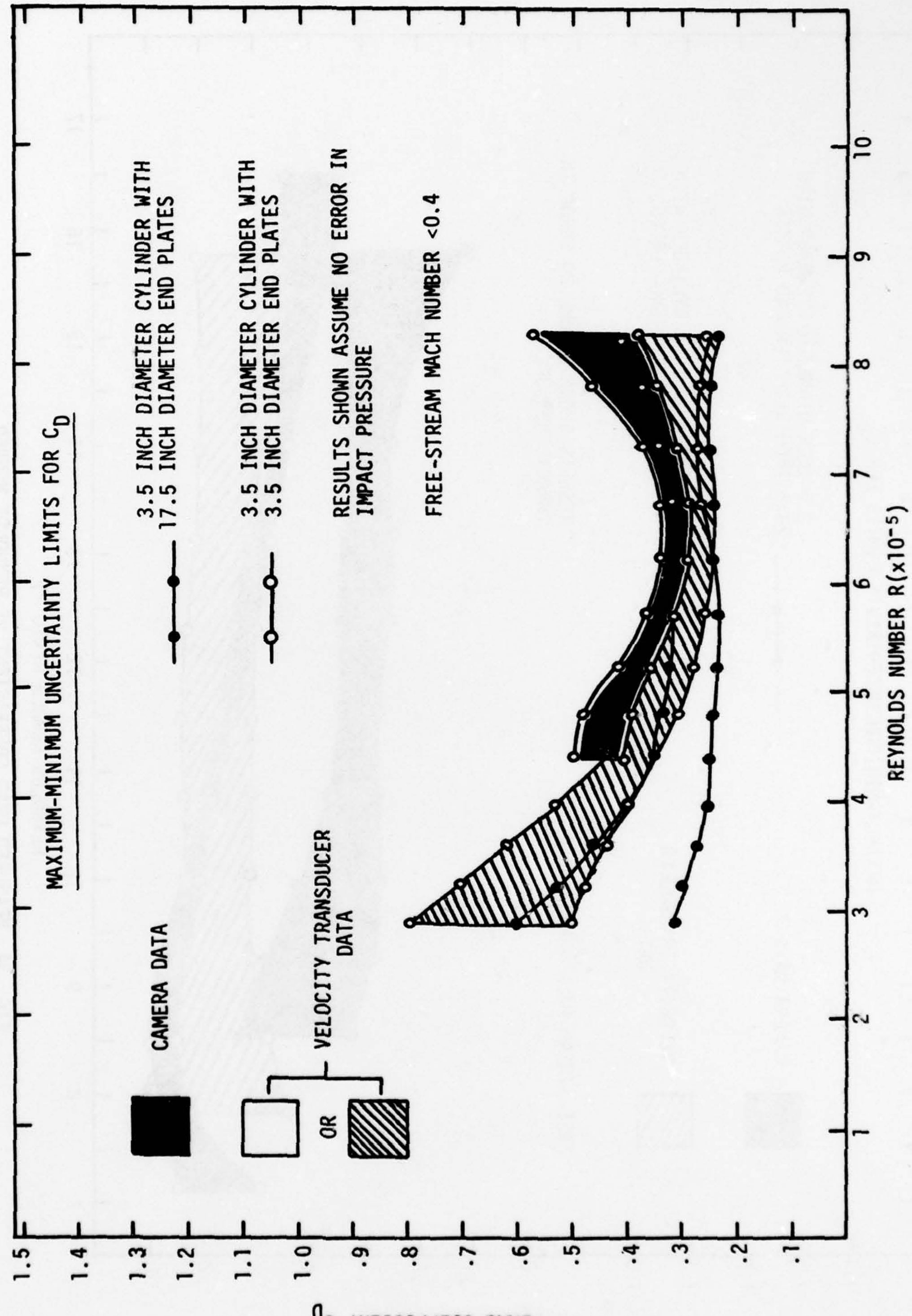

FIG. 33 MEASURED DRAG COEFFICIENT VS REYNOLDS NUMBER - 3.5 INCH DIAMETER CYLINDER

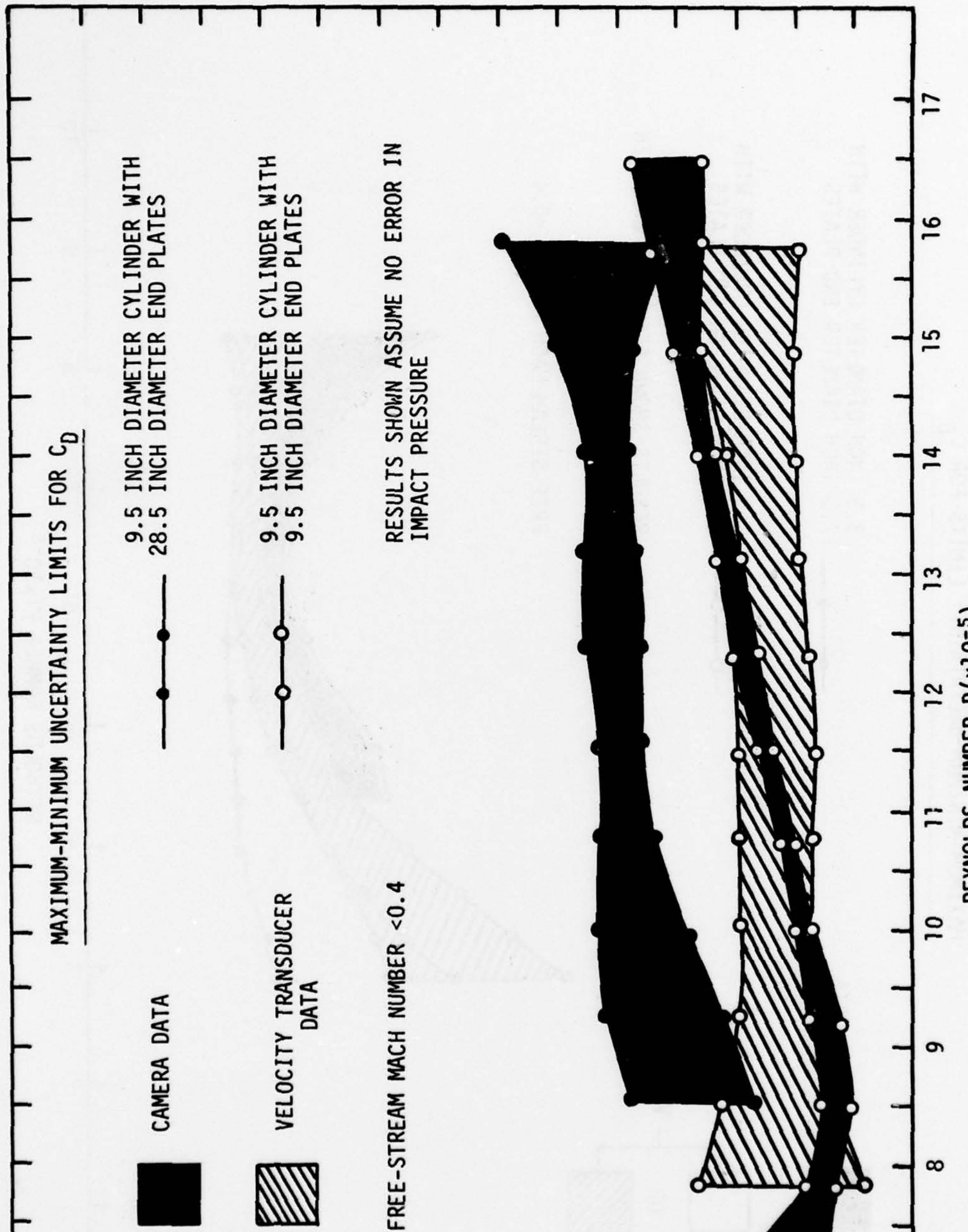

FIG. 34 MEASURED DRAG COEFFICIENT VS REYNOLDS NUMBER - 9.5 INCH DIAMETER CYLINDER

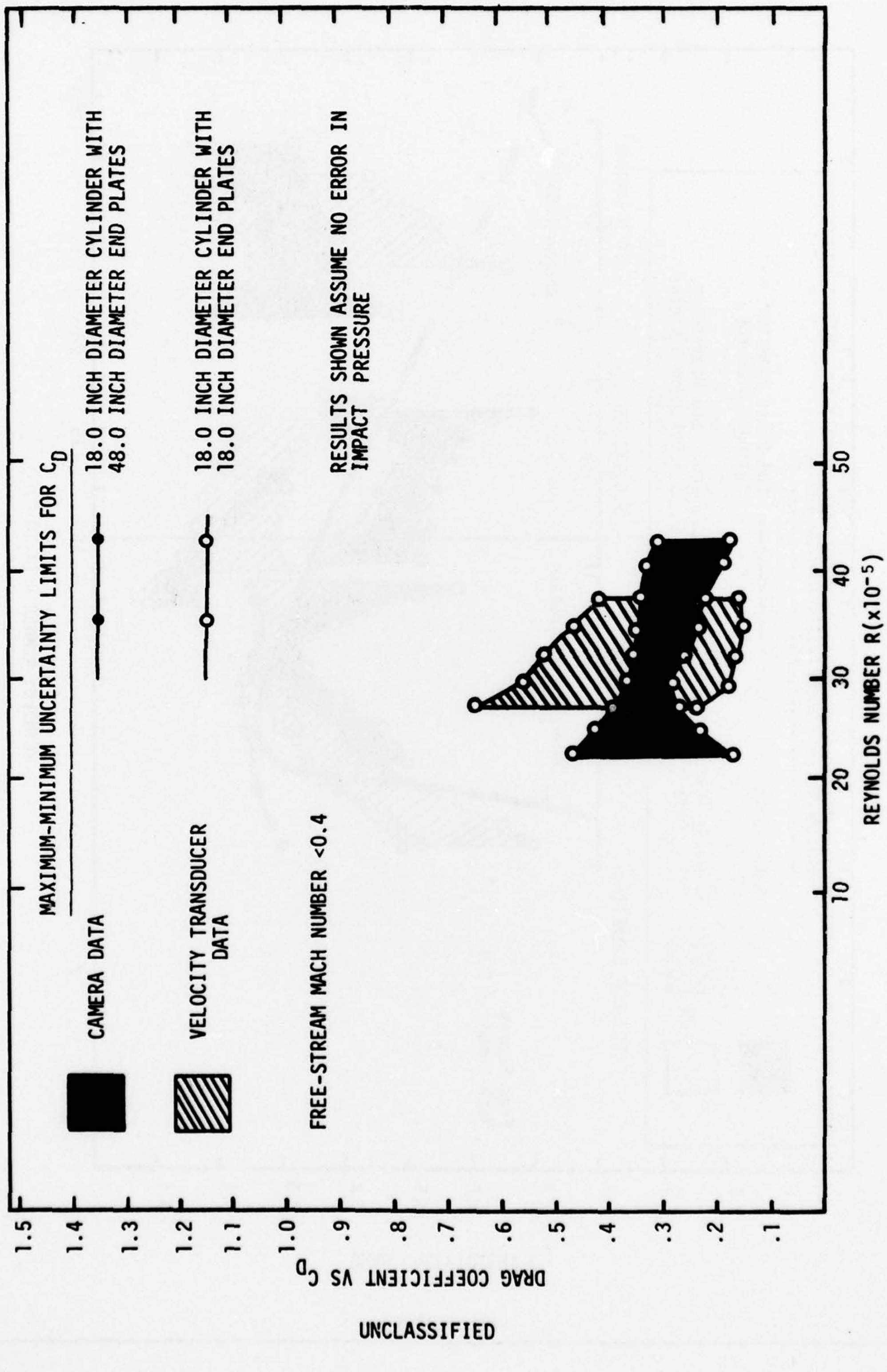

FIG. 35 MEASURED DRAG COEFFICIENT VS REYNOLDS NUMBER - 18.0 INCH DIAMETER CYLINDER

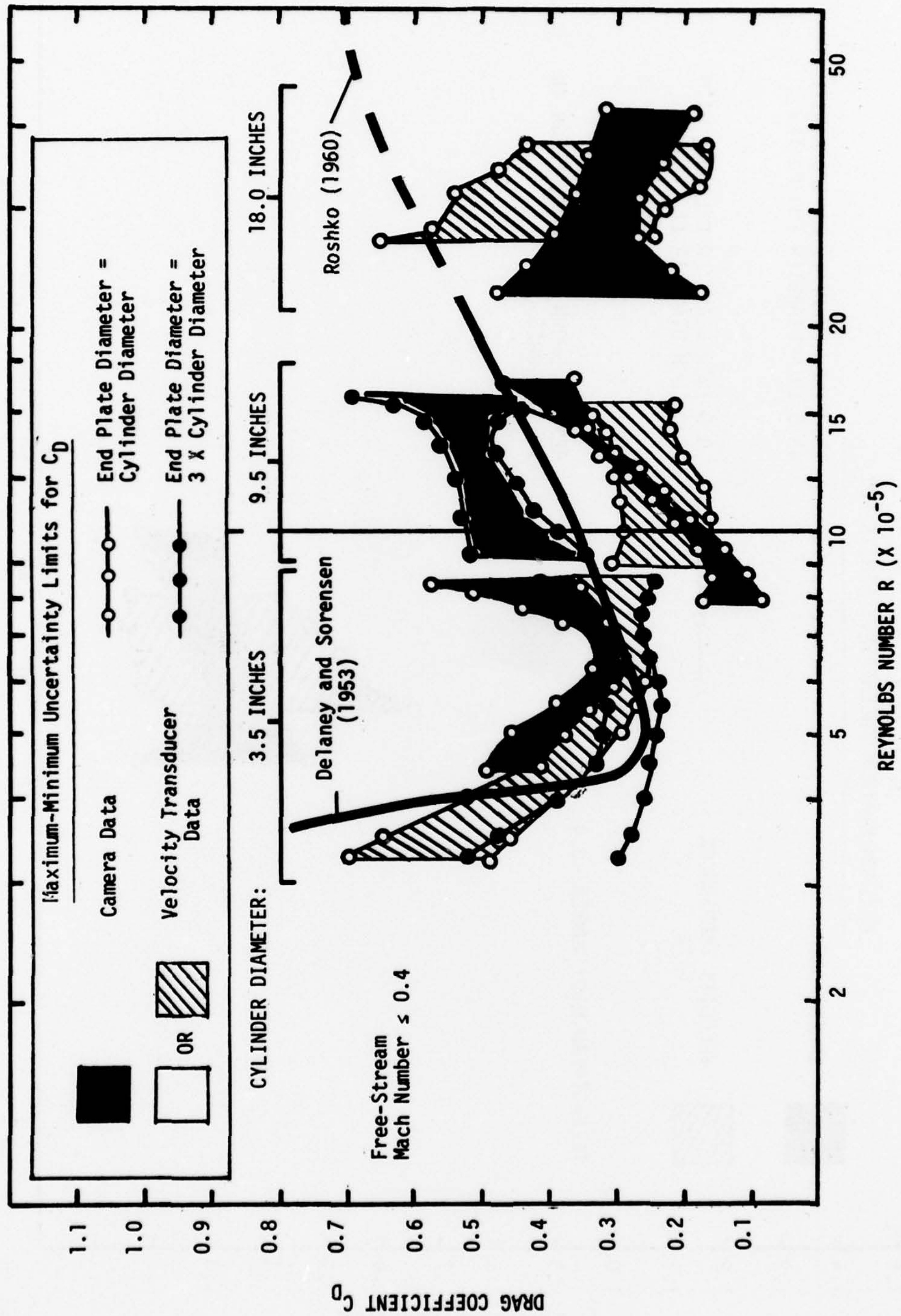

FIG. 36 MEASURED DRAG COEFFICIENT VS REYNOLDS NUMBER - COMPOSITE PLOT FOR ALL CYLINDER DIAMETERS

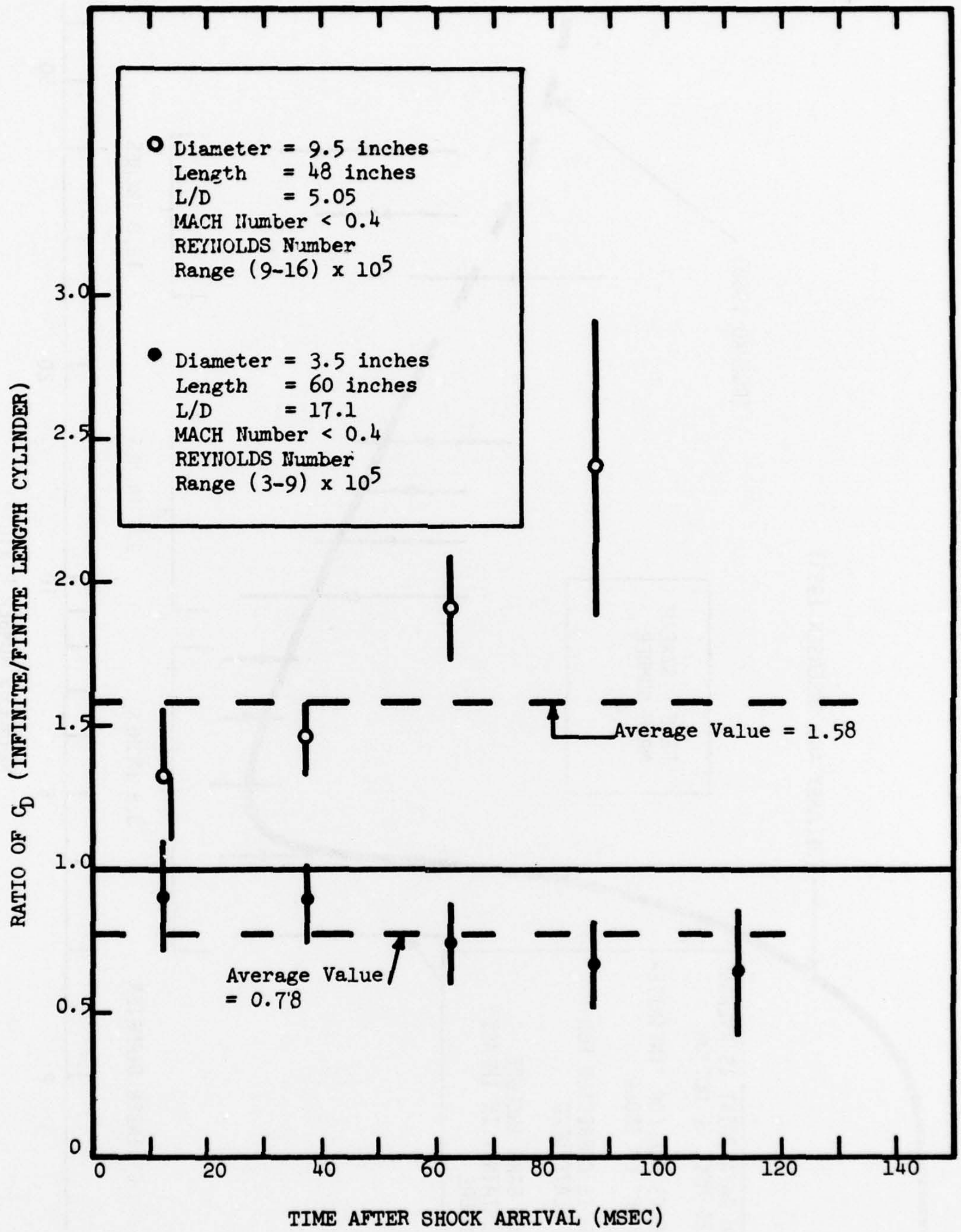

FIG. 37 MEASURED END EFFECTS FOR FINITE-LENGTH CYLINDERS

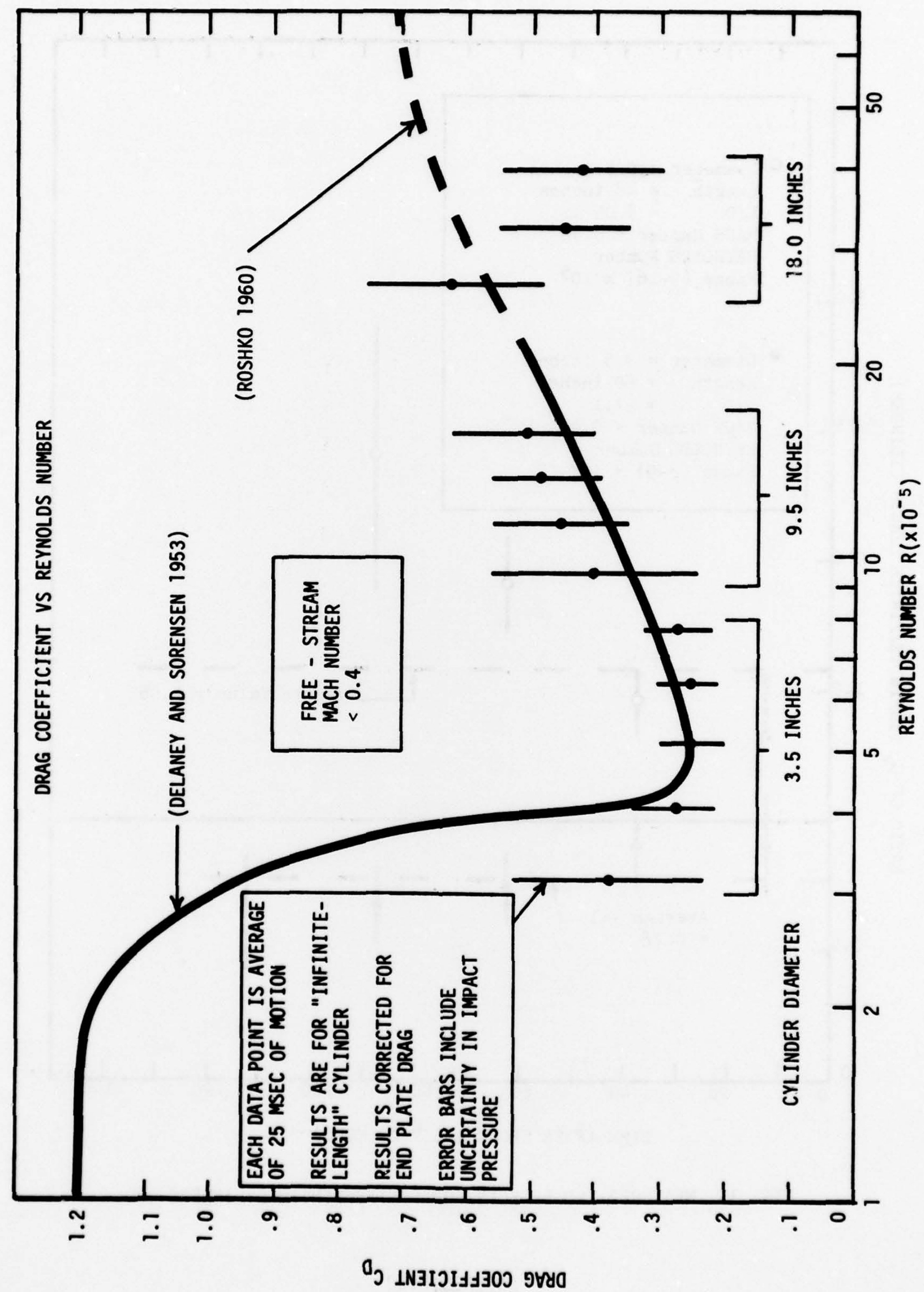

FIG. 38 DRAG COEFFICIENT VS REYNOLDS NUMBER - BEST VALUES (AFTER CORRECTIONS)

UNCLASSIFIED

Security Classification

DOCUMENT CONTROL DATA – R & D

(Security classification of title, body of abstract and indexing annotation must be entered when the overall document is classified)

1. ORIGINATING ACTIVITY DEFENCE RESEARCH ESTABLISHMENT SUFFIELD	2a. DOCUMENT SECURITY CLASSIFICATION UNCLASSIFIED 2b. GROUP

3. DOCUMENT TITLE
FREE-FLIGHT MEASUREMENT OF THE DRAG FORCES ON CYLINDERS IN EVENT DICE THROW (U)

4. DESCRIPTIVE NOTES (Type of report and inclusive dates) Technical Paper

5. AUTHOR(S) (Last name, first name, middle initial)
Gibb, A.W.M. and Hill, D.A.

6. DOCUMENT DATE February 1979	7a. TOTAL NO. OF PAGES 150	7b. NO. OF REFS 32
8a. PROJECT OR GRANT NO. 21K52	9a. ORIGINATOR'S DOCUMENT NUMBER(S) SUFFIELD TECHNICAL PAPER NO. 453	
8b. CONTRACT NO.	9b. OTHER DOCUMENT NO.(S) (Any other numbers that may be assigned this document)	

10. DISTRIBUTION STATEMENT
"UNLIMITED DISTRIBUTION"

11. SUPPLEMENTARY NOTES	12. SPONSORING ACTIVITY

13. ABSTRACT

Results are presented from an experiment to measure aerodynamic drag on smooth circular cylinders in a decaying blast wave generated by a large-scale chemical explosion (Event DICE THROW). Drag coefficients are reported from a set of measurements with Mach number 0.48 and Reynolds numbers ranging from 3×10^5 to 40×10^5. Values were in general consistent with steady-state values. Measurement of drag coefficients for identical cylinders with and without extended end plates provided an indication of the importance of end effects for cylinders of small length-to-diameter ratio at high Reynolds number.

(U)

DSIS
70-070

UNCLASSIFIED

Security Classification

KEY WORDS

Cylinder
Drag
DICE THROW
End Effect
Unsteady Flow
Chemical Explosion

INSTRUCTIONS

1. ORIGINATING ACTIVITY: Enter the name and address of the organization issuing the document.

2a. DOCUMENT SECURITY CLASSIFICATION: Enter the overall security classification of the document including special warning terms whenever applicable.

2b. GROUP: Enter security reclassification group number. The three groups are defined in Appendix 'M' of the DRB Security Regulations.

3. DOCUMENT TITLE: Enter the complete document title in all capital letters. Titles in all cases should be unclassified. If a sufficiently descriptive title cannot be selected without classification, show title classification with the usual one-capital-letter abbreviation in parentheses immediately following the title.

4. DESCRIPTIVE NOTES: Enter the category of document, e.g. technical report, technical note or technical letter. If appropriate, enter the type of document, e.g. interim, progress, summary, annual or final. Give the inclusive dates when a specific reporting period is covered.

5. AUTHOR(S): Enter the name(s) of author(s) as shown on or in the document. Enter last name, first name, middle initial. If military, show rank. The name of the principal author is an absolute minimum requirement.

6. DOCUMENT DATE: Enter the date (month, year) of Establishment approval for publication of the document.

7a. TOTAL NUMBER OF PAGES: The total page count should follow normal pagination procedures, i.e., enter the number of pages containing information.

7b. NUMBER OF REFERENCES: Enter the total number of references cited in the document.

8a. PROJECT OR GRANT NUMBER: If appropriate, enter the applicable research and development project or grant number under which the document was written.

8b. CONTRACT NUMBER: If appropriate, enter the applicable number under which the document was written.

9a. ORIGINATOR'S DOCUMENT NUMBER(S): Enter the official document number by which the document will be identified and controlled by the originating activity. This number must be unique to this document.

9b. OTHER DOCUMENT NUMBER(S): If the document has been assigned any other document numbers (either by the originator or by the sponsor), also enter this number(s).

10. DISTRIBUTION STATEMENT: Enter any limitations on further dissemination of the document, other than those imposed by security classification, using standard statements such as:

(1) "Qualified requesters may obtain copies of this document from their defence documentation center."

(2) "Announcement and dissemination of this document is not authorized without prior approval from originating activity."

11. SUPPLEMENTARY NOTES: Use for additional explanatory notes.

12. SPONSORING ACTIVITY: Enter the name of the departmental project office or laboratory sponsoring the research and development. Include address.

13. ABSTRACT: Enter an abstract giving a brief and factual summary of the document, even though it may also appear elsewhere in the body of the document itself. It is highly desirable that the abstract of classified documents be unclassified. Each paragraph of the abstract shall end with an indication of the security classification of the information in the paragraph (unless the document itself is unclassified) represented as (TS), (S), (C), (R), or (U).

The length of the abstract should be limited to 20 single-spaced standard typewritten lines; 7½ inches long.

14. KEY WORDS: Key words are technically meaningful terms or short phrases that characterize a document and could be helpful in cataloging the document. Key words should be selected so that no security classification is required. Identifiers, such as equipment model designation, trade name, military project code name, geographic location, may be used as key words but will be followed by an indication of technical context.